

America, Oslo, Norway !  
Dominique Fourcade  
Le sujet monotype  
P.O.L. (1997)

2000 Primary 60D 05; Secondary 81T 40, 05C 80, 60J65, 60J45, 30C 85, 60K 35, 82B 20, 82B 41, 82B 43

CONFORMAL FRACTAL GEOMETRY  
& BOUNDARY QUANTUM GRAVITY

Bertrand Duplantier

Abstract. This article gives a comprehensive description of the fractal geometry of conformally-invariant (CI) scaling curves, in the plane or half-plane. It focuses on deriving critical exponents associated with interacting random paths, by exploiting an underlying quantum gravity (QG) structure, which uses KPZ maps relating exponents in the plane to those on a random lattice, i.e., in a fluctuating metric. This is accomplished within the framework of conformal field theory (CFT), with applications to well-recognized critical models, like  $O(N)$  and Potts models, and to the Stochastic Loewner Evolution (SLE). Two fundamental ingredients of the QG construction are relating bulk and Dirichlet boundary exponents, and establishing additivity rules for QG boundary conformal dimensions associated with mutually-avoiding random sets. From these we derive the non-intersection exponents for random walks (RW's) or Brownian paths, self-avoiding walks (SAW's), or arbitrary mixtures thereof. The multifractal (MF) function  $f(\nu; c)$  of the harmonic measure (i.e., electrostatic potential, or diffusion field) near any conformally invariant fractal boundary, is given as a function of the central charge  $c$  of the associated CFT. A Brownian path, a SAW in the scaling limit, or a critical percolation cluster have identical spectra corresponding to the same central charge  $c = 0$ , with a Hausdorff dimension  $D = \sup_{\nu} f(\nu; c = 0) = 4/3$ , which nicely vindicates Mandelbrot's conjecture for the Brownian frontier dimension. The Hausdorff dimensions  $D_H$  of a non-simple scaling curve or cluster hull, and  $D_{EP}$  of its external perimeter or frontier, are shown to obey the "superuniversal" duality equation  $(D_H - 1)(D_{EP} - 1) = \frac{1}{4}$ , valid for any value of the central charge  $c$ . Higher multifractal functions, like the double spectrum  $f_2(\nu; \nu'; c)$  of the double-sided harmonic measure, are also considered. The universal fixed MF spectrum  $f(\nu; \nu'; c)$  describing the local winding rate and singularity exponent of the harmonic measure near any CI scaling curve is given. The fundamental duality which exists between simple and non-simple random paths is established via an algebraic symmetry of the KPZ quantum gravity map. An extended dual KPZ relation is then introduced for the SLE, which commutes with the  $\nu = 16/\nu'$  duality for SLE. This allows us to calculate the SLE exponents from simple QG rules. These rules are established from the general structure of correlation functions of arbitrary interacting random sets on a random lattice, as derived from random matrix theory.

arXiv:math-ph/0303034v2 14 Mar 2003

1991 Mathematics Subject Classification. [.

## Contents

1. Introduction	2
2. Intersections of Random Walks	8
3. Mixing Random & Self-Avoiding Walks	18
4. Harmonic Measure of Brownian and Self-Avoiding Paths	23
5. Percolation Clusters	32
6. Conformally Invariant Frontiers and Quantum Gravity	37
7. Higher Universal Multifractal Spectra	49
8. Winding of Conformally Invariant Curves	55
9. Duality for $O(N)$ and Potts Models and the Stochastic Loewner Evolution	63
10. Duality in KPZ	67
11. SLE and KPZ	70
12. Multifractal Exponents for the SLE	75
Acknowledgements	84
Appendix A. Brownian Intersection Exponents from Quantum Gravity	85
Appendix B. $O(N)$ Model Multi-Line Exponents from Quantum Gravity	95
Appendix C. Boundary-Bulk Exponents & Boundary Fusion Rules in Quantum Gravity	108
References	115

## 1. Introduction

## 1.1. A Brief Chronological History.

1.1.1. Brownian Paths, Critical Phenomena, and Quantum Field Theory. Brownian motion is the archetype of a random process, hence its great importance in probability theory. The Brownian path is also the archetype of a scale invariant set, and in two dimensions is a conformally-invariant one, as shown by P. Levy [1]. It is therefore perhaps the most natural random fractal [2]. On the other hand, Brownian paths are intimately linked with quantum field theory (QFT). Intersections of Brownian paths indeed provide the random geometrical mechanism underlying QFT [3]. In a Feynman diagram, any propagator line can be represented by a Brownian path, and the vertices are intersection points of the Brownian paths. This equivalence is widely used in polymer theory [4, 5] and in rigorous studies of second-order phase transitions and field theories [6]. Families of universal critical exponents are in particular associated with non-intersection probabilities of collections of random walks (RW's) or Brownian paths, and these play an important role both in probability theory and quantum field theory [7, 8, 9, 10].

A perhaps less known fact is the existence of highly non-trivial geometrical, actually fractal (or multifractal), properties of Brownian paths or their subsets [2]. These types of geometrical fractal properties generalize to all universality classes of, e.g., random walks (RW's), loop-erased random walks (LERW's), self-avoiding walks (SAW's) or polymers, Ising, percolation and Potts models,  $O(N)$  models, which are related in an essential way to standard critical phenomena and field theory. The random fractal geometry is particularly rich in two dimensions.

1.1.2. Conformal Invariance and Coulomb Gas. In two dimensions (2D), the notion of conformal invariance [11, 12, 13], and the introduction of the so-called "Coulomb gas techniques" have brought a wealth of exact results (see, e.g., [14, 15, 16, 17, 18, 19, 20, 21]). Conformal field theory (CFT) has lent strong support to the conjecture that statistical systems at their critical point, in their scaling (continuum) limit, produce conformally-invariant (CI) fractal structures, examples of which are the continuum scaling limits of RW's, LERW's, SAW's, critical Ising or Potts clusters. A prominent role was played by Cardy's equation for the crossing probabilities in 2D percolation [21]. To understand conformal invariance in a rigorous way presented a mathematical challenge (see, e.g., [22, 23, 24]).

In the particular case of planar Brownian paths, Benoît Mandelbrot [2] made the following famous conjecture in 1982: in two dimensions, the external frontier of a planar Brownian path has a Hausdorff dimension

$$(1.1) \quad D_{\text{Brownian:fr}} = \frac{4}{3};$$

identical to that of a planar self-avoiding walk [15]. This identity has played an important role in probability theory and theoretical physics in recent years, and will be a central theme in this article. We shall understand this identity in the light of "quantum gravity", to which we turn now.

1.1.3. Quantum Gravity and the KPZ Relation. Another breakthrough, not widely noticed at the time, was the introduction of "2D quantum gravity" (QG) in the statistical mechanics of 2D critical systems. V.A. Kazakov gave the solution of the Ising model on a random planar lattice [25]. The astounding discovery by Knizhnik, Polyakov, and Zamolodchikov of the "KPZ" map between critical exponents in the standard plane and in a random 2D metric [26] led to the relation of the exponents found in [25] to those of Onsager (see also [27]). The first other explicit solutions and checks of KPZ were obtained for SAW's [28] and for the  $O(N)$  model [29].

1.1.4. Multifractality. The concepts of generalized dimensions and associated multifractal (MF) measures were developed in parallel two decades ago [30, 31, 32, 33]. It was later realized that multifractals and field theory have deep connections, since the algebras of their respective correlation functions reveal striking similarities [34].

A particular example is given by classical potential theory, i.e., that of the electrostatic or diffusion field near critical fractal boundaries, or near diffusion limited aggregates (DLA). The self-similarity of the fractal boundary is indeed reflected in a multifractal behavior of the moments of the potential. In DLA, the potential, also called harmonic measure, actually determines the growth process [35, 36, 37]. For equilibrium statistical fractals, a first analytical example of multifractality was studied in Ref. [38], where the fractal boundary was chosen to be a simple RW, or a SAW, both accessible to renormalization group methods near four dimensions. In two dimensions, the existence of a multifractal spectrum for the Brownian path frontier was established rigorously [39].

In 2D, in analogy to the simplicity of the classical method of conformal transforms to solve electrostatics of Euclidean domains, a universal solution could be expected for the distribution of potential near any CI fractal in the plane. It was clear that these multifractal spectra should be linked with the conformal invariance

classification, but outside the realm of the usual rational exponents. That presented a second challenge to the theory.

## 1.2. Elaborating Conformal Geometrical Structures.

1.2.1. Brownian Intersection Exponents. It was already envisioned in the mid-eighties that the critical properties of planar Brownian paths, whose conformal invariance was well established [1], could be the opening gate to rigorous studies of two-dimensional critical phenomena<sup>1</sup>. Michael Aizenman, in a seminar in the Probability Laboratory of University of Paris VI in 1984, promised a good bottle of Bordeaux wine for the resolution of the  $\gamma_2$  exponent governing in two dimensions the non-intersection probability up to time  $t$ ,  $P_2(t) \sim t^{-\gamma_2}$ , of two Brownian paths<sup>2</sup>. The precise values of the family  $\gamma_1$  governing the similar non-intersection properties of L Brownian paths were later conjectured from conformal invariance and numerical studies in [40] (see also [41, 42]). They correspond to a CFT with central charge  $c = 0$ . Interestingly enough, however, their analytic derivation resisted attempts by standard "Coulomb-gas" techniques.

1.2.2. Spanning Trees and LERW. The related random process, the "loop-erased random walk", introduced in [43], in which the loops of a simple RW are erased sequentially, could also be expected to be accessible to a rigorous approach. Indeed, it can be seen as the backbone of a spanning tree, and the Coulomb gas predictions for the associated exponents [44, 45] were obtained rigorously by determinant or Pfaffian techniques by R. Kenyon [46], in addition to the conformal invariance of crossing probabilities [47]. They correspond to a CFT with central charge  $c = -2$ .

1.2.3. Conformal Invariance and Brownian Cascade Relations. The other route was followed by W. Werner [48], joined later by G.F. Lawler, who concentrated on Brownian path intersections, and on their general conformal invariance properties. They derived in particular important "cascade relations" between Brownian intersection exponents of packets of Brownian paths [49], but still without a derivation of the conjectured values of the latter.

## 1.3. Quantum Gravity.

1.3.1. QG and Brownian Paths, SAW's and Percolation. In the Brownian cascade structure the author recognized an underlying quantum gravity structure. This led to an analytical derivation of the (non-)intersection exponents for Brownian paths [50]. The same QG structure, properly understood, also gave access to exponents of mixtures of RW's and SAW's, to the harmonic measure multifractal spectra of the latter two [51], of a percolation cluster [52], and to the rederivation of path-crossing exponents in percolation of ref. [53]. Mandelbrot's conjecture (1.1) also follows from

$$(1.2) \quad D_{\text{Brownian fract}} = 2 - 2\frac{\gamma_2}{3} = \frac{4}{3}:$$

It was also observed there that the whole class of Brownian paths, self-avoiding walks, and percolation clusters, possesses the same harmonic MF spectrum in two

<sup>1</sup> It is perhaps interesting to note that P.-G. de Gennes originally studied polymer theory with the same hope of understanding from that perspective the broader class of critical phenomena. It turned out to be historically the converse: the Wilson-Fisher renormalization group approach to spin models with  $O(N)$  symmetry yielded the polymer critical exponents as the special case of the  $N \rightarrow 0$  limit [4].

<sup>2</sup> The Château Margaux 1982 bottle was finally drunk in 2001 Chez Panisse, Berkeley CA.

dimensions, corresponding to a unique central charge  $c = 0$ . Higher MF spectra were also calculated [54]. Related results were obtained in [55, 56].

1.3.2. General C I C Curves and Multifractality. The general solution for the potential distribution near any conformal fractal in 2D was naturally obtained from the same quantum gravity structure [57]. The exact multifractal spectra describing the singularities of the harmonic measure along the fractal boundary depend only on the so-called central charge  $c$ , the parameter which labels the universality class of the underlying CFT.

1.3.3. Duality. A corollary is the existence of a subtle geometrical duality structure in boundaries of random paths or clusters [57]. For instance, in the Potts model, the external perimeter (EP) of a Fortuin-Kasteleyn cluster, which bears the electrostatic charge and is a simple (i.e., double point free) curve, differs from the full cluster's hull, which bounces onto itself in the scaling limit. The EP's Hausdorff dimension  $D_{EP}$ , and the hull's Hausdorff dimension  $D_H$  obey a duality relation:

$$(1.3) \quad (D_{EP} - 1)(D_H - 1) = \frac{1}{4};$$

where  $D_{EP} = D_H$ . This generalizes the case of percolation hulls [58], elucidated in [53], for which:  $D_{EP} = 4/3; D_H = 7/4$ . Notice that the symmetric point of (1.3),  $D_{EP} = D_H = 3/2$ , gives the maximum dimension of a simple conformally-invariant random curve in the plane.

#### 1.4. Stochastic Lower Evolution.

1.4.1. SLE and Brownian Paths. Meanwhile, O. Schramm, trying to reproduce by a continuum stochastic process both the conformal invariance and Markov properties of the scaling limit of loop-erased random walks, invented in 1999 the so-called "Stochastic Lower Evolution" (SLE) [59], a process parametrized by an auxiliary one-dimensional Brownian motion of speed  $\kappa$ . It became quickly recognized as a breakthrough since it provided a powerful analytical tool to describe conformally-invariant scaling curves for various values of  $\kappa$ . It in particular describes LERW for  $\kappa = 2$ , and hulls of critical percolation clusters for  $\kappa = 6$ . More generally, it was clear that it described the continuum limit of hulls of critical clusters, and that the  $\kappa$  parameter is actually in one-to-one correspondence to the usual Coulomb gas coupling constant  $g$ ,  $g = 4 - \frac{2}{\kappa}$  (see, e.g., [60]).

Lawler, Schramm and Werner were then able to rigorously derive the Brownian intersection exponents [62], as well as Mandelbrot's conjecture [63] by relating them to the properties of  $SLE_{\kappa=6}$ . S. Smirnov related the continuum limit of site percolation on the triangular lattice to the  $SLE_{\kappa=6}$  process [64], and derived Cardy's equation [21] from it. Other well-known percolation scaling behaviors follow from this [65, 66]. The scaling limit of the LERW has also been rigorously shown to be the  $SLE_{\kappa=2}$  [67], as anticipated in [59], while that of SAW's is expected to correspond to  $\kappa = 8/3$  [60, 68].

1.4.2.  $\kappa = 16$  Duality for the SLE. The SLE trace essentially describes boundaries of conformally-invariant random clusters. For  $\kappa < 4$ , it is a simple path, while for  $\kappa > 4$  it bounces onto itself. One can establish a dictionary between the results obtained by quantum gravity and Coulomb gas techniques for Potts and  $O(N)$  models [57], and those concerning the SLE [60] (see below). The duality equation (1.3) then brings in a  $\kappa = 16$  duality property [57, 60] between

Hausdorff dimensions:

$$(1.4) \quad \mathbb{D}_{EP}(\kappa) = 1 + \mathbb{D}_H(\kappa) = \frac{1}{4}; \quad \kappa = 4;$$

where

$$\mathbb{D}_{EP}(\kappa) = \mathbb{D}_H(\kappa = 16\kappa); \quad \kappa = 4$$

gives the dimension of the frontier of a non-simple SLE $_{\kappa}$  trace as the Hausdorff dimension of the simple SLE $_{16\kappa}$  trace. Actually, this extends to the whole multifractal spectrum of the harmonic measure near the SLE $_{\kappa}$ , which is identical to that of the SLE $_{16\kappa}$  [57, 60]. From that result was originally stated the duality prediction that the frontier of the non-simple SLE $_{\kappa}$  path is locally a simple SLE $_{16\kappa}$  path [57, 60, 61].

The SLE geometrical properties per se are an active subject of investigations [69]. The value of the Hausdorff dimension of the SLE trace,  $\mathbb{D}_H(\kappa) = 1 + \frac{1}{\kappa}$ , has been obtained rigorously by V. Beara [70], in agreement with the value predicted by the Coulomb gas approach [15, 20, 57, 60]. The duality (1.4) predicts  $\mathbb{D}_{EP}(\kappa) = 1 + \frac{1}{\kappa} = \frac{1}{4}$  for the dimension of the SLE frontier [57, 60].

1.4.3. Recent Developments. The mixed multifractal spectrum [71] describing the local rotations and singularities of the harmonic measure near the SLE boundary has been obtained [72]. A two-parameter family of Stochastic Loewner Evolution processes, the SLE $(\kappa; \nu)$  processes, has been introduced recently [73]. The relationship of SLE to standard conformal field theory has been pointed out and developed recently [73, 74, 75]. Boundary correlators in 2D quantum gravity, which were originally calculated via the Liouville field theory [76, 77], and are related to our quantum gravity approach, have been recovered from discrete models on a random lattice [78]. A description of collections of SLE's in terms of Dyson's circular ensembles has been proposed [79]. The two-parameter family SLE $(\kappa; \nu)$  has been studied further [80], in particular in relation to the duality property mentioned above [81].

1.5. Synopsis.<sup>3</sup> The aim of the present article is to give a comprehensive description of conformally-invariant fractal geometry, and of its underlying quantum gravity structure. In particular, we show how the repeated use of KPZ maps between the critical exponents in the complex plane  $\mathbb{C}$  and those in quantum gravity allows the determination of a very large class of critical exponents arising in planar critical statistical systems, including the multifractal ones, and their reducing to simple irreducible elements. Two key elements are relating the bulk exponents in quantum gravity to the Dirichlet boundary ones, and establishing simple additivity rules for the latter. Within this unifying perspective, we cover many well-recognized geometrical models, like RW's or SAW's and their intersection properties, Potts and  $O(N)$  models, and the multifractal properties thereof.

We also adapt the quantum gravity formalism to the SLE process, revealing there a hidden algebraic duality in the KPZ map itself, which in turn translates into the geometrical  $! \kappa = 16\kappa$  duality between simple and non-simple SLE

<sup>3</sup>The first part of this paper (sections 2-7) is a slightly expanded version of ref. [60]. The second part (sections 8-12 and appendices) gives a detailed description of local windings and singularities along CI scaling curves. It then focuses on SLE and quantum gravity, and on their various dualities, mirrored in that relating simple and non-simple paths. Finally, it offers detailed arguments leading to the quantum gravity approach to interacting random paths.

traces. This KPZ algebraic duality also explains the duality which exists within the class of Potts and  $O(N)$  models between hulls and external frontiers.

In section 2 we first establish the values of the intersection exponents of random walks or Brownian paths from quantum gravity. The combinatorial details are given in appendix A. In section 3 we then move to the critical properties of arbitrary sets mixing simple random walks or Brownian paths and self-avoiding walks, with arbitrary interactions thereof. The multifractal spectrum of the harmonic measure near Brownian paths or self-avoiding ones is studied in section 4, including the case of the double-sided potential. Section 5 yields the related multifractal spectrum for percolation clusters. This completes the description of the universality class of central charge  $c = 0$ .

We address in section 6 the general solution for the multifractal potential distribution near any conformal fractal in 2D, which allows determination of the Hausdorff dimension of the frontier. The multifractal spectra depend only on the central charge  $c$ , which labels the universality class of the underlying CFT.

Another feature is the consideration in section 7 of higher multifractality, which occurs in a natural way in the joint distribution of potential on both sides of a random CI scaling path, or more generally, in the distribution of potential between the branches of a star made of an arbitrary number of CI paths. The associated universal multifractal spectrum will depend on two variables, or more generally, on  $m$  variables in the case of an  $m$ -arm star.

Section 8 describes the more subtle mixed multifractal spectrum associated with the local rotations and singularities along a conformally-invariant curve, as seen by the harmonic measure [71, 72]. Here quantum gravity and Coulomb gas techniques must be fused.

Section 9 focuses on the  $O(N)$  and Potts models, on the SLE, and on the correspondence between them. This is exemplified for the geometric duality existing between their frontiers and full boundaries or hulls. The various Hausdorff dimensions of  $O(N)$  lines, Potts cluster boundaries, and SLE's traces are given.

Conformally invariant paths have quite different critical properties and obey different quantum gravity rules, depending on whether they are simple paths or not. The next sections are devoted to the elucidation of this difference, and its treatment within a unified framework.

A fundamental algebraic duality which exists in the KPZ map is studied in section 10, and applied to the construction rules for critical exponents associated with non-simple paths versus simple ones. These dual rules are established in appendices B and C from considerations of quantum gravity.

In section 11, we construct an extended KPZ formalism for the SLE process, which is valid for all values of the parameter  $\kappa$ . It corresponds to the usual KPZ formalism for  $\kappa \leq 4$  (simple paths), and to the algebraic dual one for  $\kappa > 4$  (non-simple paths). The composition rules for calculating critical exponents involving several random paths in the SLE process are given, as well as some short-distance expansion results. The multi-line exponents for the SLE, and the equivalent ones for  $O(N)$  and Potts models are listed.

Finally, in section 12 the extended SLE quantum gravity formalism is applied to the calculation of all harmonic measure exponents near multiple SLE traces, near a boundary or in open space.

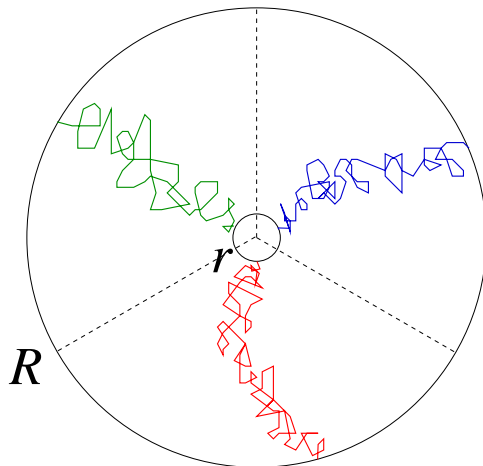


Figure 1. Three non-intersecting planar random walks crossing an annulus from  $r$  to  $R$ .

Appendix A details the calculation of Brownian non-intersection exponents in quantum gravity. Appendix B describes the calculation of  $O(N)$  model exponents from quantum gravity, and establishes the relation between boundary and bulk exponents and the additivity rules for Dirichlet boundary ones. These QG relations are actually sufficient to determine all exponents without further calculations. Finally, appendix C establishes the general relation between boundary and bulk exponents in quantum gravity, as well as the boundary additivity rules. They follow from a fairly universal structure of correlation functions in quantum gravity.

The quantum gravity techniques used here are perhaps not widely known in the statistical mechanics community at-large, since they originally belonged to string or random matrix theory. These techniques, moreover, are not yet within the realm of rigorous mathematics. However, the correspondence extensively used here, which exists between scaling laws in the plane, and on a random Riemann surface appears to be fundamental, and, in my opinion, illuminates many of the geometrical properties of conformally-invariant random curves in the plane.

## 2. Intersections of Random Walks

### 2.1. Non-Intersection Probabilities.

2.1.1. Planar Case. Let us first define the so-called (non-)intersection exponents for random walks or Brownian motions. While simpler than the multifractal exponents considered above, in fact they generate the latter. Consider a number  $L$  of independent random walks  $B^{(l)}$ ;  $l = 1, \dots, L$  in  $\mathbb{R}^2$  (or Brownian paths in  $\mathbb{R}^2 = \mathbb{C}$ ); starting at fixed neighboring points, and the probability

$$(2.1) \quad P_L(t) = P \left[ \bigcap_{l=1}^L (B^{(l)}[0;t] \cap B^{(l')}[0;t]) = \emptyset \right];$$

that the intersection of their paths up to time  $t$  is empty [7, 10]. At large times one expects this probability to decay as

$$(2.2) \quad P_L(t) \sim t^{-L};$$



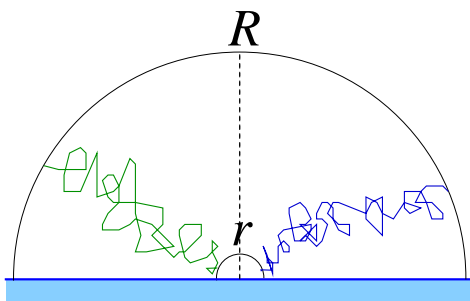


Figure 2. Two mutually-avoiding random walks crossing a half-annulus from  $r$  to  $R$  in the halfplane  $H$ .

where  $\nu_L$  is a universal exponent depending only on  $L$ . Similarly, the probability that the Brownian paths altogether traverse the annulus  $D(r;R)$  in  $C$  from the inner boundary circle of radius  $r$  to the outer one at distance  $R$  (Fig. 1) scales as

$$(2.3) \quad P_L(R) \sim (r=R)^{2\nu_L};$$

These exponents can be generalized to  $d$  dimensions. Above the upper critical dimension  $d = 4$ , RW's almost surely do not intersect and  $\nu_L(d = 4) = 0$ . The existence of exponents  $\nu_L$  in  $d = 2,3$  and their universality have been proven [42], and they can be calculated near  $d = 4$  by renormalization theory [10].

2.1.2. Boundary Case. A generalization was introduced [40] for  $L$  walks constrained to stay in the halfplane  $H$  with Dirichlet boundary conditions on  $\partial H$ , and starting at neighboring points near the boundary. The non-intersection probability  $\tilde{P}_L(t)$  of their paths is governed by a boundary critical exponent  $\tilde{\nu}_L$  such that

$$(2.4) \quad \tilde{P}_L(t) \sim t^{-\tilde{\nu}_L};$$

One can also consider the probability that the Brownian paths altogether traverse the halfannulus  $D(r;R)$  in  $H$ , centered on the boundary line  $\partial H$ , from the inner boundary circle of radius  $r$  to the outer one at distance  $R$  (Fig. 2). It scales as

$$(2.5) \quad \tilde{P}_L(R) \sim (r=R)^{2\tilde{\nu}_L};$$

2.1.3. Conformal Invariance and Weights. It was first conjectured from conformal invariance arguments and numerical simulations that in two dimensions [40]

$$(2.6) \quad \nu_L = h_{0;L}^{(c=0)} = \frac{1}{24} (4L^2 - 1);$$

and for the halfplane

$$(2.7) \quad 2\tilde{\nu}_L = h_{1;2L+2}^{(c=0)} = \frac{1}{3} L (1 + 2L);$$

where  $h_{p;q}^{(c)}$  denotes the Kac conformal weight

$$(2.8) \quad h_{p;q}^{(c)} = \frac{[(m+1)p - m q]^2 - 1}{4m(m+1)};$$

of a minimal conformal field theory of central charge  $c = 1 - 6/m(m+1)$ ;  $m \geq 2$  [12]. For Brownian motions  $c = 0$ ; and  $m = 2$ :

2.1.4. Disconnection Exponent. A discussion of the intersection exponents of random walks a priori requires a number  $L \geq 2$  of them. Nonetheless, for  $L = 1$ , the exponent has a meaning: the non-trivial value  $\gamma_1 = 1/8$  actually gives the disconnection exponent governing the probability that the origin of a single Brownian path remains accessible from infinity without the path being crossed, hence stays connected to infinity. On a Dirichlet boundary,  $\tilde{\gamma}_1$  retains its standard value  $\tilde{\gamma}_1 = 1$ , which can be derived directly, e.g., from the Green function formalism. It corresponds to a path extremity located on the boundary, which always stays accessible due to Dirichlet boundary conditions.

## 2.2. Quantum Gravity.

2.2.1. Introduction. To derive the intersection exponents above, the idea [50] is to map the original random walk problem in the plane onto a random lattice with planar geometry, or, in other words, in presence of two-dimensional quantum gravity [26]. The key point is that the random walk intersection exponents on the random lattice are related to those in the plane. Furthermore, the RW intersection problem can be solved in quantum gravity. Thus, the exponents  $\gamma_L$  (eq. (2.6)) and  $\tilde{\gamma}_L$  (eq. (2.7)) in the standard complex plane or half-plane are derived from this mapping to a random lattice or Riemann surface with fluctuating metric.

Random surfaces, in relation to string theory [82], have been the subject and source of important developments in statistical mechanics in two dimensions. In particular, the discretization of string models led to the consideration of abstract random lattices  $G$ , the connectivity fluctuations of which represent those of the metric, i.e., pure 2D quantum gravity [83].

2.2.2. KPZ Relation. One can put any 2D statistical model (e.g., Ising model [25], self-avoiding walks [28]) on the random planar graph  $G$ , thereby obtaining a new critical behavior, corresponding to the confluence of the criticality of the finite random surface  $G$  with the critical point of the original model. The critical system "dressed by gravity" has a larger symmetry under diffeomorphisms. This allowed Knizhnik, Polyakov, and Zamolodchikov (KPZ) [26] (see also [27]) to establish the existence of a fundamental relation between the conformal dimensions  $\Delta^{(0)}$  of scaling operators in the plane and those in presence of gravity,  $\Delta$ :

$$(2.9) \quad \Delta^{(0)} = \Delta - \frac{c}{12} = \frac{\Delta}{1};$$

where  $\Delta$ , the string susceptibility exponent, is related to the central charge of the statistical model in the plane:

$$(2.10) \quad c = 1 - 6\Delta^2 = (1 - \Delta); \quad \Delta \geq 0;$$

The same relation applies between conformal weights  $\tilde{\Delta}^{(0)}$  in the half-plane  $H$  and  $\tilde{\Delta}$  near the boundary of a disk with fluctuating metric:

$$(2.11) \quad \tilde{\Delta}^{(0)} = \tilde{\Delta} - \frac{c}{24} = \frac{\tilde{\Delta}}{1};$$

For a minimal model of the series (2.8),  $\gamma = 1-m$ , and the conformal weights in the plane  $C$  or half-plane  $H$  are  $h_{p;q}^{(0)} = h_{p;q}^{(c)}$ :

2.2.3. Random Walks in Quantum Gravity. Let us now consider as a statistical model random walks on a random graph. We know [40] that the central charge  $c = 0$ , whence  $m = 2$ ,  $\gamma = 1=2$ : Thus the KPZ relation becomes

$$(2.12) \quad \gamma^{(0)} = \gamma_{m=2} = \frac{1}{3} (1 + 2\gamma) = \gamma;$$

which has exactly the same analytical form as equation (2.7)! Thus, from this KPZ equation one infers that the conjectured planar Brownian intersection exponents in the complex plane  $C$  (2.6) and in  $H$  (2.7) must be equivalent to the following Brownian intersection exponents in quantum gravity:

$$(2.13) \quad \chi_L = \frac{1}{2} \chi_L + \frac{1}{2} \chi;$$

$$(2.14) \quad \tilde{\chi}_L = \chi_L;$$

Let us now sketch the derivation of these quantum gravity exponents [50]. A more detailed proof is given in appendix A.

2.3. Random Walks on a Random Lattice.

2.3.1. Random Graph Partition Function. Consider the set of planar random graphs  $G$ , built up with, e.g., trivalent vertices tied together in a random way. The topology is fixed here to be that of a sphere ( $S$ ) or a disk ( $D$ ). The partition function is defined as

$$(2.15) \quad Z(\gamma; c) = \sum_{G(c)} \frac{1}{S(G)} e^{-\gamma \sum_j j};$$

where  $\chi$  denotes the fixed Euler characteristic of graph  $G$ ;  $\chi = 2$  ( $S$ );  $1$  ( $D$ );  $\sum_j j$  is the number of vertices of  $G$ ,  $S(G)$  its symmetry factor. The partition sum converges for all values of the parameter  $\gamma$  larger than some critical  $\gamma_c$ . At  $\gamma = \gamma_c$  a singularity appears due to the presence of infinite graphs in (2.15)

$$(2.16) \quad Z(\gamma; c) = (c - \gamma)^{2 - \chi_{str}(\gamma)};$$

where  $\chi_{str}(\gamma)$  is the string susceptibility exponent, which depends on the topology of  $G$  through the Euler characteristic. For pure gravity as described in (2.15), the embedding dimension  $d = 0$  coincides with the central charge  $c = 0$ ; and [84]

$$(2.17) \quad \chi_{str}(\gamma) = 2 - \frac{5}{4} \gamma; (c = 0):$$

In particular  $\chi_{str}(2) = \frac{1}{2}$  for the spherical topology, and  $\chi_{str}(1) = \frac{3}{4}$ . The string susceptibility exponent appearing in KPZ formula (2.9) is the planar one

$$\chi_{str}(\gamma) = \chi_{str}(\gamma = 2):$$

A particular partition function will play an important role later, that of the doubly punctured sphere. It is defined as

$$(2.18) \quad Z[\text{doubly punctured sphere}] = \frac{g^2}{g^2} Z(\gamma; c=2) = \sum_{G(c=2)} \frac{1}{S(G)} \sum_j j^2 e^{-\gamma \sum_j j};$$

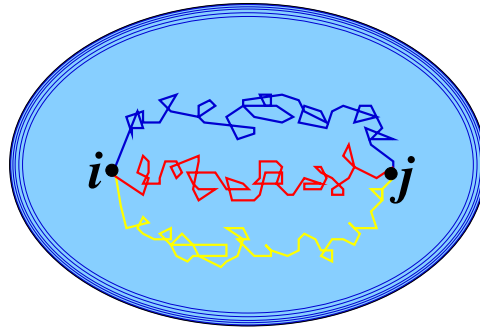


Figure 3.  $L = 3$  mutually-avoiding random walks on a random sphere.

Owing to (2.16) it scales as

$$(2.19) \quad Z[\bullet \circlearrowleft \bullet] \sim (\frac{c}{\epsilon})^{\text{str}(\epsilon=2)};$$

2.3.2. Random Walk Partition Functions. Let us now consider a set of  $L$  random walks  $B = \{B_{ij}^{(l)}; l = 1, \dots, L\}$  on the random graph  $G$  with the special constraint that they start at the same vertex  $i \in G$ ; end at the same vertex  $j \in G$ , and have no intersections in between. We introduce the  $L$  walk partition function on the random lattice [50]:

$$(2.20) \quad Z_L(\epsilon; z) = \sum_{\text{planar } G} \frac{1}{S(G)} e^{-\epsilon \beta_j} \sum_{i, j \in G} \sum_{\substack{B_{ij}^{(l)} \\ l=1, \dots, L}} z^{\beta_j};$$

where a fugacity  $z$  is associated with the total number  $\beta_j = \sum_{l=1}^L \beta_{ij}^{(l)}$  of vertices visited by the walks (Fig. 3).

2.3.3. RW Boundary Partition Functions. We generalize this to the boundary case where  $G$  now has the topology of a disk and where the random walks connect two sites  $i$  and  $j$  on the boundary  $\partial G$ :

$$(2.21) \quad Z_L(\epsilon; \epsilon^0; z) = \sum_{\text{disk } G} e^{-\epsilon \tilde{\beta}_j} \sum_{i, j \in \partial G} \sum_{\substack{B_{ij}^{(l)} \\ l=1, \dots, L}} z^{\beta_j};$$

where  $e^{-\tilde{\beta}_j}$  is the fugacity associated with the boundary's length (Fig. 4). A gain, a particular boundary partition function will play a central role, that of the disk with two punctures on the boundary. It corresponds to the  $L = 0$  case of the  $Z_L$ 's, and is defined as

$$(2.22) \quad Z(\bullet \circlearrowleft \bullet) = Z_{L=0}(\epsilon; \epsilon^0) = \sum_{\text{disk } G} e^{-\epsilon \tilde{\beta}_j} \sum_{i, j \in \partial G} \epsilon_j^2;$$

The double grand canonical partition functions (2.20) and (2.21) associated with non-intersecting RW's on a random lattice can be calculated exactly [50]. The detailed calculations are given in appendix A. One in particular uses an equivalent representation of the random walks by their forward (or backward) trees, which are

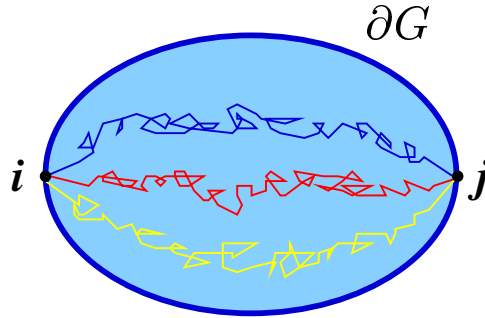


Figure 4.  $L = 3$  mutually-avoiding random walks traversing a random disk.

trees uniformly spanning the sets of visited sites. This turns the RW 's problem into the solvable one of random trees on random graphs (see, e.g., [28]).

2.3.4. Scaling Laws for Partition Functions. The critical behavior of  $Z_L$  is characterized by the existence of two critical values of the parameters,  $c_c$  where the random lattice size diverges, and  $z_c$  where the set of sites visited by the random walks also diverges. The critical behavior of  $Z_L(\gamma; z)$  is then obtained by taking the double scaling limit  $\gamma \rightarrow c_c^+$  (infinite random surface) and  $z \rightarrow z_c$  (infinite RW 's), such that the average lattice and RW 's sizes respectively scale as

$$(2.23) \quad \mathbb{E} j \sim (\gamma - c_c)^{-1}; \mathbb{E} j \sim (z_c - z)^{-1};$$

The analysis of the singular behavior in terms of conformal weights is performed by using finite-size scaling (FSS) [28], where one must have (see appendix A)

$$\mathbb{E} j \sim \mathbb{E} j^{\frac{1}{2}}(\gamma) z_c - z \sim (\gamma - c_c)^{1-2};$$

One obtains in this regime the global scaling of the full partition function [50]:

$$(2.24) \quad Z_L(\gamma; z) \sim (\gamma - c_c)^L \mathbb{E} j^L;$$

The interpretation of partition function  $Z_L$  (2.20) is the following: It represents a random surface with two punctures where two conformal operators, of conformal weight  $\Delta_L$ , are located (here two vertices of  $L$  non-intersecting RW 's), and, using a graphical notation, scales as

$$(2.25) \quad Z_L = Z[\odot \odot] \sim \mathbb{E} j^{2-L};$$

where the partition function of the doubly punctured surface is the second derivative of  $Z(\gamma; \Delta = 2)$  (2.18):

$$(2.26) \quad Z[\odot \odot] = \frac{\partial^2}{\partial \Delta^2} Z(\gamma; \Delta = 2);$$

From (2.19) we find

$$(2.27) \quad Z_L \sim \mathbb{E} j^{\text{str}(\Delta = 2) - 2 - L};$$

Comparing the latter to (2.24) yields

$$(2.28) \quad 2 - L - \text{str}(\Delta = 2) = L;$$

where we recall that  $\text{str}(\gamma = 2) = \gamma - 1 = 2$ . We thus get the first previously-announced result

$$(2.29) \quad L = \frac{1}{2} L \frac{1}{2} :$$

2.3.5. Boundary Scaling. For the boundary partition function  $Z_L$  (2.21) a similar analysis can be performed near the triple critical point  $(c; \tilde{c}; z_c)$ , where the boundary length also diverges. One finds that the average boundary length  $\langle \ell_G \rangle$  must scale with the area  $|G|$  in a natural way (see appendix A)

$$(2.30) \quad \langle \ell_G \rangle \sim |G|^{1/2} :$$

The boundary partition function  $Z_L$  corresponds to two boundary operators of conformal weights  $\tilde{L}$ ; integrated over  $\partial G$ ; on a random surface with the topology of a disk, or in terms of scaling behavior

$$(2.31) \quad Z_L \sim Z(\text{disk with two punctures}) \sim |G|^{2\tilde{L}} ;$$

using the graphical representation of the two-puncture partition function (2.22).

2.3.6. Bulk-Boundary Relation. From the exact calculation of the boundary partition function (2.21), and of the boundary puncture disk one (2.22), one gets the further scaling equivalence to the bulk partition function (2.20):

$$(2.32) \quad Z_L \sim \frac{Z_L}{Z(\text{disk with two punctures})} ;$$

where the equivalence holds true in terms of scaling behavior. It intuitively means that carving away from the  $L$ -walk boundary partition function the contribution of one connected domain with two boundary punctures brings us back to the  $L$ -walk bulk partition function. This fundamental scaling equivalence is explained in appendix A. Comparing eqs. (2.31), (2.32), and (2.27), and using the FSS (2.30) gives

$$(2.33) \quad \tilde{L} = 2L - \text{str}(\gamma = 2) :$$

This relation between bulk and Dirichlet boundary behaviors in quantum gravity is quite general and will also play a fundamental role in the study of other critical systems in two dimensions. It is studied in full detail in appendices B and C. From (2.28) we finally find the second announced result:

$$(2.34) \quad \tilde{L} = L :$$

Applying the quadratic KPZ relation (2.12) to  $L$  (2.29) and  $\tilde{L}$  (2.34) above finally yields the values in the plane  $\mathbb{C}$  or halfplane  $\mathbb{H}$

$$\begin{aligned} L &= U_{\gamma=2}(L) = \frac{1}{24} (4L^2 - 1) \\ 2\tilde{L} &= U_{\gamma=2}(\tilde{L}) = \frac{1}{3} L (1 + 2L) ; \end{aligned}$$

as previously announced.

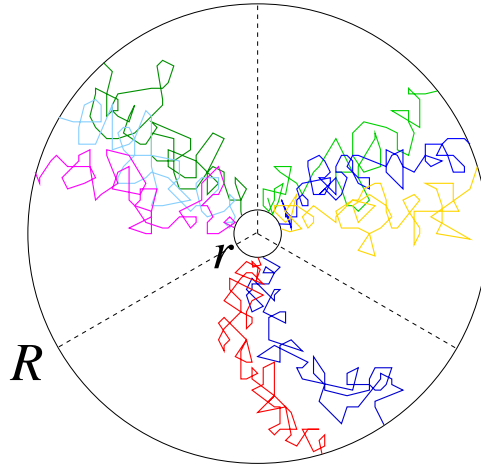


Figure 5. Packets of  $n_1 = 3; n_2 = 3$ , and  $n_3 = 2$  independent planar random walks, in a mutually-avoiding star configuration, and crossing an annulus from  $r$  to  $R$ .

2.4. Non-Intersections of Packets of Walks.

2.4.1. Definition. Consider configurations made of  $L$  mutually-avoiding bunches  $l = 1; \dots; L$ , each of them made of  $n_l$  independent RW's [48]. All of them start at neighboring points (Fig. 5). The probability of non-intersection of the  $L$  packets up to time  $t$  scales as

$$(2.35) \quad P_{n_1; \dots; n_L}(t) \sim t^{-(n_1 + \dots + n_L)}$$

and near a Dirichlet boundary (Fig. 6)

$$(2.36) \quad \tilde{P}_{n_1; \dots; n_L}(t) \sim t^{-\tilde{n}_1 - \dots - \tilde{n}_L}$$

The original case of  $L$  mutually-avoiding RW's corresponds to  $n_1 = \dots = n_L = 1$ . The probability for the same  $L$  Brownian path packets to cross the annulus  $D(r; R)$  in  $C$  (Fig. 5) scales accordingly as

$$(2.37) \quad P_{n_1; \dots; n_L}(r) \sim (r=R)^{-2(n_1 + \dots + n_L)}$$

and, near a Dirichlet boundary in  $H$  (Fig. 6), as

$$(2.38) \quad \tilde{P}_{n_1; \dots; n_L}(r) \sim (r=R)^{-2\tilde{n}_1 - \dots - 2\tilde{n}_L}$$

The generalizations of former exponents  $n_l$ , as well as  $\tilde{n}_l$ , describing these  $L$  packets can be written as conformal weights

$$(n_1; \dots; n_L) \equiv \sum_{l=1}^L n_l \epsilon_l^{(0)} \epsilon_l g$$

in the plane  $C$ , and

$$2\tilde{n}_1; \dots; 2\tilde{n}_L \equiv \sum_{l=1}^L \tilde{n}_l \epsilon_l^{(0)} \epsilon_l g$$

in the halfplane  $H$ . They can be calculated from quantum gravity, via their counterparts  $\epsilon_l g$  and  $\tilde{\epsilon}_l g$ . The details are given in appendix A. We here sketch the main steps.

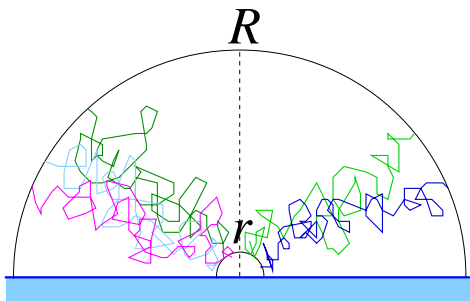


Figure 6. Packets of  $n_1 = 3$ , and  $n_2 = 2$  independent random walks, in a mutually-avoiding star configuration, and crossing the halfannulus from  $r$  to  $R$  in the halfplane  $H$ .

2.4.2. Boundary Case. One introduces the analogue  $Z^{fn_1; \quad Lg;n}$  of partition function (2.21) for the  $L$  packets of walks. In presence of gravity each bunch contributes its own normalized boundary partition function as a factor, and this yields a natural generalization of the scaling equation (2.32) (see appendix A)

$$(2.39) \quad \frac{Z^{fn_1; \quad Lg;n}}{Z(\bullet \circlearrowleft \bullet)} \stackrel{X^L}{=} \prod_{l=1}^L ? \frac{Z^{(n_l)}}{Z(\bullet \circlearrowleft \bullet)} ;$$

where the star product is to be understood as a scaling equivalence. Given the definition of boundary conformal weights (see (2.31)), the normalized left-hand fraction is to be identified with  $j^G j^{2\tilde{fn}_1; \quad Lg;n}$ , while each normalized factor  $Z^{(n_l)} = Z(\bullet \circlearrowleft \bullet)$  is to be identified with  $j^G j^{2\tilde{(n_l)}}$ . Here  $\tilde{(n)}$  is the boundary dimension of a single packet of  $n$  mutually transparent walks on the random surface. The factorization property (2.39) therefore immediately implies the additivity of boundary conformal dimensions in presence of gravity

$$(2.40) \quad \tilde{fn}_1; \quad Lg;n \stackrel{X^L}{=} \prod_{l=1}^L \tilde{(n_l)} :$$

In the standard plane  $C$ , a packet of  $n$  independent random walks has a trivial boundary conformal dimension  $\tilde{(0)}(n) = n \tilde{(0)}(1) = n$ ; since for a single walk  $\tilde{(0)}(1) = 1$ ; as can be seen using the Green function formalism. We therefore know  $\tilde{(n)}$  exactly, since it suffices to take the positive inverse of the KPZ map (2.12) to get

$$(2.41) \quad \tilde{(n)} = U_{l=1}^1 \tilde{(n)} = \frac{1}{4} \left( \frac{p}{24n+1} - 1 \right) :$$

One therefore finds:

$$(2.42) \quad \tilde{fn}_1; \quad Lg;n \stackrel{X^L}{=} \prod_{l=1}^L U_{l=1}^1 \tilde{(n_l)} = \prod_{l=1}^L \frac{1}{4} \left( \frac{p}{24n_l+1} - 1 \right) :$$

2.4.3. Relation to the Bulk. One similarly defines for  $L$  mutually-avoiding packets of  $n_1; \quad L$  independent walks the generalization  $Z^{fn_1; \quad Lg;n}$  of the bulk partition function (2.20) for  $L$  walks on a random sphere. One then establishes on



a random surface the identification, similar to (2.32), of this bulk partition function with the normalized boundary one (see appendix A):

$$(2.43) \quad Z_{\text{fn}_1; \text{Lg}; n} = \frac{Z_{\text{fn}_1; \text{Lg}; n}}{Z(\bullet \circlearrowleft)}$$

By definition of quantum conformal weights (appendix A), the left-hand term of (2.43) scales as  $\mathfrak{J} j^{2 \text{fn}_1; \text{Lg}^{\text{str}(\text{=2})}}$ , while the right-hand term scales, as written above, as  $\mathfrak{J} G j^{2 \sim \text{fn}_1; \text{Lg}}$ . Using the area to perimeter scaling relation (2.30), we thus get the identity existing in quantum gravity between bulk and boundary conformal weights, similar to (2.28):

$$(2.44) \quad 2 \text{fn}_1; \text{Lg}; n_{\text{str}(\text{=2})} = \sim \text{fn}_1; \text{Lg}; n$$

with  $\text{str}(\text{=2}) = \frac{1}{2}$  for pure gravity.

2.4.4. Back to the Complex Plane. In the plane, using once again the KPZ relation (2.12) for  $\sim \text{fn}_1 \text{g}$  and  $\text{fn}_1 \text{g}$ , we obtain the general results [50]

$$\begin{aligned} 2 \sim (n_1; \text{L}); n &= \sim^{(0)} \text{fn}_1; \text{Lg}; n U \sim \text{fn}_1; \text{Lg}; n \\ (n_1; \text{L}); n &= {}^{(0)} \text{fn}_1; \text{Lg}; n U ( \text{fn}_1; \text{Lg}; n ) \end{aligned}$$

where we set  $U = U_{=1=2}$ . One can naturally write, using (2.41) and (2.42)

$$(2.45) \quad 2 \sim (n_1; \text{L}); n U(x) = \frac{1}{3} x(1 + 2x)$$

$$(2.46) \quad (n_1; \text{L}); n U(x) = U \frac{1}{2} x \frac{1}{2} = \frac{1}{24} (4x^2 - 1);$$

$$(2.47) \quad x = \prod_{l=1}^{X^L} U^{-1}(n_1) = \prod_{l=1}^{X^L} \frac{1}{4} \left( \frac{1}{24n_1 + 1} - 1 \right);$$

Lawler and Werner [49] established the existence of two functions  $U$  and  $V$  satisfying the structure (2.45-2.47) by purely probabilistic means, using the geometrical conformal invariance of Brownian motions. The quantum gravity approach here explains this structure in terms of linearity of boundary quantum gravity (2.40, 2.42), and yields the explicit functions

$$(2.48) \quad U(x) = U_{=1=2}(x)$$

$$(2.49) \quad V(x) = U \frac{1}{2} x \frac{1}{2} ;$$

as KPZ maps (2.45-2.46). The same expressions for these functions has also been derived in probability theory from the equivalence to SLE<sub>6</sub> [62].

2.4.5. Particular Values and Mandelbrot's Conjecture. The first few values are:

$$\begin{aligned} \sim(n=1) &= U_{=1=2}(1) = 1 \\ \sim(n=2) &= U_{=1=2}(2) = \frac{3}{2} \\ \sim(n=3) &= U_{=1=2}(3) = \frac{1}{4} \left( \frac{1}{73} - 1 \right); \end{aligned}$$

Let us introduce the notation  $1^{(L)} = 1;1;$  for  $L$  mutually-avoiding walks in a star con guration. Then the exponent  $(2;1^{(L)})$  describing a two-sided walk and  $L$  one-sided walks, all mutually-avoiding, has the value

$$\begin{aligned} (2;1^{(L)}) &= V_{L+1} U^{-1}(1) + U^{-1}(2) = V(L + \frac{3}{2}) \\ &= \frac{1}{L + \frac{3}{2}} = \frac{1}{6} (L + 1)(L + 2); \end{aligned}$$

For  $L = 1$ ,  $(2;1) = \frac{1}{5} = 1$  correctly gives the exponent governing the escape probability of a RW from a given origin near another RW [85]. (By construction the second one indeed appears as made of two independent RW 's di using away from the origin.)

For  $L = 0$  one finds the non-trivial result

$$(2;1^{(0)}) = \frac{1}{3} = 1/3;$$

which describes the accessible points along a RW. It is formally related to the Hausdor dimension of the Brownian frontier by  $D = 2 - 2$  [86]. Thus we obtain for the dimension of the Brownian frontier [50]

$$(2.50) \quad D_{Br:fr} = 2 - 2 \frac{1}{3} = \frac{4}{3};$$

ie., the famous Mandelbrot conjecture. Notice that the accessibility of a point on a Brownian path is a statistical constraint equivalent to the non-intersection of  $L = 3/2$  paths. (The relation of this Hausdor dimension to the exponent  $3/2 = 1/3$  was actually made in December 1997, after a discussion in the Institute for Advanced Study at Princeton with M. Aizenman and R. Langlands about the meaning of half-integer indices in critical percolation exponents.) The Mandelbrot conjecture was later established in probability theory [63], using the analytic properties of the non-intersection exponents derived from the stochastic Loewner evolution  $SLE_6$  [59].

The quantum geometric structure made explicit here allows generalizations to self-avoiding walks and percolation, which we now describe.

### 3. Mixing Random & Self-Avoiding Walks

We now generalize the scaling structure obtained in the preceding section to arbitrary sets of random or self-avoiding walks interacting together [51] (see also [49, 55])

#### 3.1. General Star Con gurations.

3.1.1. Star Algebra. Consider a general copolymer  $S$  in the plane  $C$  (or in  $Z^2$ ), made of an arbitrary mixture of RW 's or Brownian paths (set  $B$ ); and SAW 's or polymers (set  $P$ ), all starting at neighboring points, and di using away, ie., in a star con guration. In the plane, any successive pair  $(A;B)$  of such paths,  $A;B \in B$  or  $P$ ; can be constrained in a speci c way: either they avoid each other ( $A \setminus B = \emptyset$ ; denoted  $A \wedge B$ ); or they are independent, ie., "transparent" and can cross each other (denoted  $A \_ B$ ) [51, 87]. This notation allows any nested interaction structure [51]; one can decide for instance that the branches  $FP \setminus 2 P g_{= 1;::;L}$  of an  $L$ -star polymer, all mutually-avoiding, further avoid a collection of Brownian

paths  $\{B_k\}_{k=1, \dots, n}$ ; all transparent to each other, which structure is represented by:

$$(3.1) \quad S = \bigwedge_{k=1}^L P \setminus \bigwedge_{k=1}^n B_k :$$

A priori in 2D the order of the branches of the star polymer matters and is intrinsic to the  $(\wedge; \setminus)$  notation.

3.1.2. Conformal Operators and Scaling Dimensions. To each specific star copolymer center  $S$  is attached a local conformal scaling operator  $\phi_S$ , which represents the presence of the star vertex, with a scaling dimension  $x(S)$  [18, 19, 51]. When the star is constrained to stay in a half-plane  $H$ , with Dirichlet boundary conditions, and its core placed near the boundary  $\partial H$ , a new boundary scaling operator  $\tilde{\phi}_S$  appears, with a boundary scaling dimension  $\varkappa(S)$  [18, 19]. To obtain proper scaling, one has to construct the partition functions of Brownian paths and polymers having the same mean size  $R$  [18]. These partition functions then scale as powers of  $R$ , with an exponent which mixes the scaling dimension of the star core ( $x(S)$  or  $\varkappa(S)$ ), with those of star dangling ends.

3.1.3. Partition Functions. It is convenient to define for each star  $S$  a grand canonical partition function [18, 19, 87], with fugacities  $z$  and  $z^0$  for the total lengths  $\beta$  and  $\beta^0$  of RW or SAW paths:

$$(3.2) \quad Z_R(S) = \sum_{B;P \in S} z^{\beta} z^{0\beta^0} 1_R(S);$$

where one sums over all RW and SAW configurations respecting the mutual-avoidance constraints built in star  $S$  (as in (3.1)), further constrained by the indicatrix  $1_R(S)$  to stay within a disk of radius  $R$  centered on the star. At the critical values  $z_c = z_B^{-1}; z_c^0 = z_P^{-1}$ ; where  $z_B$  is the coordination number of the underlying lattice for the RW 's, and  $z_P$  the effective one for the SAW 's,  $Z_R$  has a power law decay [18]

$$(3.3) \quad Z_R(S) \sim R^{-x(S) - \varkappa} :$$

Here  $x(S)$  is the scaling dimension of the operator  $\phi_S$ , associated only with the singularity occurring at the center of the star where all critical paths meet, while  $\varkappa$  is the contribution of the independent dangling ends. It reads  $\varkappa = k_B k_{x_{B;1}} + k_P k_{x_{P;1}} - 2V$ ; where  $k_B$  and  $k_P$  are respectively the total numbers of Brownian or polymer paths of the star;  $x_{B;1}$  or  $x_{P;1}$  are the scaling dimensions of the extremities of a single RW ( $x_{B;1} = 0$ ) or SAW ( $x_{P;1} = \frac{5}{48}$ ) [18, 15]. The last term in (3.3), in which  $V = k_B + k_P$  is the number of dangling vertices, corresponds to the integration over extremity positions in the disk of radius  $R$ .

When the star is constrained to stay in a half-plane with its core placed near the boundary, its partition function scales as [18, 40]

$$(3.4) \quad \tilde{Z}_R(S) \sim R^{-\varkappa(S) - \varkappa} ;$$

where  $\varkappa(S)$  is the boundary scaling dimension,  $x$  staying the same for star extremities in the bulk.

### 3.2. Quantum Gravity for SAW's & RW's.

3.2.1. Scaling Dimensions and Conformal Weights. Any scaling dimension  $x$  in the plane is twice the conformal weight  $\tilde{x}^{(0)}$  of the corresponding operator, while near a boundary they are identical [11, 13]

$$(3.5) \quad x = 2 \tilde{x}^{(0)}; \quad \tilde{x} = \tilde{x}^{(0)};$$

3.2.2. KPZ map. As in section 2, the idea is to use the representation where the RW's or SAW's are on a 2D random lattice, or a random Riemann surface, i.e., in the presence of 2D quantum gravity (QG) [26]. The general relation (2.12) for Brownian paths depends only on the central charge  $c = 0$ , which also applies to self-avoiding walks or polymers. For a critical system with central charge  $c = 0$ , the two universal functions:

$$(3.6) \quad U(x) = U_{\frac{1}{2}}(x) = \frac{1}{3}x(1+2x); \quad V(x) = \frac{1}{24}(4x^2 - 1);$$

with  $\tilde{V}(x) := U_{\frac{1}{2}}(x) - \frac{1}{2}$ , generate all the scaling exponents. They transform the conformal weights in bulk quantum gravity, or in boundary QG,  $\tilde{x}$ , into the plane and half-plane ones (3.5):

$$(3.7) \quad \tilde{x}^{(0)} = U^{-1}(\tilde{x}); \quad \tilde{x}^{(0)} = U^{-1}(\tilde{x}); \quad x^{(0)} = V^{-1}(\tilde{x});$$

3.2.3. Composition Rules. Consider two stars  $A; B$  joined at their centers, and in a random mutually-avoiding star-configuration  $A \wedge B$ . Each star is made of an arbitrary collection of Brownian paths and self-avoiding paths with arbitrary interactions of type (3.1). Their respective bulk partition functions (3.2), (3.3), or boundary partition functions (3.4) have associated planar scaling exponents  $x(A); x(B)$ ; or planar boundary exponents  $\tilde{x}(A); \tilde{x}(B)$ . The corresponding scaling dimensions in quantum gravity are then, for instance for  $A$ :

$$(3.8) \quad \tilde{x}(A) = U^{-1}(\tilde{x}(A)); \quad x(A) = U^{-1}\left(\frac{1}{2}\tilde{x}(A)\right);$$

where  $U^{-1}(x)$  is the positive inverse of the KPZ map  $U$

$$(3.9) \quad U^{-1}(x) = \frac{1}{4} \left( \sqrt{24x + 1} - 1 \right);$$

The key properties are given by the following propositions:

In  $c = 0$  quantum gravity the boundary and bulk scaling dimensions of a given random path set are related by:

$$(3.10) \quad \tilde{x}(A) = 2x(A) \quad \text{str}(c=0) = 2x(A) + \frac{1}{2};$$

This generalizes the relation (2.33) for non-intersecting Brownian paths.

In quantum gravity the boundary scaling dimensions of two mutually-avoiding sets is the sum of their respective boundary scaling dimensions:

$$(3.11) \quad \tilde{x}(A \wedge B) = \tilde{x}(A) + \tilde{x}(B);$$

It generalizes identity (2.40) for mutually-avoiding packets of Brownian paths. The boundary-bulk relation (3.10) and the fusion rule (3.11) come from simple convolution properties of partition functions on a random lattice [50, 51]. They are studied in detail in appendices A and C.

The planar scaling exponents  $x(A \wedge B)$  in  $C$ , and  $\varkappa(A \wedge B)$  in  $H$  of the two mutually-avoiding stars  $A \wedge B$  are then given by the KPZ map (3.7) in terms of (3.11)

$$(3.12) \quad x(A \wedge B) = \frac{h_i}{2V} \tilde{\sim}(A \wedge B) = 2V \frac{h_i}{h_i} \tilde{\sim}(A) + \frac{h_i}{h_i} \tilde{\sim}(B)$$

$$(3.13) \quad \varkappa(A \wedge B) = U \tilde{\sim}(A \wedge B) = U \tilde{\sim}(A) + \tilde{\sim}(B) :$$

Owing to (3.8), these scaling exponents thus obey the star algebra [50, 51]

$$(3.14) \quad x(A \wedge B) = 2V U^{-1}(\varkappa(A)) + U^{-1}(\varkappa(B))$$

$$(3.15) \quad \varkappa(A \wedge B) = U U^{-1}(\varkappa(A)) + U^{-1}(\varkappa(B)) :$$

On a random surface,  $U^{-1}(\varkappa)$  is the boundary conformal weight corresponding to the value  $\varkappa$  in the upper-half plane  $H$ , and the sum of  $U^{-1}$  functions in eq. (3.14) linearly represents the mutually-avoiding juxtaposition  $A \wedge B$  of two sets of random paths near the random frontier, i.e., the operator product of two "boundary operators" on the random surface. The latter sum is mapped by the functions  $U, V$ , into the scaling dimensions in  $H$  or  $C$  [51].

These fusion rules (3.11), (3.14) and (3.15), which mix bulk and boundary exponents are already apparent in the derivation of non-intersection exponents for Brownian paths given in section 2 and appendix A. They also apply to the  $O(N)$  model, as shown in appendix B, and are established in all generality in appendix C. They can also be seen as recurrence "cascade" relations in  $C$  between successive conformal Riemann maps of the frontiers of mutually-avoiding paths onto the half-plane boundary  $@H$ , as in the original work [49] on Brownian paths.

When the random sets  $A$  and  $B$  are independent and can overlap, their scaling dimensions in the standard plane or halfplane are additive by trivial factorization of partition functions or probabilities [51]

$$(3.16) \quad x(A \_ B) = x(A) + x(B); \quad \varkappa(A \_ B) = \varkappa(A) + \varkappa(B) :$$

This additivity no longer applies in quantum gravity, since overlapping paths get coupled by the fluctuations of the metric, and are no longer independent. In contrast, it is replaced by the additivity rule (3.11) for mutually-avoiding paths (see appendix C for a thorough discussion of this additivity property).

It is clear at this stage that the set of equations above is complete. It allows for the calculation of any conformal dimensions associated with a star structure  $S$  of the most general type, as in (3.1), involving  $(\wedge; \_)$  operations separated by nested parentheses [51]. Here follow some examples.

3.3. RW-SAW Exponents. The single extremity scaling dimensions are for a RW or a SAW near a Dirichlet boundary  $@H$  [16]

$$(3.17) \quad \varkappa_B(1) = \tilde{\sim}_B^{(0)}(1) = 1; \quad \varkappa_P(1) = \tilde{\sim}_P^{(0)}(1) = \frac{5}{8};$$

or in quantum gravity

$$(3.18) \quad \tilde{\sim}_B(1) = U^{-1}(1) = 1; \quad \tilde{\sim}_P(1) = U^{-1}\left(\frac{5}{8}\right) = \frac{3}{4}:$$

Because of the star algebra described above these are the only numerical seeds, i.e., generators, we need.

Consider packets of  $n$  copies of transparent RW 's or  $m$  transparent SAW 's. Their boundary conformal dimensions in  $H$  are respectively, by using (3.16) and (3.17),  $\tilde{\gamma}_B^{(0)}(n) = n$  and  $\tilde{\gamma}_P^{(0)}(m) = \frac{5}{8}m$ . The inverse mapping to the random surface yields the quantum gravity conformal weights  $\tilde{\gamma}_B(n) = U^{-1}(n)$  and  $\tilde{\gamma}_P(m) = U^{-1}(\frac{5}{8}m)$ . The star made of  $L$  packets  $\setminus 2 \text{ fl}; \dots; Lg$ , each of them made of  $n$  transparent RW 's and of  $m$  transparent SAW 's, with the  $L$  packets mutually-avoiding, has planar scaling dimensions

$$(3.19) \quad \tilde{\gamma}^{(0)}(fn, m, g) = U^{-1}(\tilde{\gamma}(fn, m, g))$$

$$(3.20) \quad \tilde{\gamma}^{(0)}(fn, m, g) = V^{-1}(\tilde{\gamma}(fn, m, g));$$

$$(3.21) \quad \begin{aligned} \tilde{\gamma}(fn, m, g) &= \sum_{\nu=1}^X L U^{-1}(n + \frac{5}{8}m, \nu) \\ &= \sum_{\nu=1}^X L \frac{1}{4} \frac{\Gamma(24n + \frac{5}{8}m + 1) \Gamma(1 - \nu)}{\Gamma(24n + \frac{5}{8}m + 1 - \nu)} \end{aligned}$$

Take, as an example, a copolymer star  $S_{L, L^0}$  made of  $L$  RW 's and  $L^0$  SAW 's, all mutually-avoiding ( $\delta = 1$ ;  $\nu = 0$ ;  $\delta^0 = 1$ ;  $\nu^0 = 0$ ;  $m = 0$ ;  $m^0 = 1$ ). In quantum gravity the linear boundary conformal weight (3.21) is simply  $\tilde{\gamma}(S_{L, L^0}) = L + \frac{3}{4}L^0$ . By the  $U$  and  $V$  maps, it gives the scaling dimensions in  $\mathcal{H}$  and  $\mathcal{C}$

$$\begin{aligned} \tilde{\gamma}^{(0)}(S_{L, L^0}) &= \frac{1}{3} L + \frac{3}{4} L^0 \quad 1 + 2L + \frac{3}{2} L^0 \\ &\quad \# \\ \tilde{\gamma}^{(0)}(S_{L, L^0}) &= \frac{1}{24} (4L + \frac{3}{4} L^0)^2 - 1; \end{aligned}$$

recovering for  $L = 0$  the SAW star-exponents [19] and for  $L^0 = 0$  the RW non-intersection exponents in  $\mathcal{H}$  and  $\mathcal{C}$  obtained in section 2

$$\begin{aligned} 2\tilde{\gamma}_L &= \tilde{\gamma}^{(0)}(S_{L, L^0=0}) = \frac{1}{3} L (1 + 2L) \\ \tilde{\gamma}_L &= \tilde{\gamma}^{(0)}(S_{L, L^0=0}) = \frac{1}{24} (4L^2 - 1); \end{aligned}$$

This encompasses all previously known exponents for RW 's and SAW 's [40, 18, 19]. In particular we arrive at a striking scaling equivalence: a self-avoiding walk is exactly equivalent to  $5=8$  of a Brownian motion [51]. Similar results were later obtained in probability theory, based on the general structure of "completely conformally-invariant processes", which correspond exactly to  $c = 0$  central charge conformal field theories [55, 62]. The construction of the scaling limit of SAW 's still eludes a rigorous approach, though it is predicted to correspond to "stochastic Loewner evolution" SLE with  $\kappa = 8=3$ , equivalent to a Coulomb gas with  $g = 4 = 3=2$  (see section 9 below).

4. Harmonic Measure of Brownian and Self-Avoiding Paths

4.1. Harmonic Measure and Potential.

4.1.1. Introduction. The harmonic measure, i.e., the diffusion or electrostatic potential field near an equipotential fractal boundary [88], or, equivalently, the electric charge appearing on the frontier of a perfectly conducting fractal, possesses a self-similarity property, which is reflected in a multifractal behavior. Cates and Witten [38] considered the case of the Laplacian diffusion field near a simple random walk, or near a self-avoiding walk. The associated exponents can be recast as those of star copolymers made of a bunch of independent RW's diffusing away from a generic point of the absorber. The exact solution to this problem in two dimensions is as follows [51]. From a mathematical point of view, it can also be derived from the results of refs [49, 55, 62, 63] taken altogether.

4.1.2. Harmonic Measure. Consider a two-dimensional very large "absorber"  $S$ . One defines the harmonic measure  $H(w)$  as the probability that a random walker launched from infinity, first hits the outer "hull's frontier" or accessible frontier  $F(S)$  at point  $w \in F(S)$ . For a given point  $w \in F$ , let  $B(w; a)$  be the ball (i.e., disk) of radius  $a$  centered at  $w$ . Then  $H(F \setminus B(w; a))$  is the total harmonic measure of the points of  $F$  inside the ball  $B(w; a)$ .

4.1.3. Potential Theory. One can also consider potential theory near the same fractal boundary, now charged. One assumes the absorber to be perfectly conducting, and introduces the harmonic potential  $H(z)$  at an exterior point  $z \in C$ , with Dirichlet boundary conditions  $H(w \in F) = 0$  on the outer (simply connected) frontier  $F$ , and  $H(w) = 1$  on a circle "at 1", i.e., of a large radius scaling like the average size  $R$  of  $F$ . As is well-known from a theorem due to Kakutani [89],  $H(z)$  is identical to the probability that a Brownian path started at  $z$  escapes to  $\infty$  without having hit  $F$ . The harmonic measure  $H(F \setminus B(w; a))$  defined above then also appears as the integral of the Laplacian of  $H$  in the disk  $B(w; a)$ , i.e., the boundary charge in that disk.

4.1.4. Multifractal Local Behavior. The multifractal formalism [30, 31, 32, 33] further involves characterizing subsets  $F'$  of sites of the frontier  $F$  by a Holder exponent  $\alpha$ ; such that the  $H$ -measure of the frontier points in the ball  $B(w; a)$  of radius  $a$  centered at  $w \in F'$  scales as

$$(4.1) \quad H(F' \setminus B(w; a)) \sim a^{-\alpha} \quad (\alpha = R^{-\alpha}) :$$

The Hausdorff or "fractal dimension"  $f(\alpha)$  of the set  $F'$  is such that

$$(4.2) \quad \text{Card} F' \cap B(w; a) \sim a^{f(\alpha)} :$$

Then the local behavior of the potential near point  $w \in F'$ ,

$$(4.3) \quad H(z \in B(w; r)) \sim r^{-\alpha} ; r = |z - w| ;$$

scales with the same  $\alpha$ -exponent as the harmonic measure (4.1) around point  $w \in F'$ ; and  $f(\alpha) = \dim F'$  thus appears as the Hausdorff dimension of boundary points inducing the local behavior (4.3).

4.1.5. Harmonic Moments. One then considers a covering of  $F'$  by balls  $B(w; a)$  of radius  $a$ , and centered at points  $w$  forming a discrete subset  $F' = \{w_i\}$  of  $F'$ . We are

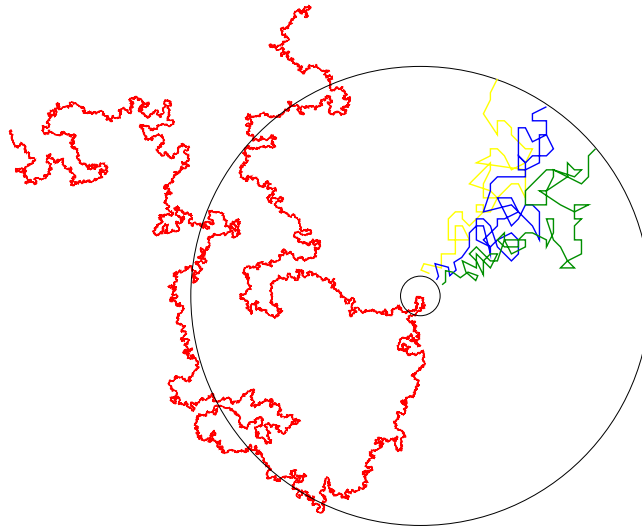


Figure 7. Representation of moments (4.4) by a packets of  $n$  independent Brownian paths di using away of a SAW , from short distance  $a$  to large distance  $R$  .

interested in the moments of  $H^*$  , averaged over all realizations of RW 's and of  $S$

$$(4.4) \quad Z_n = \sum_{w \in F, a} H^n (F \setminus B(w;a)) ;$$

where  $n$  is, a priori, a real number. For very large absorbers  $S$  and frontiers  $F(S)$  of average size  $R$  ; one expects these moments to scale as

$$(4.5) \quad Z_n \sim (a=R)^{D(n)} ;$$

where the radius  $a$  serves as a microscopic cut-off, reminiscent of the lattice structure, and where the multifractal scaling exponents  $D(n)$  encode generalized dimensions

$$(4.6) \quad D(n) = \frac{D(n)}{n-1} ;$$

which vary in a non-linear way with  $n$  [30, 31, 32, 33]. Several a priori results are known.  $D(0)$  is the Hausdorff dimension of the accessible frontier of the fractal. By construction,  $H$  is a normalized probability measure, so that  $D(1) = 0$ : Makarov's theorem [90], here applied to the Hölder regular curve describing the frontier [91], gives the so-called information dimension  $D^0(1) = D(1) = 1$ .

The multifractal spectrum  $f(\alpha)$  appearing in (4.2) is given by the symmetric Legendre transform of  $D(n)$ :

$$(4.7) \quad \alpha = \frac{d}{dn} D(n); \quad D(n) + f(\alpha) = n; \quad n = \frac{df}{d\alpha}(\alpha) ;$$

Because of the statistical ensemble average (4.4), values of  $f(\alpha)$  can become negative for some domains of  $\alpha$  [38]. (The existence of the harmonic multifractal spectrum  $f(\alpha)$  for a Brownian path has been rigorously established in ref. [39].)



4.2. Multifractal Exponents.

4.2.1. Representation by Random Walks. By the very definition of the measure,  $n$  independent RW's starting away from the absorber give a geometric representation of the  $n^{\text{th}}$  moment  $H^n$ ; for  $n$  integer, and convexity arguments give the complete continuation to real values (Fig. 7).

When the absorber is a RW or a SAW of size  $R$ ; the site average of its moments  $H^n$  is represented by a copolymer star partition function  $Z_R(S^n)$  of the type (3.2), where we have introduced the short-hand notation  $S^n := S(B)^n$  for describing the copolymer star made by the absorber  $S$  hit by the bunch  $(B)^n$  at the apex only [38, 51]. More precisely, the sum (4.4) is normalized in such a way that

$$(4.8) \quad Z_{n=1} = \sum_{w \in F=a} H(F \setminus B(w;a)) = 1;$$

since  $H$  is a (first hit) probability. The correct normalization is therefore:

$$(4.9) \quad H^n(w) = Z_R(S^n) = Z_R(S^1);$$

Because of the scaling (3.3), we have

$$(4.10) \quad H^n(w) = (a=R)^{x(S^n) - x(S^1)};$$

The normalizing star partition function  $Z_R(S^1)$  is governed by an exponent which is identically  $x(S^1) = 2$ :  $n = 1$  indeed corresponds to a single brownian path escaping from the absorber, which represents the potential itself, and this identity can be seen as a consequence of Gauss's theorem in two dimensions [38]. We therefore conclude that

$$(4.11) \quad Z_n = R^2 Z_R(S^n);$$

Owing to eqs.(4.5), and (4.10), we get the scaling relation

$$(4.12) \quad (n) = x(S^n) - x(S^1) = x(S^n) - 2;$$

4.2.2. Quantum Gravity Formalism. The absorber  $S$  near the ball center  $w$  (Fig. 7) is either a two-RW star  $S = B \_ B$ , where the two strands are independent and mutually-intersecting, or a two-SAW star  $S = P \wedge P$ ; made of two non-intersecting SAW's.

Our formalism (3.14) immediately gives the scaling dimension of the mutually-avoiding set  $S^n$  as

$$(4.13) \quad x(S^n) = 2\tilde{V}(S) + U^{-1}(n);$$

where  $\tilde{V}(S) = U^{-1}(x(S))$  is as above the quantum gravity boundary conformal dimension of the absorber  $S$  alone. The quantity  $U^{-1}(n)$  represents the quantum gravity boundary conformal dimension (2.41) of a packet of  $n$  independent paths. For a RW absorber, we have

$$\tilde{V}(S) = \tilde{V}(B \_ B) = U^{-1}(2) = \frac{3}{2};$$

while for a SAW (see (3.11) and (3.18))

$$\tilde{V}(S) = \tilde{V}(P \wedge P) = 2\tilde{V}_P(1) = 2U^{-1}\left(\frac{5}{8}\right) = \frac{3}{2};$$

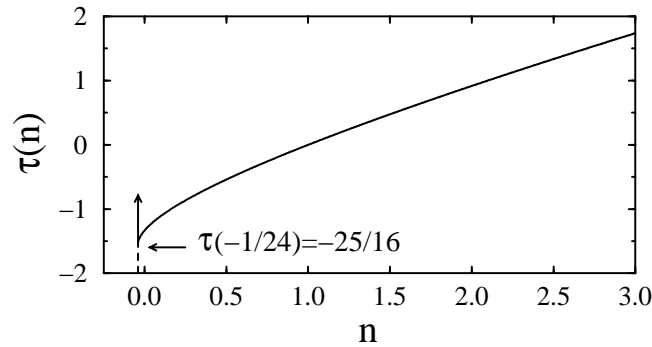


Figure 8. Harmonic multifractal dimensions  $\tau(n)$  of a two-dimensional RW or SAW .

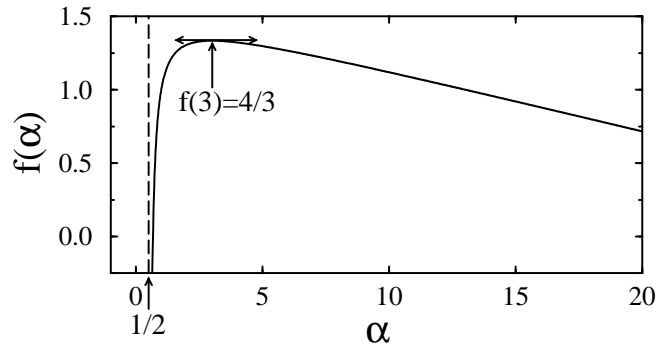


Figure 9. Harmonic multifractal spectrum  $f(\alpha)$  of a two-dimensional RW or SAW .

The coincidence of these two values gives us the general result:

In two dimensions the harmonic multifractal exponents  $\tau(n)$  and spectra  $f(\alpha)$  of a random walk and a self-avoiding walk are identical.

4.2.3. Multifractal Spectrum . Calculation using (4.12-4.13) gives [51]

$$(4.14) \quad \tau(n) = \frac{1}{2} (n - 1) + \frac{5}{24} \sqrt{24n + 1} - 5 ;$$

$$(4.15) \quad D(n) = \frac{1}{2} + \frac{5}{24\sqrt{24n + 1} + 5} ; \quad n \geq \frac{1}{24} + 1 ;$$

The Legendre transform (4.7) gives

$$(4.16) \quad f(\alpha) = \frac{d}{dn} \tau(n) = \frac{1}{2} + \frac{5}{2} \frac{1}{\sqrt{24n + 1}} ;$$

$$(4.17) \quad f(\alpha) = \frac{25}{48} \left( 3 - \frac{1}{2} \frac{1}{\alpha} - \frac{1}{24} \right) ; \quad \alpha \geq \frac{1}{2} + 1 ;$$

4.2.4. Geometrical Properties of Multifractal Curves. The corresponding universal curves are shown in Figures 8 and 9:  $f_1(x)$  is half a parabola, and  $f_2(x)$  a hyperbola.  $D(1) = f_1(1) = 1$  is Minkowski's theorem. The singularity at  $x = \frac{1}{2}$  in the multifractal functions  $f(x)$  corresponds to points on the fractal boundary  $F$  where the latter has the local geometry of a needle. The mathematical version of this statement is given by Beurling's theorem [92], which states that at distance from the boundary, the harmonic measure is bounded above by

$$(4.18) \quad H(z : \inf_{w \in F} |z - w|^{-2}) \leq C^{-1};$$

where  $C$  is a constant. This insures that the spectrum of multifractal Holder exponents is bounded below by  $\frac{1}{2}$ . The right branch of the  $f(x)$  curve has a linear asymptote

$$(4.19) \quad \lim_{n \rightarrow \infty} \frac{1}{n} f\left(\frac{1}{n}\right) = \frac{1}{24};$$

Its linear shape is quite reminiscent of that of the multifractal function of the growth probability as in the case of a 2D DLA cluster [93]. The domain of large values of  $n$  corresponds to the lowest part  $n = \frac{1}{24}$  of the spectrum of dimensions, which is dominated by almost inaccessible sites, and the existence of a linear asymptote to the multifractal function  $f$  implies a peculiar behavior for the number of those sites in a lattice setting. Indeed define  $N(H)$  as the number of sites having a probability  $H$  to be hit:

$$(4.20) \quad N(H) = \text{Card}\{w \in F : H(w) = H\};$$

Using the MF formalism to change from the variable  $H$  to  $x$  (at fixed value of  $a=R$ ), shows that  $N(H)$  obeys, for  $H \rightarrow 0$ ; a power law behavior

$$(4.21) \quad N(H) \sim H^{-n}$$

with an exponent

$$(4.22) \quad n = 1 + \lim_{n \rightarrow \infty} \frac{1}{n} f\left(\frac{1}{n}\right) = 1 + \frac{1}{24};$$

Thus we predict

$$(4.23) \quad f\left(\frac{1}{24}\right) = \frac{23}{24};$$

Let us remark that  $f(0) = \sup f(x) = f(3) = \frac{4}{3}$  is the Hausdorff dimension of the Brownian frontier or of a SAW. Thus Mandelbrot's classical conjecture identifying the latter two is derived and generalized to the whole  $f(x)$  harmonic spectrum.

4.3. An Invariance Property of  $f(x)$ . The expression for  $f(x)$  simplifies if one considers the combination:

$$(4.24) \quad f(x) = \frac{25}{24} - \frac{1}{2}x^2 + \frac{1}{2}x^{-1};$$

Thus the multifractal function possesses the invariance symmetry [94]

$$(4.25) \quad f(x) = f\left(\frac{1}{x}\right);$$

for  $x$  and  $\frac{1}{x}$  satisfying the duality relation:

$$(4.26) \quad (2-x)(2-\frac{1}{x}) = 1;$$

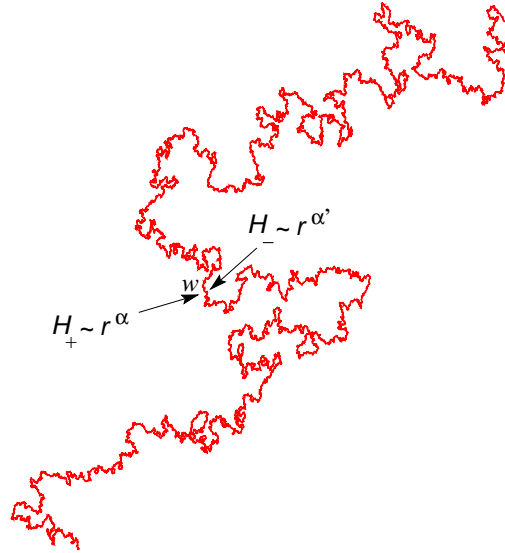


Figure 10. Double distribution of harmonic potential  $H$  on both sides of a simple scaling curve (here a SAW, courtesy of T. G. Kennedy). The local exponents on both sides of point  $w = w ; 0$  are  $\alpha$  and  $\alpha'$ . The Hausdorff dimension of such points along the SAW is  $f_2(\alpha ; \alpha')$ .

or, equivalently

$$(4.27) \quad \alpha + \alpha' = 2 :$$

When associating an equivalent electrostatic wedge angle  $\theta = \theta$  to each local singularity exponent (see section 6), one gets the complementary rule for angles in the plane [94]

$$(4.28) \quad \theta + \theta' = \pi - \frac{\pi}{2} = \frac{\pi}{2} :$$

Notice that by definition of the multifractal dimension  $f(\alpha)$ ,  $R^{f(\alpha)}$  is the total harmonic measure content of points of type  $\alpha$  or equivalent angle  $\theta = \theta$  along the multifractal frontier. The symmetry (4.25) thus means that this harmonic content is invariant when taken at the complementary angle in the plane  $\mathbb{R}^2$ . The basic symmetry (4.25) thus seems to reflect that of the frontier itself under the exchange of interior and exterior domains (ref. [94]).

It is also interesting to note that, owing to the explicit forms (4.16) of  $f(\alpha)$  and (4.15) of  $D(\alpha)$ , the condition (4.27) becomes, after a little algebra,

$$(4.29) \quad D(\alpha) + D(\alpha') = 2 :$$

4.4. Higher Multifractality for Brownian or Self-Avoiding Paths. It is interesting to note that one can define higher multifractal spectra as those depending on several variables [54]. A first example is given by the double moments of the harmonic measure on both sides of a random fractal, taken here to be either a

Brownian motion or a self-avoiding walk. (The general case will be further described in section 7).

4.4.1. Double-Sided Potential. When it is simple, i.e., double point free, a conformally scaling curve  $F$  can be reached from both sides. A SAW is naturally such a simple curve, therefore accessible from both sides. For a Brownian motion, one can consider the subset of the pinching or cut points, of Hausdorff dimension  $D = 2 - 2_2 = 3/4$ , where the path splits into two non-intersecting parts. The Brownian path is then locally accessible from both directions.

Taking Dirichlet boundary conditions on a random curve, one can then consider the joint distribution of potential on both sides, namely  $H_+$  on one side, and  $H_-$  on the other, such that

$$(4.30) \quad H_+(z; w; \epsilon) = r; H_-(z; w; \epsilon) = r^0;$$

when approaching a point  $w; \epsilon$  of the subset  $F; \epsilon$  at distance  $r = |z - w; \epsilon|$  (Fig. 10). Then a double-multifractal spectrum  $f_2(\epsilon; \epsilon^0) = \dim F; \epsilon$  yields the Hausdorff dimension of the set of points of type  $(\epsilon; \epsilon^0)$ .

4.4.2. Double Harmonic Moments. As before, instead of considering directly the potential  $H$ , one can consider equivalently the harmonic measure content of a covering by small balls centered along the random fractal. Let us now define:

$$(4.31) \quad Z_{n,n^0} = \sum_{w \in F; a} [H_+(w; a)]^n [H_-(w; a)]^{n^0};$$

where  $H_+(w; a) := H_+(F \setminus B(w; a))$  and  $H_-(w; a) := H_-(F \setminus B(w; a))$  are respectively the harmonic measure contents of the same ball  $B(w; a)$  on "left" or "right" sides of the random fractal. The ball's center  $w$  is taken in a discrete set of points  $w \in F; a$ .

They are represented by two packets of  $n$  and  $n^0$  independent Brownian paths diffusing away from the fractal object (Fig. 11). These moments have a multifractal scaling behavior

$$(4.32) \quad Z_{n,n^0} \sim (a=R)^{2(n;n^0)};$$

where the exponents  $2(n;n^0)$  now depend on two moment orders  $n$  and  $n^0$ .

4.4.3. Double Legendre Transform. The generalization of the Legendre transform (4.7) reads

$$(4.33) \quad \begin{aligned} f_2(\epsilon; \epsilon^0) &= \frac{\partial}{\partial n} 2(n;n^0); \quad \epsilon^0 = \frac{\partial}{\partial n^0} 2(n;n^0); \\ f_2(\epsilon; \epsilon^0) &= n + n^0 2_2(n;n^0); \\ n &= \frac{\partial f_2}{\partial \epsilon}(\epsilon; \epsilon^0); \quad n^0 = \frac{\partial f_2}{\partial \epsilon^0}(\epsilon; \epsilon^0); \end{aligned}$$

It yields the dimension of the subset  $F; \epsilon$  of frontier points  $w; \epsilon$ , where the potential  $H$  scales as in eqs. (4.31), or where the harmonic content of a ball  $B(w; \epsilon; a)$  scales as  $(a=R)^n$  on one side, and  $(a=R)^{n^0}$  on the other.

4.4.4. Star Fusion Algebra. We find the exponents from the star algebra (3.14):

$$(4.34) \quad 2_2(n;n^0) = 2V a^0 + U^{-1}(n) + U^{-1}(n^0) - 2;$$

where  $a^0$  corresponds to the quantum gravity boundary scaling dimension of the fractal set near where the potential or harmonic measure is evaluated, i.e., the

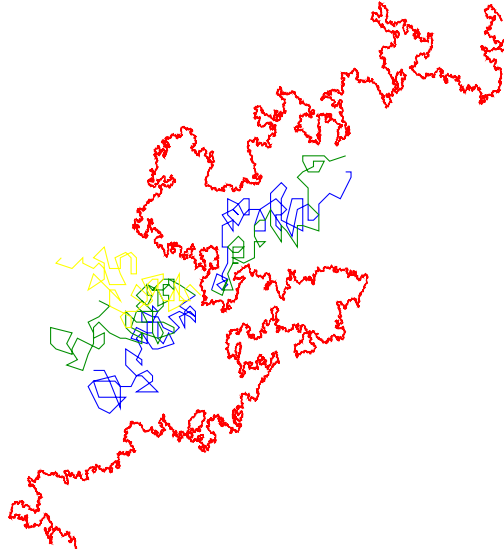


Figure 11. Representation of the double moment (4.31) by two packets of  $n$  and  $n^0$  independent Brownian paths disjoint away from a SAW.

simple SAW curve or the Brownian cut-point set. For Brownian motion near a cut-point, the two-strands appear as two mutually-avoiding parts  $B \wedge B$ , (further separated by the two sets of auxiliary Brownian motions which represent the harmonic measure moments). Thus we have from (3.11) and (3.18):

$$(4.35) \quad a_B^0 = \tilde{\nu}(B \wedge B) = 2 \tilde{\nu}_B(1) = 2U^{-1}(1) = 2:$$

Near a point on a self-avoiding walk, the latter appears by construction as made of two mutually-avoiding SAW's, and we have from (3.11) and (3.18):

$$(4.36) \quad a_P^0 = \tilde{\nu}(P \wedge P) = 2 \tilde{\nu}_P(1) = 2U^{-1}\left(\frac{5}{8}\right) = \frac{3}{2}:$$

After performing the double Legendre transform and some calculations (generalized and detailed in section 7), we find

$$(4.37) \quad f_2(\cdot; \cdot^0) = 2 + \frac{1}{12} \frac{1}{3} a^{\omega^2} \left(1 - \frac{1}{2} \frac{1}{-} + \frac{1}{0}\right)^{-1} \frac{1}{24} (\cdot + \cdot^0);$$

$$(4.38) \quad = 2 \frac{1}{24n+1} a^{\omega} + \frac{1}{4} \frac{P}{24n+1} + \frac{P}{24n^0+1};$$

and a similar symmetric equation for  $a^0$ . Here  $a^0$  has the shifted values:

$$(4.39) \quad a^0 = a^0 + \frac{1}{2} = a^0 + \frac{1}{2}$$

$$(4.40) \quad a_B^0 = \frac{3}{2} \text{ (RW)}; \text{ or } a_P^0 = 1 \text{ (SAW)};$$

These doubly multifractal spectra thus are different for RW's and SAW's. The SAW spectrum possesses the required property

$$f_p(\cdot) = \sup_{\epsilon} f_p(\cdot; \epsilon) = f(\cdot);$$

where  $f(\cdot)$  is (4.17) above. For a Brownian path, the one-sided spectrum

$$f_B(\cdot) = \sup_{\epsilon} f_B(\cdot; \epsilon) = 2 \frac{45}{48} \frac{49}{48} \frac{1}{2} = \frac{1}{24};$$

such that  $f_B(\cdot) < f(\cdot)$ , gives the MF spectrum of cut-points along the Brownian frontier. This set of Hausdorff dimension  $\frac{3}{4} < 1$  is disconnected, and  $f_B(\cdot = 1) (= \frac{49}{48}) \notin 1$ , in contrast to Makarov's theorem,  $f(\cdot = 1) = 1$ , for any connected set in the plane.

4.4.5. Poly-Multifractality. The results above can be generalized to a star configuration made of  $m$  random walks or  $m$  self-avoiding walks, where one looks at the simultaneous behavior of the potential in each sector between the  $m$  mutually-avoiding arms of the star (see section 7 below for a precise description and calculation in the general case). The quantum gravity boundary dimensions of these stars are respectively from (3.11) and (3.18):

$$(4.41) \quad a^0 = a_B^0(m) = \tilde{\alpha}_B^m = \tilde{\alpha}_B(1) = m U^{-1}(1) = m;$$

for  $m$ -cut Brownian paths, and

$$(4.42) \quad a^0 = a_P^0(m) = \tilde{\alpha}_P^m = \tilde{\alpha}_P(1) = m U^{-1}\left(\frac{5}{8}\right) = \frac{3}{4}m;$$

for a star made of  $m$  self-avoiding walks, all being mutually-avoiding. We give here only these poly-multifractal results, which read for Brownian cut-points or self-avoiding paths:

$$(4.43) \quad f_m(f_{i=1, \dots, m} g) = 2 + \frac{1}{12} \frac{1}{3} a^{00}(m) + \frac{1}{2} \sum_{i=1}^m \frac{1}{i} \frac{X^n}{i^{n-1}};$$

with

$$(4.44) \quad \frac{1}{i} = 2 \sum_{j=1}^m \frac{1}{24n_j + 1} a^0(m) + \frac{1}{4} \sum_{j=1}^m \frac{1}{24n_j + 1} A;$$

and where

$$(4.45) \quad a^{00}(m) = a_B^{00}(m) = a_B^0(m) + \frac{1}{4}m = \frac{3}{4}m;$$

for  $m$  random walks pinched in a mutually-avoiding  $m$ -star configuration, and

$$(4.46) \quad a^{00}(m) = a_p^{00}(m) = a_p^0(m) \frac{1}{4}m = \frac{1}{2}m;$$

for  $m$  self-avoiding walks in a mutually-avoiding star configuration. The two-sided case (4.37) (4.40) above is recovered for  $m = 2$ . The domain of definition of the poly-multifractal function  $f$  is given by

$$(4.47) \quad 1 - \frac{1}{2} \sum_{i=1}^N x_i \geq 0;$$

as verified by eq. (4.44).

## 5. Percolation Clusters

5.1. Cluster Hull and External Perimeter. Let us consider, for definiteness, site percolation on the 2D triangular lattice. By universality, the results are expected to apply to other 2D (e.g., bond) percolation models in the scaling limit. Consider then a very large two-dimensional incipient cluster  $C$ , at the percolation threshold  $p_c = 1/2$ . Figure 12 depicts such a connected cluster.

5.1.1. Hull. The boundary lines of a site percolation cluster, i.e., of connected sets of occupied hexagons, form random lines on the dual hexagonal lattice. (They are actually known to obey the statistics of random loops in the  $O(N=1)$  model, where  $N$  is the loop fugacity, in the so-called "low-temperature phase", or of boundaries of Fortuin-Kasteleyn clusters in the  $Q=1$  Potts model [20].) Each critical connected cluster thus possesses an external closed boundary, its hull, the fractal dimension of which is known to be  $D_H = 7/4$  [20].

In the scaling limit, however, the hull, which possesses many pairs of points at relative distances given by a finite number of lattice meshes, coils onto itself to become a non-simple curve [58]; it thus develops a smoother outer (accessible) frontier  $F(C)$  or external perimeter (EP).

5.1.2. External Perimeter and Crossing Paths. The geometrical nature of this external perimeter has recently been elucidated and its Hausdorff dimension found to equal  $D_{EP} = 4/3$  [53]. For a site  $w = (\cdot)$  to belong to the accessible part of the hull, it must remain, in the continuous scaling limit, the source of at least three non-intersecting crossing paths, noted  $S_3 = P \wedge P_1 \wedge P_2$ , reaching to a (large) distance  $R$  (Fig. 12). (Recall the notation  $A \wedge B$  for two sets,  $A, B$ , of random paths, required to be mutually non-intersecting, and  $A \_ B$  for two independent, thus possibly intersecting, sets.) Each of these paths is "monochromatic": one path  $P$  runs only through occupied sites, which simply means that  $w$  belongs to a particular connected cluster; the other two dual lines  $P_{i=1,2}$  run through empty sites, and doubly connect the external perimeter site  $w$  to "infinity" in open space [53]. The definition of the standard hull requires only the origination, in the scaling limit, of a "bichromatic" pair of lines  $S_2 = P \wedge P$ , with one path running on occupied sites, and the dual one on empty ones. Such hull points lacking a second dual line will not necessarily remain accessible from the outside after the scaling limit is taken, because their single exit path becomes a strait pinched by parts of the occupied cluster. In the scaling limit, the hull is thus a self-coiling and conformally-invariant (CI) scaling curve which is not simple, while the external perimeter is a simple CI scaling curve.



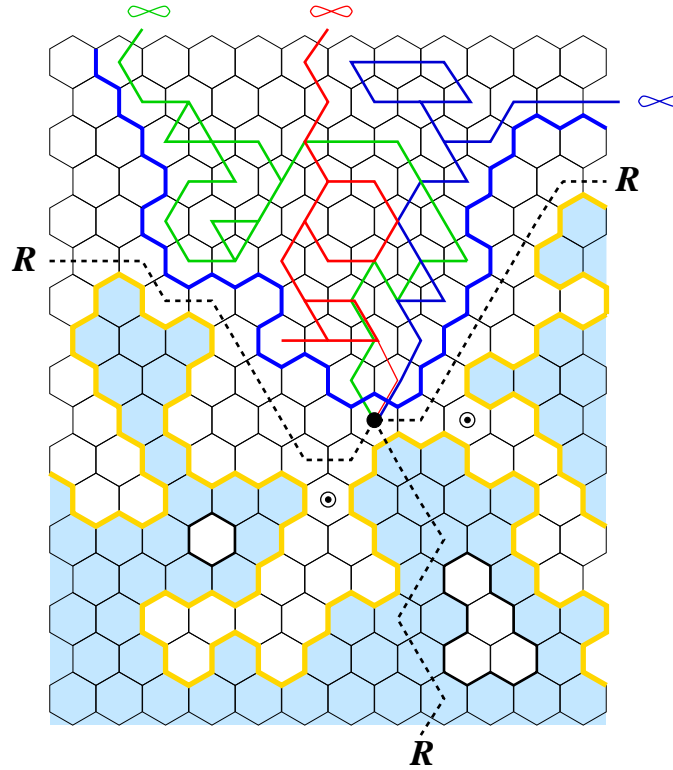


Figure 12. An accessible site ( ) on the external perimeter for site percolation on the triangular lattice. It is defined by the existence, in the scaling limit, of three non-intersecting, and connected paths  $S_3$  (dotted lines), one on the incipient cluster, the other two on the dual empty sites. The entrances of fjords close in the scaling limit. Point ( ) is first reached by three independent RW's (red, green, blue), contributing to  $H^3$  ( ). The hull of the incipient cluster (golden line) avoids the outer frontier of the RW's (thick blue line). A Riemann map of the latter onto the real line  $\partial H$  reveals the presence of an underlying  $\nu = 3$  path-crossing boundary operator, i.e, a two-cluster boundary operator, with dimension in the half-plane  $\kappa_{\nu=3} = \kappa_{\kappa=2}^C = 2$ : Both accessible hull and Brownian paths have a frontier dimension  $\frac{4}{3}$ .

The (bichromatic) set  $S_3$  of three non-intersecting connected paths in the percolation system is governed by a new critical exponent  $\chi(S_3) (= 2=3)$  such that  $D_{EP} = 2 - \chi(S_3)$ , while a bichromatic pair of non-intersecting paths  $S_2$  has an exponent  $\chi(S_2) (= 1=4)$  such that  $D_H = 2 - \chi(S_2)$  (see below).

5.2. Harmonic Measure of Percolation Frontiers. Define  $H(w;a) := H(F \setminus B(w;a))$  as the probability that a random walker, launched from infinity, first hits the outer (accessible) percolation hull's frontier or external perimeter  $F(C)$  in the ball  $B(w;a)$  centered at point  $w \in F(C)$ . The moments  $H^n$  of  $H$  are averaged

over all realizations of RW 's and  $C$ , as in eq.(4.4) above:

$$(5.1) \quad Z_n = \sum_{w \in F, a} H^n(F \setminus B(w; a)) :$$

For very large clusters  $C$  and frontiers  $F(C)$  of average size  $R$ ; one expects again these moments to scale as in eq. (4.5):  $Z_n \sim (a=R)^{\chi(n)}$ . These exponents  $\chi(n)$  have been obtained recently [52], and we shall see that they are identical to those obtained in the preceding section 4 for Brownian paths and self-avoiding walks.

As before, by the very definition of the  $H$ -measure,  $n$  independent RW 's diffusing away or towards a neighborhood of a EP point  $w$ , give a geometric representation of the  $n^{\text{th}}$  moment  $H^n(w)$ ; for  $n$  integer. The values so derived for  $n \leq N$  will be enough, by convexity arguments, to obtain the analytic continuation for arbitrary  $n$ 's. Figure 12 depicts such  $n$  independent random walks, in a bunch, first hitting the external frontier of a percolation cluster at a site  $w = (\cdot)$ : The packet of independent RW 's avoids the occupied cluster, and defines its own envelope as a set of two boundary lines separating it from the occupied part of the lattice. The  $n$  independent RW 's, or Brownian paths  $B$  in the scaling limit, in a bunch denoted  $(\underline{B})^n$ ; thus avoid the set  $S_3$  of three non-intersecting connected paths in the percolation system, and this system is governed by a new family of critical exponents  $\chi(S_3 \wedge n)$  depending on  $n$ : The main lines of the derivation of the latter exponents by generalized conformal invariance are as follows.

### 5.3. Harmonic and Path Crossing Exponents.

5.3.1. Generalized Harmonic Crossing Exponents. The  $n$  independent Brownian paths  $B$ , in a bunch  $(\underline{B})^n$ ; avoid a set  $S \wedge (\wedge P)$  of  $\wedge$  non-intersecting crossing paths in the percolation system. They originate from the same hull site, and each passes only through occupied sites, or only through empty (dual) ones [53]. The probability that the Brownian and percolation paths altogether traverse the annulus  $D(a; R)$  from the inner boundary circle of radius  $a$  to the outer one at distance  $R$ , i.e., are in a "star" configuration  $S \wedge (\underline{B})^n$ , is expected to scale for  $a=R \rightarrow 0$  as

$$(5.2) \quad P_R(S \wedge n) \sim (a=R)^{\chi(S \wedge n)} ;$$

where we used  $S \wedge n = S \wedge (\underline{B})^n$  as a shorthand notation, and where  $\chi(S \wedge n)$  is a new critical exponent depending on  $\wedge$  and  $n$ . It is convenient to introduce similar boundary probabilities  $\tilde{P}_R(S \wedge n) \sim (a=R)^{\tilde{\chi}(S \wedge n)}$  for the same star configuration of paths, now crossing through the half-annulus  $\tilde{D}(a; R)$  in the half-plane  $H$ .

5.3.2. Bichromatic Path Crossing Exponents. When  $n \rightarrow 0$ , the probability  $P_R(S \cdot) = P_R(S \wedge 0) \sim (a=R)^{\chi(S \cdot)}$  [resp.  $\tilde{P}_R(S \cdot) = \tilde{P}_R(S \wedge 0) \sim (a=R)^{\tilde{\chi}(S \cdot)}$ ] is the probability of having  $\wedge$  simultaneous non-intersecting path-crossings of the annulus  $D(a; R)$  in the plane  $C$  [resp. half-plane  $H$ ], with associated exponents  $\chi \cdot = \chi(S \wedge 0)$  [resp.  $\tilde{\chi} \cdot = \tilde{\chi}(S \wedge 0)$ ]. Since these exponents are obtained from the limit  $n \rightarrow 0$  of the harmonic measure exponents, at least two paths run on occupied sites or empty sites, and these are the bichromatic path crossing exponents [53]. The monochromatic ones are different in the bulk [53, 95].

5.4. Quantum Gravity for Percolation.

5.4.1.  $c = 0$  KPZ mapping. Critical percolation is described by a conformal field theory with the same vanishing central charge  $c = 0$  as RW's or SAW's (see, e.g., [96]). Using again the fundamental mapping of this conformal field theory (CFT) in the plane  $C$ , to the CFT on a fluctuating random Riemann surface, i.e., in presence of quantum gravity [26], the two universal functions  $U$  and  $V$  only depend on the central charge  $c$  of the CFT, and are the same as for RW's, and SAW's:

$$(5.3) \quad U(x) = \frac{1}{3}x(1+2x); \quad V(x) = \frac{1}{24}(4x^2 - 1);$$

with  $V(x) = U(\frac{1}{2}x - \frac{1}{2})$ :

They suffice to generate all geometrical exponents involving mutual-avoidance of random star-shaped sets of paths of the critical percolation system. Consider two arbitrary random sets  $A; B$ ; involving each a collection of paths in a star configuration, with proper scaling crossing exponents  $x(A); x(B)$ ; or, in the half-plane, crossing exponents  $\kappa(A); \kappa(B)$ : If one fuses the star centers and requires  $A$  and  $B$  to stay mutually-avoiding, then the new crossing exponents,  $x(A \wedge B)$  and  $\kappa(A \wedge B)$ ; obey the same star fusion algebra as in (3.14) [50, 51]

$$(5.4) \quad \begin{aligned} x(A \wedge B) &= 2V(U^{-1}(\kappa(A)) + U^{-1}(\kappa(B))) \\ \kappa(A \wedge B) &= U(U^{-1}(\kappa(A)) + U^{-1}(\kappa(B))); \end{aligned}$$

where  $U^{-1}(x)$  is the inverse function

$$(5.5) \quad U^{-1}(x) = \frac{1}{4} \sqrt{24x + 1} - \frac{1}{4} :$$

This structure immediately gives both the percolation crossing exponents  $x, \kappa$ , [53], and the harmonic crossing exponents  $x(S \wedge n)$  (5.2).

5.4.2. Path Crossing Exponents. First, for a set  $S = (\wedge P)$  of  $\setminus$  crossing paths, we have from the recurrent use of (5.4)

$$(5.6) \quad x_S = 2V(U^{-1}(\kappa_1)); \quad \kappa_S = U(U^{-1}(\kappa_1)) :$$

For percolation, two values of halfplane crossing exponents  $\kappa_S$  are known by elementary means:  $\kappa_2 = 1; \kappa_3 = 2$ : [23, 53] From (5.6) we thus find  $U^{-1}(\kappa_1) = \frac{1}{2}U^{-1}(\kappa_2) = \frac{1}{3}U^{-1}(\kappa_3) = \frac{1}{2}$ ; (thus  $\kappa_1 = \frac{1}{3}$  [16]), which in turn gives

$$x_S = 2V\left(\frac{1}{2}\right) = \frac{1}{12} \sqrt{2} - \frac{1}{12}; \quad \kappa_S = U\left(\frac{1}{2}\right) = \frac{1}{6}(\sqrt{2} + 1) :$$

We thus recover the identity [53]  $x_S = x_{L=, N=1}^0; \kappa_S = \kappa_{L=, N=1}^0$  with the  $L$ -line exponents of the associated  $O(N=1)$  loop model, in the "low-temperature phase". For  $L$  even, these exponents also govern the existence of  $k = \frac{1}{2}L$  spanning clusters, with the identity  $x_k^C = x_{\setminus=2k} = \frac{1}{12}(4k^2 - 1)$  in the plane, and  $\kappa_k^C = \kappa_{\setminus=2k-1} = \frac{1}{3}k(2k-1)$  in the halfplane [20, 44, 97].

5.4.3. Brownian Non-Intersection Exponents. The non-intersection exponents (2.6) and (2.7) of  $L$  Brownian paths seen in section 2 are identical to the percolation path crossing exponents for

$$(5.7) \quad 2L = x_S; \quad 2\tilde{L} = \kappa_S; \quad \setminus = 2L;$$

so we obtain a complete scaling equivalence between a Brownian path and two percolating crossing paths, in both the plane and half-plane [52].

5.4.4. Harmonic Crossing Exponents. Finally, for the harmonic crossing exponents in (5.2), we fuse the two objects  $S_\nu$  and  $(\underline{B})^n$  into a new star  $S_\nu \wedge n$ , and use (5.4). We just have seen that the boundary  $\nu$ -crossing exponent of  $S_\nu$ ,  $\kappa_\nu$ , obeys  $U^{-1}(\kappa_\nu) = \frac{1}{2}\nu$ : The bunch of  $n$  independent Brownian paths have their own half-plane crossing exponent  $\kappa((\underline{B})^n) = n\kappa(B) = n$ ; since the boundary conformal weight of a single Brownian path is trivially  $\kappa(B) = 1$ . Thus we obtain

$$(5.8) \quad \chi(S_\nu \wedge n) = 2\nu - 1 + U^{-1}(n) :$$

Specializing to the case  $\nu = 3$  finally gives from (5.3-5.5)

$$\chi(S_3 \wedge n) = 2 + \frac{1}{2}(n-1) + \frac{5}{24} \frac{\Gamma(2n+1)}{\Gamma(2n+5)} :$$

5.5. Multifractality of Percolation Clusters.

5.5.1. Multifractal Dimensions and Spectrum. In terms of probability (5.2), the harmonic measure moments (5.1) scale simply as  $Z_n = R^2 P_R(S_{\nu=3} \wedge n)$  [34], which leads to

$$(5.9) \quad \chi(n) = \chi(S_3 \wedge n) - 2 :$$

Thus

$$(5.10) \quad \chi(n) = \frac{1}{2}(n-1) + \frac{5}{24} \frac{\Gamma(2n+1)}{\Gamma(2n+5)}$$

is found to be identical to (4.14) for RW's and SAW's; the generalized dimensions  $D(n)$  are then:

$$(5.11) \quad D(n) = \frac{1}{n-1} \chi(n) = \frac{1}{2} + \frac{5}{24} \frac{\Gamma(2n+1)}{\Gamma(2n+5)}; \quad n \geq 2, \quad \frac{1}{24}; +1 ;$$

valid for all values of moment order  $n$ ;  $U^{-1}(\frac{1}{24})$ : The Legendre transform reads again exactly as in eq. (4.17):

$$(5.12) \quad f(\tau) = \frac{25}{48} - 3 \frac{1}{2} \frac{1}{\tau-1} - \frac{1}{24}; \quad \tau \geq 2, \quad \frac{1}{2}; +1 :$$

5.5.2. Comparison to Numerical Results. Only in the case of percolation has the harmonic measure been systematically studied numerically, by Meakin et al. [98]. We show in Figure 13 the exact curve  $D(n)$  (5.11) [52] together with the numerical results for  $n \geq 2$ ; [98], showing fairly good agreement.

The average number  $N(H)$  (4.21) has been also determined numerically for percolation clusters in [99], and for  $c=0$ , our prediction (4.23)  $= \frac{23}{24} = 0.95833...$  compares very well with the result  $= 0.951 - 0.030$ , obtained for  $10^5$   $H$   $10^4$ .

The dimension of the measure's support  $D(0) = \frac{4}{3} \notin D_H$ ; where  $D_H = \frac{7}{4}$  is the Hausdorff dimension of the standard hull, i.e., the outer boundary of critical percolating clusters [20]. The value  $D(0) = \frac{4}{3}$  corresponds to the dimension of the accessible external perimeter. A direct derivation of its exact value is given in [53]. The complement of the accessible perimeter in the hull is made of deep fjords, which do close in the scaling limit and are not probed by the harmonic measure. This is in agreement with the instability phenomenon observed on a lattice for the hull dimension [58]. A striking fact is the complete identity of the multifractal spectrum for percolation to the corresponding results, eqs.(4.14-4.17), both for random walks and self-avoiding walks. Seen from outside, these three fractal simple curves are not distinguished by the harmonic measure. In fact they are the same, and one of the

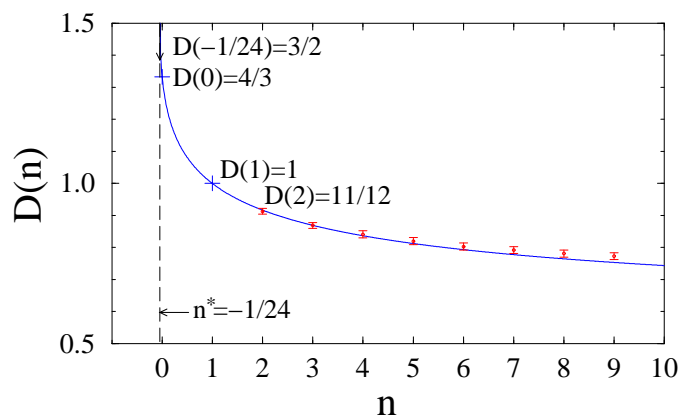


Figure 13. Universal generalized dimensions  $D(n)$  as a function of  $n$ , corresponding to the harmonic measure near a percolation cluster, or to self-avoiding or random walks, and comparison with the numerical data obtained by Meakin et al. (1988) for percolation.

main conclusions of this study is that the external frontiers of a planar Brownian motion, or of a critical percolation cluster are, in the scaling limit, identical to a critical self-avoiding walk, with Hausdorff dimension  $D = \frac{4}{3}$ . As we have seen, this fact is linked to the presence of a single universal conformal field theory (with a vanishing central charge  $c = 0$ ), and to the underlying presence of quantum gravity, which organizes the associated conformal dimensions. Note that in a recent work, Smirnov [64] proved that critical site percolation on the triangular lattice has a conformally-invariant scaling limit, and that the discrete cluster interfaces (hulls) converge to the same stochastic Loewner evolution process as the one involved for Brownian paths, opening the way to a rigorous derivation of percolation exponents [65, 66], previously derived in the physics literature [4, 16, 20, 53].

5.5.3. Double Layer Impedance. Let us finally consider the different, but related, problem of the double layer impedance of a rough electrode. In some range of frequencies  $\omega$ , the impedance contains an anomalous "constant phase angle" (CPA) term  $(i\omega)^{-\alpha}$ , where  $\alpha < 1$ . From a natural RW representation of the impedance, a scaling law was recently proposed:  $\alpha = \frac{D(2)}{D(0)}$  (here in 2D), where  $D(2)$  and  $D(0)$  are the multifractal dimensions of the H-measure on the rough electrode [100]. In the case of a 2D porous percolative electrode, our results (5.11) give  $D(2) = \frac{11}{12}$ ;  $D(0) = \frac{4}{3}$ , whence  $\alpha = \frac{11}{16} = 0.6875$ : This compares very well with a numerical RW algorithm result [99], which yields an effective CPA exponent  $\alpha \approx 0.69$ ; nicely vindicating the multifractal description [100].

## 6. Conformally Invariant Frontiers and Quantum Gravity

In the next sections, we present a universal description of multifractal functions for arbitrary conformally-invariant curves. They are derived from conformal field

theory and quantum gravity. The geometrical findings are described in detail, including cases like Ising clusters, or  $Q = 4$  Potts Fortuin-Kasteleyn clusters, which are of particular interest. We also make explicit the relation between a conformally-invariant scaling curve with CFT central charge  $c$  [57], and the stochastic Loewner process SLE [59]. A fundamental geometric duality property for the external boundaries in  $O(N)$  and Potts models, and SLE is obtained. For several simple paths we also define and calculate higher multifractal spectra.

### 6.1. Harmonic Measure and Potential near a Fractal Frontier.

6.1.1. Local Behavior of the Potential. Consider a single (conformally-invariant) critical random cluster, generically called  $C$ . Let  $H(z)$  be the potential at an exterior point  $z \in \mathbb{C}$ , with Dirichlet boundary conditions  $H(w \in \partial C) = 0$  on the outer (simply connected) boundary  $\partial C$  of  $C$ , (or frontier  $F = \partial C$ ), and  $H(w) = 1$  on a circle  $\partial B(w; R)$ , i.e., of a large radius scaling like the average size  $R$  of  $C$ . As is well-known [89],  $H(z)$  is identical to the harmonic measure of the circle  $\partial B(w; R)$  seen from  $z$ , i.e., the probability that a random walker (more precisely, a Brownian motion) launched from  $z$ , escapes to  $\partial B(w; R)$  without having hit  $C$ .

The multifractal formalism [30, 31, 32, 33] characterizes subsets  $\partial C$  of boundary sites by a Hölder exponent  $\alpha$ ; and a Hausdorff dimension  $f(\alpha) = \dim(\partial C)$ , such that their potential locally scales as

$$(6.1) \quad H(z \in \partial B(w; R)) \sim (|z - w|/R)^\alpha;$$

in the scaling limit  $a \rightarrow 0$  ( $R = |z - w|/a$  with  $a$  the underlying lattice constant if one starts from a lattice description before taking the scaling limit  $a \rightarrow 0$ ).

6.1.2. Equivalent Wedge Angle. In 2D the complex potential  $\phi(z)$  (such that the electrostatic potential  $H(z) = |\phi(z)|^2$  and the field's modulus  $\mathbb{E}(z) = |\phi'(z)|^2$ ) for a wedge of angle  $\theta$ , centered at  $w$ , is

$$(6.2) \quad \phi(z) = (z - w)^{\theta/\pi};$$

By eq. (6.1) a Hölder exponent  $\alpha$  thus defines a local equivalent "electrostatic" angle  $\theta = \alpha\pi$ ; and the MF dimension  $\hat{f}(\alpha)$  of the boundary subset with such  $\alpha$  is

$$(6.3) \quad \hat{f}(\alpha) = f(\theta = \alpha\pi):$$

6.1.3. Moments. It is convenient to define the harmonic measure  $H(w; r) = H(\partial C \setminus B(w; r))$  in a ball  $B(w; r)$  of radius  $r$  centered at  $w \in \partial C$ , as the probability that a Brownian path started at infinity first hits the frontier  $F = \partial C$  inside the ball  $B(w; r)$ . It is the integral of the Laplacian of potential  $H$  in the ball  $B(w; r)$ , i.e., the boundary charge in that ball. It scales as  $r^\alpha$  with the same exponent as in (6.1).

Of special interest are the moments of  $H$ , averaged over all realizations of  $C$ , and defined as

$$(6.4) \quad Z_n = \sum_{z \in \partial C, r}^* H^n(w; r);$$

where points  $w \in \partial C, r$  are the centers of a covering of the frontier  $\partial C$  by balls of radius  $r$ , and form a discrete subset  $\partial C, r \subset \partial C$ . The moment order  $n$  can be a real number. In the scaling limit, one expects these moments to scale as

$$(6.5) \quad Z_n \sim (r=R)^{\hat{f}(n)};$$

where the multifractal scaling exponents  $\chi(n)$  vary in a non-linear way with  $n$  [30, 31, 32, 33]. As above, they obey the symmetric Legendre transform  $\chi(n) + f(\chi) = n$ ; with  $n = f'(\chi)$ ;  $\chi = f'^{-1}(n)$ . By normalization:  $\chi(1) = 0$ : As noted above, because of the ensemble average (6.4), values of  $f(\chi)$  can become negative for some domains of  $\chi$  [34, 38].

6.2. Calculation of Exponents from Quantum Gravity. Let us now give the main lines of the derivation of exponents  $\chi(n)$ , hence  $f(\chi)$ , via generalized conformal invariance.

6.2.1. Brownian Representation of Moments. As above,  $n$  independent RW's, or Brownian paths  $B$  in the scaling limit, started at the same point a distance  $r$  away from the cluster's hull's frontier  $@C$ , and discussing without hitting  $@C$ , give a geometric representation of the  $n^{\text{th}}$  moment;  $H^n$ ; in eq.(4.4) for  $n$  integer. Convexity yields the analytic continuation to arbitrary  $n$ 's. Let us recall the notation  $A \wedge B$  for two random sets required to traverse, without mutual intersection, the annulus  $D(r;R)$  from the inner boundary circle of radius  $r$  to the outer one at distance  $R$ , and  $A \_ B$  for two independent, thus possibly intersecting, sets [51]. With this notation, one can define, as in eq. (3.3), a grand canonical partition function which describes the star configuration of the Brownian paths and cluster:  $@C \wedge n = (@C \wedge \_ B)^n$ . At the critical point, it is expected to scale for  $r=R \rightarrow 0$  as

$$(6.6) \quad Z_R (@C \wedge n) \sim (r=R)^{\chi(n)+}$$

where the scaling exponent

$$(6.7) \quad \chi(n) = \chi (@C \wedge n)$$

depends on  $n$  and is associated with the conformal operator creating the star vertex  $@C \wedge n$ . The dots after exponent  $\chi(n)$  express the fact that there may be an additional contribution to the exponent, independent of  $n$ , corresponding to the entropy associated with the extremities of the random frontier (see, e.g., (3.3)).

By normalization, this contribution actually does not appear in the multifractal moments. Since  $H$  is a probability measure, the sum (6.4) is indeed normalized as in (4.8)

$$(6.8) \quad Z_{n=1} = 1;$$

or in terms of star partition functions:

$$(6.9) \quad Z_n = Z_R (@C \wedge n) = Z_R (@C \wedge 1):$$

The scaling behavior (6.6) thus gives

$$(6.10) \quad Z_n \sim (r=R)^{\chi(n) - \chi(1)};$$

The last exponent actually obeys the identity  $\chi(1) = \chi (@C \wedge 1) = 2$ , which will be obtained directly, and can also be seen as a consequence of Gauss's theorem in two dimensions [38]. Thus we can also write as in (5.2)

$$(6.11) \quad Z_n = (R=r)^2 P_R (@C \wedge n);$$

where  $P_R (@C \wedge n)$  is a (grand-canonical) excursion measure from  $r$  to  $R$  for the random set  $@C \wedge n$ , with proper scaling  $P_R \sim (r=R)^{\chi(n)}$ . The factor  $(R=r)^2$  is the area scaling factor of the annulus  $D(r;R)$ .

Owing to eqs. (6.5) (6.10) we get

$$(6.12) \quad \chi(n) = \chi(n) - \chi(1) = \chi(n) - 2:$$

6.2.2. Quantum Gravity. To calculate these exponents, we again use the fundamental mapping between the conformal field theory, describing a critical statistical system in the plane  $\mathbb{C}$  or half-plane  $\mathbb{H}$ , and the same CFT on a random planar surface, i.e., in presence of quantum gravity [26, 28, 27]. Two universal functions  $U$  and  $V$ , which now depend on the central charge  $c$  of the CFT, describe the KPZ map between conformal dimensions in bulk or boundary QG and those in the standard plane or halfplane:

$$(6.13) \quad U(x) = U(x) = x \frac{x}{1}; \quad V(x) = V(x) = \frac{1}{4} \frac{x^2}{1};$$

with

$$(6.14) \quad V(x) = U\left(\frac{1}{2}(x + \dots)\right);$$

The parameter  $\gamma$  is the string susceptibility exponent of the random 2D surface (of genus zero), bearing the CFT of central charge  $c$  [26];  $\gamma$  is the solution of

$$(6.15) \quad c = 1 - 6\gamma^2(1 - \gamma)^{-1}; \quad \gamma > 0;$$

In order to simplify the notation, we shall hereafter in this section drop the subscript from functions  $U$  and  $V$ .

The function  $U$  maps quantum gravity conformal weights, whether in the bulk or on a boundary, into their counterparts in  $\mathbb{C}$  or  $\mathbb{H}$ , as in (2.9)–(2.11). The function  $V$  has been tailored to map quantum gravity boundary dimensions to the corresponding conformal dimensions in the full plane  $\mathbb{C}$ , as in (2.46)–(2.47). The positive inverse function of  $U$ ,  $U^{-1}$ , is

$$(6.16) \quad U^{-1}(x) = \frac{1}{2} \sqrt{4(1 - \gamma)x + \dots};$$

and transforms conformal weights of a conformal operator in  $\mathbb{C}$  or  $\mathbb{H}$  into the conformal weights of the same operator in quantum gravity, in the bulk or on the boundary. Note the shift relation

$$(6.17) \quad U^{-1}(x) = \frac{1}{2} V^{-1}(x) + \frac{1}{2};$$

where the inverse of  $V$ ,

$$(6.18) \quad V^{-1}(x) = \sqrt{4(1 - \gamma)x + \dots};$$

transforms the bulk conformal weight in  $\mathbb{C}$  of a given conformal operator into the boundary conformal weight of the corresponding boundary operator in quantum gravity (see appendix C).

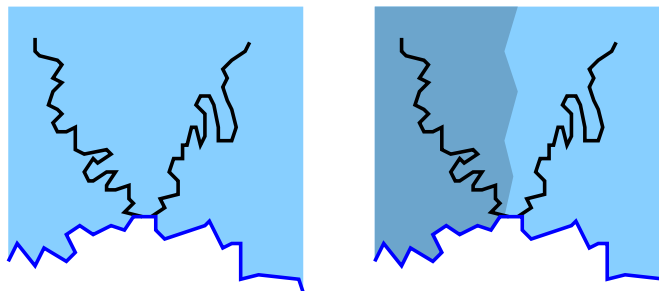
6.2.3. Boundary Additivity Rule. Consider two arbitrary random sets  $A; B$ ; with boundary scaling exponents  $\kappa(A); \kappa(B)$  in the half-plane  $\mathbb{H}$  with Dirichlet boundary conditions. When these two sets are mutually-avoiding, the scaling exponent  $\kappa(A \wedge B)$  in  $\mathbb{C}$ , as in (6.7), or  $\kappa(A \wedge B)$  in  $\mathbb{H}$  have the universal structure [51, 52, 57]

$$(6.19) \quad \kappa(A \wedge B) = 2V U^{-1}(\kappa(A)) + U^{-1}(\kappa(B));$$

$$(6.20) \quad \kappa(A \wedge B) = U U^{-1}(\kappa(A)) + U^{-1}(\kappa(B));$$

We have seen these fundamental relations in the  $c = 0$  case above; they are established for the general case in appendix C.  $U^{-1}(\kappa)$  is, on the random disk with





$$U^{-1}(\tilde{x}_2) = 2U^{-1}(\tilde{x}_1)$$

Figure 14. Illustration of the additivity rule (6.22): each of the two non-intersecting strands of a simple random path lives in its own sector of the random disk near the Dirichlet boundary.

Dirichlet boundary conditions, the boundary scaling dimension corresponding to  $\varkappa$  in the halfplane  $H$ , and in eqs. (6.19)–(6.20)

$$(6.21) \quad U^{-1}(\varkappa(A \wedge B)) = U^{-1}(\varkappa(A)) + U^{-1}(\varkappa(B))$$

is a linear boundary exponent corresponding to the fusion of two "boundary operators" on the random disk, under the Dirichlet mutual avoidance condition  $A \wedge B$ . This quantum boundary conformal dimension is mapped back by  $V$  to the scaling dimension in  $C$ , or by  $U$  to the boundary scaling dimension in  $H$  [57] (see appendix C).

6.2.4. Exponent Construction. For determining the harmonic exponents  $x(n)$  (6.7), we use (6.19) for  $A = @C$  and  $B = (\_B)^n$ .

We first need the boundary (conformal) scaling dimension (b.s.d.)  $\varkappa := \varkappa(@C)$  associated with the presence of the random frontier near the Dirichlet boundary  $H$ . Since this frontier is simple, it can be seen as made of two non-intersecting semi-infinite strands (Fig. 14). Its b.s.d. in quantum gravity thus obeys (6.21)

$$(6.22) \quad U^{-1}(\varkappa_2) = 2U^{-1}(\varkappa_1);$$

where  $\varkappa_1$  is the boundary scaling dimension of a semi-infinite frontier path originating at the boundary  $H$ .

The packet of  $n$  independent Brownian paths has  $\varkappa((\_B)^n) = n$ ; since  $\varkappa(B) = 1$ .

From (6.21) the QG boundary dimension of the whole set is (see Fig. 15):

$$(6.23) \quad \tilde{\varkappa} := U^{-1}[\varkappa(@C \wedge n)] = 2U^{-1}(\varkappa_1) + U^{-1}(n);$$

Its associated QG bulk conformal dimension is therefore  $\tilde{x} = \frac{1}{2}(\tilde{\varkappa} + \dots)$  (appendix C). From eqs. (6.14) or (6.19) we finally find

$$(6.24) \quad \begin{aligned} x(n) &= 2U^{-1}(\tilde{x}) = 2V^{-1}(\tilde{\varkappa}) \\ &= 2V^{-1}(2U^{-1}(\varkappa_1) + U^{-1}(n)) : \end{aligned}$$

The whole construction is illustrated in Fig. 15.

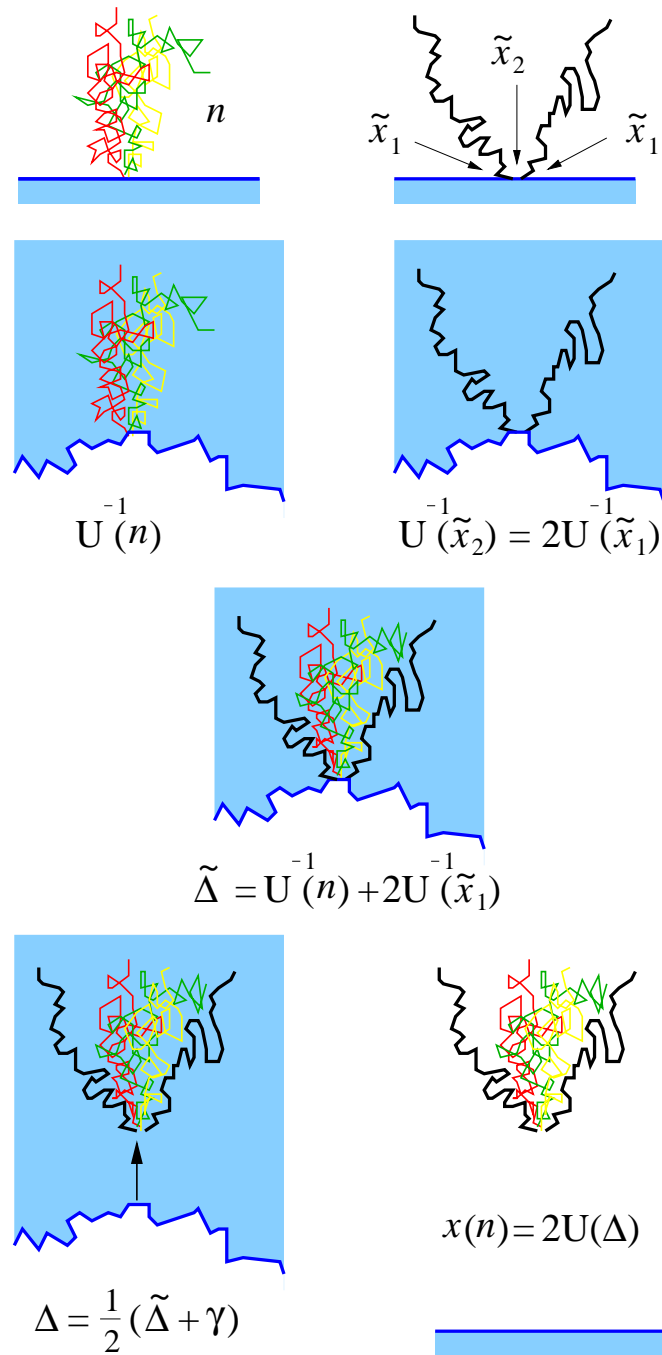


Figure 15. The quantum gravity construction (6.22) (6.23) of exponents (6.24).

The value of the QG b.s.d. of a simple semi-infinite random path is

$$(6.25) \quad U^{-1}(x_1) = \frac{1}{2}(1 \quad ):$$

It is derived in section 11 below and in appendix B from the exponents of the O(N) model, or of the SLE. It can be directly derived from Makarov's theorem :

$$(6.26) \quad \chi(n=1) = \chi'(n=1) = \frac{dx}{dn}(n=1) = 1;$$

which, applied to (6.24), leads to the same result. We thus finally get

$$(6.27) \quad \chi(n) = 2V^{-1} + U^{-1}(n) = 2U \left[ \frac{1}{2} + \frac{1}{2}U^{-1}(n) \right];$$

This result satisfies the identity:  $\chi(1) = 2U(1) = 2$ , which is related to Gauss's theorem, as mentioned above.

6.2.5. Multifractal Exponents. The multifractal exponents  $\chi(n)$  (6.12) are obtained from (6.13-6.16) as [57]

$$(6.28) \quad \begin{aligned} \chi(n) &= \chi(n) - 2 \\ &= \frac{1}{2}(n-1) + \frac{1}{4} \frac{2}{1} \left[ \frac{2}{4(1-n)^2} (2) \right]; \end{aligned}$$

Similar exponents, but associated with moments taken at the tip, later appeared in the context of the SLE process (see II in [62], and [101]; see also [102] for Laplacian random walks.) The whole family will be given in section 12.

The Legendre transform is easily performed to yield:

$$(6.29) \quad \frac{d}{dn} \chi(n) = \frac{1}{2} + \frac{1}{2} \frac{2}{4(1-n)^2};$$

$$(6.30) \quad f(\xi) = \frac{1}{8} \frac{2}{1} \xi^3 - \frac{1}{2} \frac{1}{1} - \frac{1}{4} \frac{2}{1} \xi; \quad \xi = \frac{1}{2} \xi + 1;$$

It is convenient to express the results in terms of the central charge  $c$  with the help of:

$$(6.31) \quad \frac{1}{4} \frac{2}{1} \xi = \frac{25-c}{24} \xi; \quad \frac{1}{4} \frac{2}{1} = \frac{1-c}{24};$$

We finally find the Multifractal Exponents

$$(6.32) \quad \chi(n) = \frac{1}{2}(n-1) + \frac{25-c}{24} \frac{r \frac{24n+1-c}{25-c}}{1};$$

$$(6.33) \quad \begin{aligned} D(n) &= \frac{\chi(n)}{n-1} = \frac{1}{2} + \frac{r \frac{24n+1-c}{25-c} + 1}{25-c}; \\ n-2 \quad n &= \frac{1-c}{24} \xi + 1; \end{aligned}$$

Multifractal Spectrum

$$(6.34) \quad = \frac{d}{dn} (n) = \frac{1}{2} + \frac{1}{2} \frac{25c}{24n+1} ;$$

$$(6.35) \quad f(\cdot) = \frac{25c}{48} \left( \frac{1}{2} + \frac{1}{24} \frac{c}{n} \right) ;$$

6.2.6. Other Multifractal Exponents. This formalism immediately allows generalizations. For instance, in place of a packet of  $n$  independent random walks, one can consider a packet of  $n$  independent self-avoiding walks  $P$ , which avoid the fractal boundary. The associated multifractal exponents  $\chi(C \wedge (P)^n)$  are given by (6.27), with the argument  $n$  in  $U^{-1}(n)$  simply replaced by  $\kappa((P)^n) = n\kappa(P) = \frac{5}{8}n$  [51]. These exponents govern the universal multifractal behavior of the moments of the probability that a SAW escapes from  $C$ . One then gets a spectrum  $f(\cdot)$  such that

$$f(\kappa(P)) = f(\cdot) = \hat{f}(\cdot);$$

thus unveiling the same invariant underlying wedge distribution as the harmonic measure (see also [56]).

6.3. Geometrical Analysis of Multifractal Spectra.

6.3.1. Makarov's Theorem. The generalized dimensions  $D(n)$  satisfy, for any  $c$ ,  $D(n=1) = D(n=1) = 1$ , or equivalently  $f(\cdot=1) = 1$ , i.e., Makarov's theorem [90], valid for any simply connected boundary curve. From (6.33), (6.34) we also note a fundamental relation, independent of  $c$ :

$$(6.36) \quad 3 - 2D(n) = 1 = \dots ;$$

We also have the superuniversal bounds:  $8c; 8n; \frac{1}{2} = D(1) \dots D(n) \dots D(n) = \frac{3}{2}$ , corresponding to  $0 \dots 2$ .

6.3.2. Symmetries. It is interesting to note that the general multifractal function (6.35) can also be written as

$$(6.37) \quad f(\cdot) = \frac{25c}{24} \left( \frac{1}{2} + \frac{1}{2} + \frac{1}{2} \right) ;$$

The multifractal functions  $f(\cdot) = \hat{f}(\cdot)$  - thus possess the invariance property (4.25) upon substitution of primed variables given by

$$(6.38) \quad 2 = \dots + \dots = \dots ;$$

this corresponds to the complementary domain of the wedge. This condition reads also  $D(n) + D(n^0) = 2$ : This basic symmetry, first observed [94] for the  $c=0$  result of [51] (see section 4.3), is valid for any conformally invariant boundary.

6.3.3. Equivalent Wedge Distribution. The geometrical multifractal distribution of wedges along the boundary takes the form:

$$(6.39) \quad \hat{f}(\cdot) = f - \dots = \dots \left( \frac{25c}{12} \left( \frac{1}{2} \right) \right) ;$$

Remarkably enough, the second term also describes the contribution by a wedge to the density of electromagnetic modes in a cavity [103]. The simple shift in (6.39),

25 ! 25 c, from the c = 0 case to general values of c, can then be related to results of conformal invariance in a wedge [104]. The partition function for the two sides of a wedge of angle and size R, in a CFT of central charge c, indeed scales as [105]

$$(6.40) \quad \hat{Z}(\alpha; c) \sim R^{-c(\alpha^2 - 12)};$$

Thus, one can view the c-dependence of result (6.39) as follows: the number of sites,  $R^{\hat{f}(\alpha; c)}$ , with local wedge angle along a random path with central charge c, is the same as the number of sites,  $R^{\hat{f}(\alpha; c=0)}$ , with wedge angle along a self-avoiding walk (c = 0), renormalized by the partition function  $\hat{Z}(\alpha)$  representing the presence of a c-CFT along such wedges:

$$R^{\hat{f}(\alpha; c)} / R^{\hat{f}(\alpha; c=0)} = \hat{Z}(\alpha; c);$$

6.3.4. Hausdorff Dimension of the External Perimeter. The maximum of  $f(\alpha)$  corresponds to  $n = 0$ , and gives the Hausdorff dimension  $D_{EP}$  of the support of the measure, i.e., the accessible or external perimeter as:

$$(6.41) \quad D_{EP} = \sup_{\alpha} f(\alpha) = f(\alpha(n=0))$$

$$(6.42) \quad = D(0) = \frac{3}{2} \frac{2}{(1-c)} = \frac{3}{2} \frac{1}{24} \frac{P_{1-c}}{P_{25-c}} \frac{P_{1-c}}{P_{1-c}};$$

This corresponds to a typical singularity exponent

$$(6.43)$$

$$\alpha(n=0) = 1 - \frac{1}{12} = \frac{1}{12} \frac{P_{1-c}}{P_{25-c}} \frac{P_{1-c}}{P_{1-c}} = (3 - 2D_{EP})^{-1};$$

and to a typical wedge angle

$$(6.44) \quad \alpha(n=0) = \alpha = (3 - 2D_{EP});$$

6.3.5. Probability Densities. The probability  $P(\alpha)$  to find a singularity exponent  $\alpha$  or, equivalently,  $\hat{P}(\alpha)$  to find an equivalent opening angle along the frontier is

$$(6.45) \quad P(\alpha) = \hat{P}(\alpha) / R^{\hat{f}(\alpha) - \hat{f}(\alpha^*)};$$

Using the values found above, one can recast this probability as (see also [56])

$$(6.46) \quad P(\alpha) = \hat{P}(\alpha) / \exp \left[ \frac{1}{24} \ln R \left( \frac{P_{1-c}}{P_{25-c}} \right)^{\frac{1}{1-c}} \frac{P_{25-c}}{2^{P_{1-c}}} \right];$$

where

$$\frac{1}{1-c} = - \frac{1}{2};$$

6.3.6. Universal Multifractal Data. The multifractal exponents  $\chi(n)$  (Fig. 16) or generalized dimensions  $D(n)$  (Fig. 17) appear quite similar for various values of c, and a numerical simulation would hardly distinguish the different universality classes, while the  $f(\alpha)$  functions, as we see, do distinguish these classes, especially for negative n, i.e. large  $\alpha$ . In Figure 18 we display the multifractal functions  $f(\alpha)$ , eq. (6.35), corresponding to various values of  $2 - c \leq 1$ , or, equivalently, to a number of components  $N \geq 2$  [0;2], and  $Q \geq 2$  [0;4] in the O(N) or Potts models (see below).

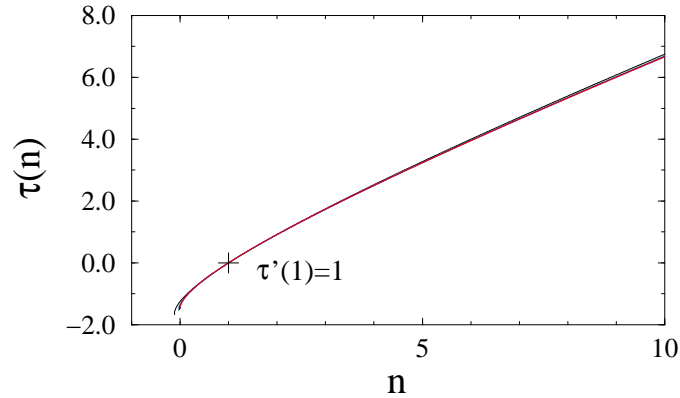


Figure 16. Universal multifractal exponents  $\tau(n)$ . The curves are indexed by the central charge  $c$ , and correspond to the same colors as in Figure 18 below: (black: 2D spanning trees ( $c = -2$ ); green: self-avoiding or random walks, and percolation ( $c = 0$ ); blue: Ising clusters or  $Q = 2$  Potts clusters ( $c = \frac{1}{2}$ ); red:  $N = 2$  loops, or  $Q = 4$  Potts clusters ( $c = 1$ )). The curves are almost indistinguishable at the scale shown.

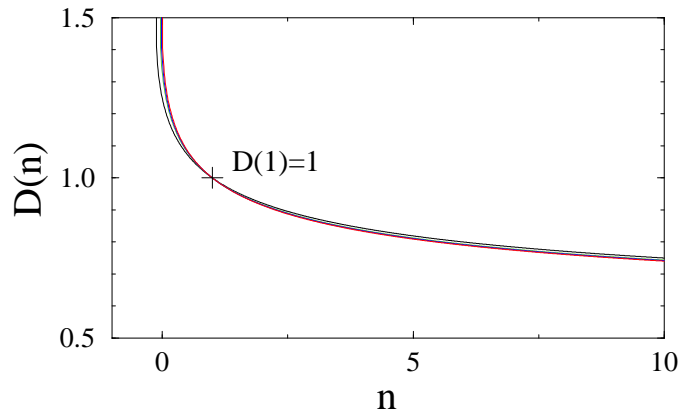


Figure 17. Universal generalized dimensions  $D(n)$ . The curves are indexed by the same colors as in Figure 18 below but are almost indistinguishable at the scale shown.

6.3.7. *Needles.* The singularity at  $\alpha = \frac{1}{2}$ , or  $\alpha = 2$ , in the multifractal functions  $f$ , or  $\hat{f}$ , corresponds to boundary points with a needle local geometry, and Beurling's theorem [92] indeed insures that the Hölder exponents are bounded below by  $\frac{1}{2}$ . This corresponds to large values of  $n$ , where, asymptotically, for any universality class,

$$(6.47) \quad 8c; \lim_{n \rightarrow 1} D(n) = \frac{1}{2};$$

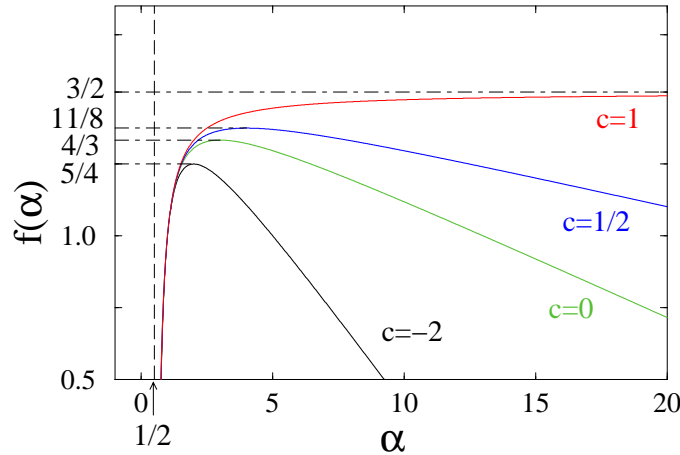


Figure 18. Universal harmonic multifractal spectra  $f(\alpha)$ . The curves are indexed by the central charge  $c$ , and correspond to: 2D spanning trees ( $c = -2$ ); self-avoiding or random walks, and percolation ( $c = 0$ ); Ising clusters or  $Q = 2$  Potts clusters ( $c = \frac{1}{2}$ );  $N = 2$  loops, or  $Q = 4$  Potts clusters ( $c = 1$ ). The maximal dimensions are those of the accessible frontiers. The left branches of the various  $f(\alpha)$  curves are largely indistinguishable, while their right branches split for large  $\alpha$ , corresponding to negative values of  $n$ .

6.3.8. Fractals. The right branch of  $f(\alpha)$  has a linear asymptote

$$(6.48) \quad \lim_{\alpha \rightarrow \infty} f(\alpha) = 1 + n = (1 - c)/24$$

The  $\alpha \rightarrow \infty$  behavior corresponds to moments of lowest order  $n \rightarrow n_*$ , where  $D(n)$  reaches its maximal value:  $8c$ ;  $D(n) = \frac{3}{2}$ , common to all simply connected, conformally-invariant, boundaries.

This describes almost inaccessible sites: Define  $N(H)$  as the number of boundary sites having a given probability  $H$  to be hit by a RW starting at infinity; the MF formalism yields, for  $H \rightarrow 0$ ; a power law behavior

$$(6.49) \quad N(H) \sim \int_0^H H^{-(1+n)}$$

with an exponent

$$(6.50) \quad 1 + n = \frac{23 + c}{24} < 1$$

6.3.9. Ising Clusters. A critical Ising cluster ( $c = \frac{1}{2}$ ) possesses a multifractal spectrum with respect to the harmonic measure:

$$(6.51) \quad \langle n \rangle = \frac{1}{2} \langle n - 1 \rangle + \frac{7}{48} \frac{P}{48n + 1} - 7$$

$$(6.52) \quad f(\alpha) = \frac{49}{96} \frac{3}{2} \frac{1}{1 - \frac{1}{48}}; \quad 2 \frac{1}{2} + 1$$

with the dimension of the accessible perimeter

$$(6.53) \quad D_{EP} = \sup f(\delta; c = \frac{1}{2}) = \frac{11}{8};$$

6.3.10.  $Q = 4$  Potts Clusters, and "ultimate Norway". The limit multifractal spectrum is obtained for  $c = 1$ , which is an upper or lower bound for all  $c$ 's, depending on the position of  $\delta$  with respect to 1:

$$\begin{aligned} f(\delta; c < 1) &< f(\delta; c = 1); \delta < 1; \\ f(\delta = 1; c) &= 1; 8c; \\ f(\delta; c < 1) &> f(\delta; c = 1); \delta > 1; \end{aligned}$$

This MF spectrum provides an exact example of a left-sided MF spectrum, with an asymptote  $f(\delta = 1; c = 1) = \frac{3}{2}$  (Fig. 18). It corresponds to singular boundaries where  $\hat{f}(\delta = 0; c = 1) = \frac{3}{2} = D_{EP}$ , i.e., where the external perimeter is everywhere dominated by "fjords", with typical angle  $\hat{\alpha} = 0$ . It is tempting to call it the "ultimate Norway".

The frontier of a  $Q = 4$  Potts Fortuin-Kasteleyn cluster, or the  $SLE_{\kappa=4}$  provide such an example for this left-handed multifractal spectrum ( $c = 1$ ) (see section 9). The MF data are:

$$(6.54) \quad \langle n \rangle = \frac{1}{2} (n-1) + \frac{P}{n-1};$$

$$(6.55) \quad f(\delta) = \frac{1}{2} \left( 3 - \frac{1}{2^{1-\delta}} \right); \quad \delta \geq \frac{1}{2};$$

with accessible sites forming a set of Hausdorff dimension

$$(6.56) \quad D_{EP} = \sup f(\delta; c = 1) = \frac{3}{2};$$

which is also the maximal value common to all multifractal generalized dimensions  $D(n) = \frac{1}{n-1} \langle n \rangle$ . The external perimeter which bears the electrostatic charge is a non-intersecting simple path. We therefore arrive at the striking conclusion that in the plane, a conformally-invariant scaling curve which is simple has a Hausdorff dimension at most equal to  $D_{EP} = 3/2$  [57]. The corresponding  $Q = 4$  Potts frontier, while still possessing a set of double points of dimension 0, actually develops a logarithmically growing number of double points [106].



### 7. Higher Universal Multifractal Spectra

#### 7.1. Double-Sided Spectrum .

7.1.1. Simple Random Paths & Double-Sided Potential. As in section 4.4, we consider here the specific case where the fractal set  $C$  is a (conformally-invariant) simple scaling curve, that is, it does not contain double points. The frontier  $\partial C$  is thus identical with the set itself:  $\partial C = C$ . Each point of the curve can then be reached from infinity, and we address the question of the simultaneous behavior of the potential on both sides of the curve. Notice, however, that one could also address the case of non-simple random paths, by concentrating on the double-sided potential near cut-points, as we did in section 4.4 for cut-points in Brownian paths.

The potential  $H$  scales as

$$(7.1) \quad H_+(z) \sim w^{2-\alpha} \text{ as } z \rightarrow w \text{ from the left;}$$

when approaching  $w$  on one side of the scaling curve, while scaling as

$$(7.2) \quad H_-(z) \sim w^{2-\alpha'} \text{ as } z \rightarrow w \text{ from the right;}$$

on the other side. The multifractal formalism now characterizes subsets  $C$  of boundary sites with two such Hölder exponents,  $\alpha$  and  $\alpha'$ , by their Hausdorff dimension  $f_2(\alpha, \alpha') = \dim(C)$ . The standard one-sided multifractal spectrum  $f(\alpha)$  is then recovered as the supremum:

$$(7.3) \quad f(\alpha) = \sup_{\alpha'} f_2(\alpha, \alpha')$$

7.1.2. Equivalent W edges. As above, one can also define two equivalent "electrostatic" angles from singularity exponents  $\alpha$  and  $\alpha'$ , as  $\alpha = \alpha'$  and the MF dimension  $\hat{f}_2(\alpha, \alpha')$  of the boundary subset with such  $\alpha$  and  $\alpha'$  is then

$$(7.4) \quad \hat{f}_2(\alpha, \alpha') = f_2(\alpha = \alpha', \alpha = \alpha')$$

7.1.3. Harmonic Moments. Consider the harmonic measure (as seen from infinity)  $H(w; r) = H(C \cap B(w; r))$  of the intersection of  $C$  and the ball  $B(w; r)$  centered at point  $w \in C$ , i.e., the probability that a Brownian path, launched from infinity, first hits the frontier  $C$  inside the ball  $B(w; r)$ . Let us consider a covering of the frontier by such balls centered at points forming a discrete subset  $C_r$  of  $C$ .

The double multifractal spectrum will be computed from the double moments of the harmonic measure on both sides of the random fractal curve:

$$(7.5) \quad Z_{n, n^0} = \sum_{w \in C_r} [H_+(w; r)]^n [H_-(w; r)]^{n^0};$$

where  $H_+(w; r)$  and  $H_-(w; r)$  are respectively the harmonic measures on the "left" or "right" sides of the random fractal. These double moments have a multifractal scaling behavior

$$(7.6) \quad Z_{n, n^0} \sim (r=R)^{2(n, n^0)};$$

where the exponent  $2(n, n^0)$  now depends on two moment orders  $n, n^0$ . As in section 4.4, the Hausdorff dimension is given by the double Legendre transform:

$$(7.7) \quad \begin{aligned} \alpha &= \frac{\partial}{\partial n} 2(n, n^0); & \alpha' &= \frac{\partial}{\partial n^0} 2(n, n^0); \\ f_2(\alpha, \alpha') &= n + n^0 - 2(n, n^0); \\ n &= \frac{\partial f_2}{\partial \alpha}(\alpha, \alpha'); & n^0 &= \frac{\partial f_2}{\partial \alpha'}(\alpha, \alpha'); \end{aligned}$$

From definition (7.5) and eq. (7.6), we recover for  $n^0 = 0$  the one-sided multifractal exponents

$$(7.8) \quad \tau(n) = \tau_2(n; n^0 = 0);$$

and putting these values in the Legendre transform (7.7) yields identity (7.3), as it must.

7.2. Higher Multifractality of Path Vertices.

7.2.1. Definition. One can consider a star configuration  $S_m$  of a number  $m$  of similar simple scaling paths, all originating at the same vertex  $w$ . Higher moments  $Z_{n_1, n_2, \dots, n_m}$  are then defined as

$$(7.9) \quad Z_{n_1, n_2, \dots, n_m} = \sum_{w \in S_m} \prod_{i=1}^m [H_i(w; r)]^{n_i} \quad ;$$

where

$$H_i(w; r) = H_i(C \setminus B(w; r))$$

is the harmonic measure (or, equivalently, local potential at distance  $r$ ) in the  $i$ th sector of radius  $r$  located between paths  $i$  and  $i + 1$ , with  $i = 1; \dots; m$ , and by periodicity  $m + 1 = 1$ . These higher moments have a multifractal scaling behavior

$$(7.10) \quad Z_{n_1, n_2, \dots, n_m}(r=R) \sim r^{-\tau_m(n_1, n_2, \dots, n_m)};$$

where the exponent  $\tau_m(n_1, n_2, \dots, n_m)$  now depends on the set of moment orders  $n_1, n_2, \dots, n_m$ . The generalization of the usual Legendre transform of multifractal formalism eqs. (4.7) (7.7) now involves a multifractal function  $f_m(\tau; \tau; \dots; \tau)$  depending on  $m$  local exponents  $\tau_i$ :

$$(7.11) \quad \begin{aligned} \tau_i &= \frac{\partial \tau_m}{\partial n_i}(\tau; \tau; \dots; \tau); \\ f_m(\tau; \tau; \dots; \tau) &= \sum_{i=1}^m n_i \tau_i^{-1}(\tau; \tau; \dots; \tau); \\ n_i &= \frac{\partial f_m}{\partial \tau_i}(\tau; \tau; \dots; \tau); \end{aligned}$$

7.2.2. Summing over Contact Points. At this point, a caveat is in order. The reader may wonder about the meaning of the sum over points  $w$  in (7.9), since there is only one  $m$ -vertex in a star. This notation is kept for consistency with the  $m = 2$  case, and can be understood as follows. Along a scaling path, one can consider the subset  $S_m$  of contact points of order  $m$ , where the path folds onto itself several times on large (macroscopic) scales  $R$ , and returns to itself at a short scale  $r$ , thereby forming local stars of order  $m$ . The sum in moment (7.9) runs over such higher contact points along the path, and for  $n_i = 0; \dots; 0$ , their number in a domain of size  $R$  then scales for  $r=R \rightarrow 0$  as

$$(7.12) \quad Z_{0;0;\dots;0}(r=R) \sim R^{D_m};$$

so that the formal Hausdorff dimension  $D_m$  associated with this set of order  $m$  contact points is

$$(7.13) \quad D_m = \tau_m(0;0;\dots;0) = \sup_{\tau} f_m(\tau; \tau; \dots; \tau);$$

One can equivalently consider the density, or the probability for these points to appear:  $P_{S_m}(r) = (r=R)^{\chi_m(0;0;\dots;0)}$ , such that

$$(7.14) \quad Z_{0;0;\dots;0} = (R=r)^2 P_{S_m}(r);$$

whence  $\chi_m(0;0;\dots;0) = \chi_m(0;0;\dots;0) - 2$ . For  $m$  large enough, the density vanishes for  $r \neq 0$  fast enough, so that  $\chi_m(0;0;\dots;0) = -2$ , and  $D_m = 0$  (see below).

7.2.3. Local Moments. Alternatively, one can define shifted exponents

$$\tilde{\chi}_m = \chi_m + D_m = \chi_m(n_1; n_2; \dots; n_m) - \chi_m(0;0;\dots;0);$$

which describe the scaling of local averages at a given  $m$ -vertex

$$(7.15) \quad h[H_1(w;r)]^{\tilde{\chi}_m^{(1)}} [H_2(w;r)]^{\tilde{\chi}_m^{(2)}} \dots [H_m(w;r)]^{\tilde{\chi}_m^{(m)}} = (r=R)^{\tilde{\chi}_m(n_1; n_2; \dots; n_m)};$$

By the Legendre transform (7.11) these exponents give the subtracted spectrum  $f_m(f_{ig}) = \sup_{f_{ig}} f_m(f_{ig})$  directly. The latter has a direct physical meaning: the probability  $P(f_{ig})$  to find a set of local singularity exponents  $f_{ig}$  in the  $m$  sectors of an  $m$ -arm star scales as:

$$(7.16) \quad P_m(f_{ig}) / R^{f_m(f_{ig})} = R^{\sup f_m};$$

7.2.4. Recursion between Spectra. From definition (7.9) and eq. (7.10), we get the lower  $(m-1)$ -multifractal spectrum as

$$(7.17) \quad \chi_m^{[m-1]}(n_1; n_2; \dots; n_m) = \chi_m(n_1; n_2; \dots; n_m) - \chi_m(n_m) = 0;$$

In these exponents, the subscript  $m$  stays unchanged since it counts the number of arms of the star, while the potential is evaluated only at  $m-1$  sectors amongst the  $m$  possible ones. More generally, one can define exponents

$$\chi_m^{[p]}(n_1; n_2; \dots; n_p) = \chi_m(n_1; n_2; \dots; n_p; n_{p+1} = 0; \dots; n_m \neq 0);$$

where  $p$  takes any value in  $1 \leq p \leq m$ . Note that according to the commutativity of the star algebra for exponents between mutually-avoiding paths (see eq.(3.14) and below), the result does not depend on the choice of the  $p$  sectors amongst  $m$ . Putting these values  $n_{p+1} = 0; \dots; n_m \neq 0$  in the Legendre transform (7.11) yields the identity:

$$(7.18) \quad f_m^{[p]}(\dots; p) = \sup_{p+1; \dots; m} f_m(\dots; p; p+1; \dots; m);$$

Note that the usual one-sided spectrum is in this notation  $f(\dots) = f_2^{[1]}(\dots)$ .

7.3. Explicit Higher Multifractal Exponents and Spectra.

7.3.1. Scaling Dimensions of Multiple-Sided Paths. In analogy to eqs. (6.12), (6.24), the exponent  $\chi_2(n; n^0)$  is associated with a scaling dimension  $x_2(n; n^0)$

$$(7.19) \quad \begin{aligned} \chi_2(n; n^0) &= x_2(n; n^0) - 2 \\ x_2(n; n^0) &= 2V^{-1} + U^{-1}(n) + U^{-1}(n^0) \end{aligned}$$

Similarly, the  $m$ -order case is given by

$$\begin{aligned} x_m(n_1; n_2; \dots; n_m) &= x_m(n_1; n_2; \dots; n_m) - 2 \\ x_m(n_1; n_2; \dots; n_m) &= 2V^{-1} \sim_m + U^{-1}(n_1) + U^{-1}(n_2) + \dots + U^{-1}(n_m) \end{aligned}$$

Here  $\sim_m$  is the quantum gravity boundary scaling dimension of the  $m$ -star  $S_m$  made of  $m$  (simple) scaling paths. According to the star algebra (6.21) valid for simple paths, we have:

$$(7.20) \quad \sim_m = m U^{-1}(x_1) = \frac{m}{2} U^{-1}(x_2) = m \frac{1}{2} ;$$

where  $x_2$  is the boundary scaling dimension of a scaling path, i.e., a 2-star, already considered in eq. (6.22), and such that  $U^{-1}(x_2) = 1$ .

7.3.2. Multiple Legendre Transform. The calculation of the multiple Legendre transform eq. (7.7) is as follows. We start from a total (boundary) quantum scaling dimension of the  $m$ -path  $S_m$  dressed by Brownian paths

$$(7.21) \quad = m \frac{1}{2} + \sum_{i=1}^{X^n} U^{-1}(n_i) ;$$

such that

$$(7.22) \quad x_m(n_1; n_2; \dots; n_m) = 2V^{-1} ;$$

Using the shift identity (6.17)

$$U^{-1}(n) = \frac{1}{2} + \frac{1}{2} V^{-1}(n) ; \quad V^{-1}(n) = \frac{P}{4(1 - )n + 2} ;$$

gives

$$(7.23) \quad = \frac{m}{2} + \frac{1}{2} \sum_{i=1}^{X^n} V^{-1}(n_i) ;$$

and

$$(7.24) \quad \frac{\partial x_m}{\partial n_i} = 2V^0( ) \frac{\partial}{\partial n_i} = V^0( ) V^{-1}(n_i)^0 ;$$

Since

$$V^0( ) = \frac{1}{2} ;$$

we get

$$(7.25) \quad \frac{\partial}{\partial n_i} = \frac{P}{4(1 - )n_i + 2} = \frac{1}{V^{-1}(n_i)} ;$$

or, equivalently

$$(7.26) \quad V^{-1}(n_i) = \frac{1}{i} ; \quad n_i = V \frac{1}{i} ;$$

One gets from eqs. (7.23) and (7.26) the useful identity

$$(7.27) \quad = \frac{m}{2} \prod_{i=1}^m \frac{1}{2} X_i^{n_i} : \quad ! \quad 1$$

This yields the simple expression for  $f_m$

$$(7.28) \quad f_m(f_{i=1}^m g) = 2 \prod_{i=1}^m V_i + \frac{X_i^n}{i} V_i : \quad ! \quad 1$$

Recalling (6.13), collecting the terms, and using identity (7.27) for  $\phi$ , finally gives after some calculations the explicit formulae

$$(7.29) \quad f_m(f_{i=1}^m g) = 2 + \frac{2}{2(1-n_1)} \frac{1}{8(1-n_1)^m} \prod_{i=1}^m \frac{1}{2} X_i^{n_i} : \quad ! \quad 1$$

$$\frac{2}{4(1-n_1)} \prod_{i=1}^m X_i^{n_i}$$

with

$$(7.30) \quad \phi = \frac{1}{4(1-n_1)^{n_1+2}} \left( \frac{m}{2} + \frac{1}{2} \sum_{j=1}^m X_j^{n_j} \right) \frac{1}{4(1-n_1)^{n_1+2} A} : \quad ! \quad 1$$

Substituting expressions (6.31) gives in terms of  $c$

$$(7.31) \quad f_m(f_{i=1}^m g) = \frac{25}{12} c \frac{1}{8(1-n_1)^m} \prod_{i=1}^m \frac{1}{2} X_i^{n_i} : \quad ! \quad 1$$

$$\frac{1}{24} c \prod_{i=1}^m X_i^{n_i}$$

where the central charge  $c$  and the parameter  $\phi$  are related by eq. (6.31). The self-avoiding walk case (4.43) is recovered for  $c=0$ ;  $\phi=1=2$ .

The domain of definition of the poly-multifractal function  $f$  is independent of  $c$  and given by

$$(7.32) \quad \prod_{i=1}^m \frac{1}{2} X_i^{n_i} > 0;$$

as verified by eq. (7.30).

### 7.3.3. One and Two-Sided Cases. Notice that the $m=1$ case,

$$(7.33) \quad f_1(\phi) = \frac{25}{12} c \frac{1}{8(1-n_1)} \frac{1}{2} \frac{1}{24} c ;$$

corresponds to the potential in the vicinity of the tip of a conformally-invariant scaling path, and naturally differs from the usual  $f(\phi) = \sup_{\phi} f_2(\phi; \phi_0)$  spectrum, which describes the potential on one side of the scaling path.

The two-sided case is obtained for  $m = 2$  as

$$(7.34) \quad f_2(\rho; \rho^0) = \frac{25}{12} c \frac{1}{2(1-\rho)} \left( 1 - \frac{1}{2} \left( \frac{1}{\rho} + \frac{1}{\rho^0} \right) \right)^{-1} \\ \frac{1}{24} c (\rho + \rho^0);$$

$$(7.35) \quad = \frac{1}{4(1-\rho)^{n+2}} \left( 1 + \frac{1}{2} \frac{\rho}{4(1-\rho)^{n+2}} + \frac{\rho}{4(1-\rho)^{n+2}} \right)^{-1};$$

This doubly multifractal spectrum possesses the desired properties, like

$$\sup_{\rho^0} f_2(\rho; \rho^0) = f(\rho);$$

where  $f(\rho)$  is (6.35) above.

7.3.4. Local Wedge Description. We can also substitute equivalent "electrostatic" angles  $\alpha_i = \frac{\rho}{\rho^0}$  for the variables  $\rho_i$ . This gives a new distribution:

$$(7.36) \quad \hat{f}_m(\alpha_{i=1;\dots;m}) = f_m(\alpha_{i=1;\dots;m}) = \frac{2}{2(1-\alpha)} \frac{2}{4(1-\alpha)} \frac{X^n}{\prod_{i=1}^m \alpha_i} \\ \frac{1}{8(1-\alpha)^{m^2}} \left( 1 - \frac{1}{2} \frac{X^n}{\prod_{i=1}^m \alpha_i} \right)^{-1};$$

The domain of definition of distribution  $\hat{f}_m$  is the image of domain (7.32) in  $\alpha$ -variables:

$$(7.37) \quad \prod_{i=1}^m \alpha_i \leq 2;$$

The total electrostatic angle is thus less than  $2$ , which simply accounts for the electrostatic screening of local wedges by fractal randomness, as expected.

7.3.5. Maxima and Global Hausdorff Dimension. The maxima of  $f_m$  or  $\hat{f}_m$  are by construction obtained for  $\rho_i = 0; \forall i = 1; \dots; m$ : Eq. (7.30) gives the values of typical singularity exponents  $\alpha_i$  at the maximum of  $f_m$ :

$$(7.38) \quad \alpha_i = \frac{\rho}{\rho^0} = \frac{m-1}{2} \frac{1}{\rho^0}; \quad \forall i = 1; \dots; m;$$

corresponding to a maximal value of  $f_m$  or  $\hat{f}_m$ :

$$D_m = \sup f_m = f_m(\alpha_{i=1;\dots;m}) = \hat{f}_m(\alpha_{i=1;\dots;m}) \\ = \frac{2}{2(1-\alpha)} \frac{1}{8(1-\alpha)^{m^2}};$$

As anticipated, for  $m$  large enough, i.e.,  $m \geq \frac{2}{1-\alpha}$ , this Hausdorff dimension  $D_m$  (7.13) formally becomes negative. Since  $1-\alpha < 1$ , and  $m$  integer, this already happens for  $m \geq 3$  (3-stars), except for  $\alpha = 0$ , which gives the condition  $m \geq 4$  and again corresponds to the  $c = 1$  "ultimate Norway" fractal boundary.

7.3.6. Local Probabilities and Shifted Spectrum. As mentioned above, the following interpretation of the poly-multifractal spectrum holds. The probability  $P(f_{i,g}) = \hat{P}(f_{i,g})$  to find a set of local singularity exponents  $f_{i,g}$  or equivalent angles  $f_{i,g}$  in the  $m$  sectors of an  $m$ -arm star is given by the ratio

$$(7.39) \quad P_m(f_{i,g}) / R^{f_m(f_{i,g})} = R^{\sup f_m}$$

of the respective number of configurations to the total one. We therefore arrive at a probability, here written in terms of the equivalent electrostatic angles:

$$(7.40) \quad \hat{P}_m(f_{i,g}) / R^{\hat{f}_m(f_{i,g})} = \hat{f}_m(\hat{f}_{i,g});$$

$$(7.41) \quad \hat{f}_m(f_{i,g}) / \hat{f}_m(\hat{f}_{i,g}) = \frac{1}{8(1 - \dots)^2} \prod_{i=1}^m \frac{2}{1 - \dots} \dots$$

For a large scaling star, the typical set of singularity exponents  $\hat{f}_{i,g}$ , or wedge angles  $\hat{f}_{i,g}$ , is thus given by the symmetric set of values (7.38).

### 8. Winding of Conformally Invariant Curves

Another important question arises concerning the geometry of the equipotential lines near a random (CI) fractal curve. These lines are expected to rotate wildly, or wind, in a spiralling motion that closely follows the boundary itself. The key geometrical object is here the logarithmic spiral, which is conformally invariant (Fig. 19). The MF description should generalize to a mixed multifractal spectrum,

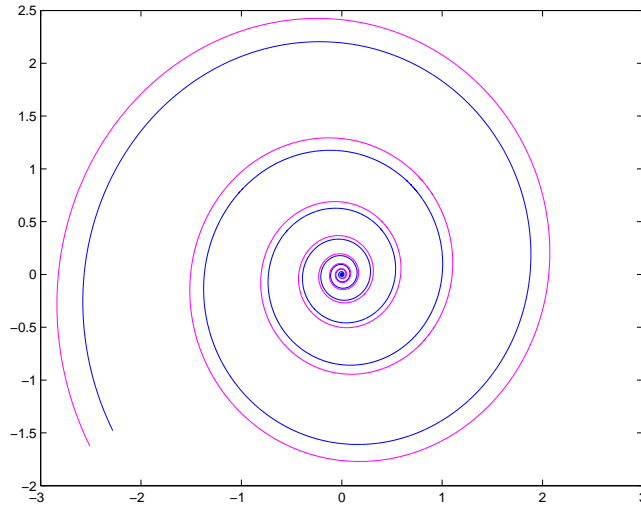


Figure 19. A double logarithmic spiral mimicking the local geometry of the two strands of the conformally-invariant frontier.

accounting for both scaling and winding of the equipotentials [71].

In this section, we describe the exact solution to this mixed MF spectrum for any random CI curve [72]. In particular, it is shown to be related by a scaling law

to the usual harmonic MF spectrum. We use the same conformal tools as before, fusing quantum gravity and Coulomb gas methods, which allow the description of Brownian paths interacting and winding with CI curves, thereby providing a probabilistic description of the potential map near any CI random curve.

8.1. Harmonic Measure and Rotations. Consider a single (CI) critical random cluster, generically called  $C$ . Let  $H(z)$  be the potential at an exterior point  $z \in \mathbb{C}$ , with Dirichlet boundary conditions  $H(w \in \partial C) = 0$  on the outer (simply connected) boundary  $\partial C$  of  $C$ , and  $H(w) = 1$  on a circle  $\partial \mathbb{D}_R$ , i.e., of a large radius scaling like the average size  $R$  of  $C$ . The potential  $H(z)$  is identical to the probability that a Brownian path started at  $z$  escapes to  $\partial \mathbb{D}_R$  without having hit  $C$ .

Let us now consider the degree with which the curves wind in the complex plane about point  $w$  and call  $\theta(z) = \arg(z - w)$ . In the scaling limit, the multifractal formalism, here generalized to take into account rotations [71], characterizes subsets  $\partial C$  of boundary sites by a Holder exponent  $\alpha$ , and a rotation rate  $\beta$ , such that their potential lines respectively scale and logarithmically spiral as

$$(8.1) \quad \begin{aligned} H(z \in \mathbb{D}_R \setminus \partial C; \alpha, \beta) &\sim r^{-\alpha}; \\ \theta(z \in \mathbb{D}_R \setminus \partial C; \alpha, \beta) &\sim \ln r; \end{aligned}$$

in the limit  $r = |z - w| \rightarrow 0$ . The Hausdorff dimension  $\dim(\partial C; \alpha, \beta) = f(\alpha, \beta)$  defines the mixed MF spectrum, which is CI since under a conformal map both  $\alpha$  and  $\beta$  are locally invariant.

As above, we consider the harmonic measure  $H(w; r)$ , which is the integral of the Laplacian of  $H$  in a disk  $B(w; r)$  of radius  $r$  centered at  $w \in \partial C$ , i.e., the boundary charge in that disk. It scales as  $r^{-\alpha}$  with the same exponent as in (8.1), and is also the probability that a Brownian path started at large distance  $R$  first hits the boundary at a point inside  $B(w; r)$ . Let  $\theta(w; r)$  be the associated winding angle of the path down to distance  $r$  from  $w$ . The mixed moments of  $H$  and  $\theta$ , averaged over all realizations of  $C$ , are defined as

$$(8.2) \quad Z_{n,p} = \sum_{w \in \partial C, r} H^n(w; r) \exp(p\theta(w; r)) \quad (r=R)^{(n,p)}$$

where the sum runs over the centers of a covering of the boundary by disks of radius  $r$ , and where  $n$  and  $p$  are real numbers. As before, the  $n^{\text{th}}$  moment of  $H(w; r)$  is the probability that  $n$  independent Brownian paths diffuse along the boundary and all first hit it at points inside the disk  $B(w; r)$ . The angle  $\theta(w; r)$  is then their common winding angle down to distance  $r$  (Fig. 20)

The scaling limit in (8.2) involves multifractal scaling exponents  $f(n;p)$  which vary in a non-linear way with  $n$  and  $p$ . They give the multifractal spectrum  $f(\alpha, \beta)$  via a symmetric double Legendre transform :

$$(8.3) \quad \begin{aligned} f(\alpha, \beta) &= \frac{\partial}{\partial n} f(n;p); \quad \beta = \frac{\partial}{\partial p} f(n;p); \\ f(\alpha, \beta) &= n + p f(n;p); \\ n &= \frac{\partial f}{\partial \alpha}(\alpha, \beta); \quad p = \frac{\partial f}{\partial \beta}(\alpha, \beta); \end{aligned}$$

Because of the ensemble average (8.2),  $f(\alpha, \beta)$  can become negative for some  $\alpha, \beta$ .



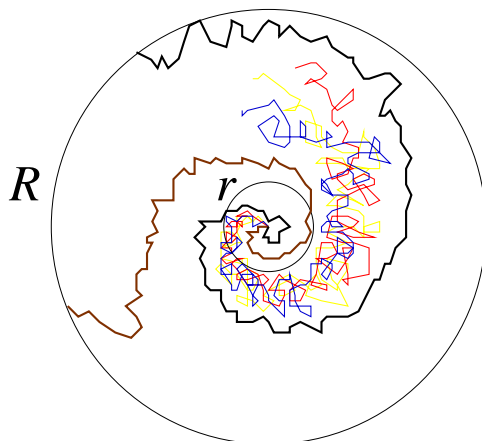


Figure 20. Two-sided boundary curve  $\partial C$  and Brownian  $n$ -packet winding together from the disk of radius  $r$  up to distances of order  $R$ , as measured by the winding angle  $\theta(w; r) = \arg(\partial C^n)$  as in (8.2) and in (8.10).

8.2. Exact Mixed Multifractal Spectra. The 2D conformally invariant random statistical system is labelled by its central charge  $c$ ,  $c \in \mathbb{Z}$  [1]. The main result is the following exact scaling law [72]:

$$(8.4) \quad f(\nu; \omega) = (1 + \omega^2) f\left(\frac{\nu}{1 + \omega^2}\right) + b \omega^2;$$

$$b = \frac{25}{12} c - 2;$$

where  $f(\nu) = f(\nu; \omega = 0)$  is the usual harmonic MF spectrum in the absence of prescribed winding, first obtained in [57], and described in section 6, eq. (6.35). It can be recast as:

$$(8.5) \quad f(\nu) = \frac{1}{2} + b \frac{b^2}{1};$$

$$b = \frac{25}{12} c;$$

We thus arrive at the very simple formula for the mixed spectrum :

$$(8.6) \quad f(\nu; \omega) = \frac{1}{2} + b \frac{b^2}{1 + \omega^2};$$

Notice that by conformal symmetry

$$\sup_{\omega} f(\nu; \omega) = f(\nu; \omega = 0);$$

i.e., the most likely situation in the absence of prescribed rotation is the same as  $\omega = 0$ , i.e. winding-free. The domain of definition of the usual  $f(\nu)$  (8.6) is  $1 \leq \nu \leq 2$  [57, 92], thus for  $\omega$ -spiralling points eq. (8.4) gives

$$(8.7) \quad \frac{1}{2} (1 + \omega^2) \leq \nu \leq 2;$$

in agreement with a theorem by Beurling [92, 71].

We have seen in section 6.3 the geometrical meaning to the exponent  $\alpha$ : For an angle with opening  $\theta$ ,  $\alpha = \frac{1}{2} \theta$ , the quantity  $\alpha$  can be regarded as a local generalized angle with respect to the harmonic measure. The geometrical MF spectrum of the boundary subset with such opening angle  $\theta$  and spiralling rate reads from (8.6)

$$\hat{f}(\alpha; \theta) = f(\alpha = -; \theta) = -\alpha + b \frac{1}{2} + \frac{1}{\frac{2}{1+\alpha^2}} \quad !$$

As in (8.7), the domain of definition in the  $\alpha$  variable is

$$0 \leq \alpha < \frac{1}{2} \theta; \quad \theta = 2\alpha = (1+\alpha^2):$$

The maximum is reached when the two frontier strands about point  $w$  locally collapse into a single  $\theta$ -spiral, whose inner opening angle is  $\theta(\alpha)$  [92].

In the absence of prescribed winding ( $\theta = 0$ ), the maximum  $D_{EP} := D_{EP}(0) = \sup f(\alpha; \theta = 0)$  gives the dimension of the external perimeter of the fractal cluster, which is a simple curve without double points, and may differ from the full hull [57, 53]. Its dimension (6.42) reads in this notation

$$D_{EP} = \frac{1}{2}(1+b) \frac{1}{2} \frac{1}{b(b-2)}; \quad b = \frac{25}{12} c:$$

It corresponds to typical values  $\alpha = 0$  ( $n = 0; p = 0$ ) and  $\alpha = \frac{1}{2} \theta = \frac{1}{2} (3 - 2D_{EP})$ :

For spirals, the maximum value  $D_{EP}(\theta) = \sup f(\alpha; \theta)$  still corresponds in the Legendre transform (8.3) to  $n = 0$ , and gives the dimension of the subset of the external perimeter made of logarithmic spirals of type  $\theta$ . Owing to (8.4) we immediately get

$$(8.8) \quad D_{EP}(\theta) = (1 + \frac{1}{2} \theta^2) D_{EP} - \frac{1}{2} \theta^2:$$

This corresponds to typical scaled values

$$\alpha(\theta) = (1 + \frac{1}{2} \theta^2)^{-1/2}; \quad \alpha(\theta) = \frac{1}{2} \theta = (1 + \frac{1}{2} \theta^2):$$

Since  $b \geq 2$  and  $D_{EP} \geq 3/2$ , the EP dimension decreases with spiralling rate, in a simple parabolic way.

Fig. 21 displays typical multifractal functions  $f(\alpha; \theta; c)$ . The example chosen,  $c = 0$ , corresponds to the cases of a SAW, or of a percolation EP, the scaling limits of which both coincide with the Brownian frontier [51, 52, 55]. The original singularity at  $\alpha = \frac{1}{2}$  in the rotation free MF functions  $f(\alpha; 0)$ , which describes boundary points with a needle local geometry, is shifted for  $\theta \neq 0$  towards the minimal value (8.7). The right branch of  $f(\alpha; \theta)$  has a linear asymptote  $\lim_{\alpha \rightarrow 1/2} f(\alpha; \theta) = \frac{1}{2} (1 - c) = 24$ : Thus the  $\theta$ -curves all become parallel for  $\theta \rightarrow 1$ , i.e.,  $\theta \rightarrow 0^+$ , corresponding to deep fjords where winding is easiest.

Limit multifractal spectra are obtained for  $c = 1$ , which exhibit exact examples of left-sided MF spectra, with a horizontal asymptote  $f(\alpha \rightarrow 1/2; \theta; c = 1) = \frac{3}{2} - \frac{1}{2} \theta^2$  (Fig. 22). This corresponds to the frontier of a  $Q = 4$  Potts cluster (i.e., the SLE<sub>4</sub>), a universal random scaling curve, with the maximum value  $D_{EP} = 3/2$ , and a vanishing typical opening angle  $\alpha = 0$ , i.e., the "ultimate Norway" where the EP is dominated by "fjords" everywhere [57, 60]. Fig. 23 displays the dimension  $D_{EP}(\theta)$  as a function of the rotation rate  $\theta$ , for various values of  $c \in [0, 1]$ , corresponding to different statistical systems. A gain, the  $c = 1$  case shows the least decay with  $\theta$ , as expected from the predominance of fjords there.

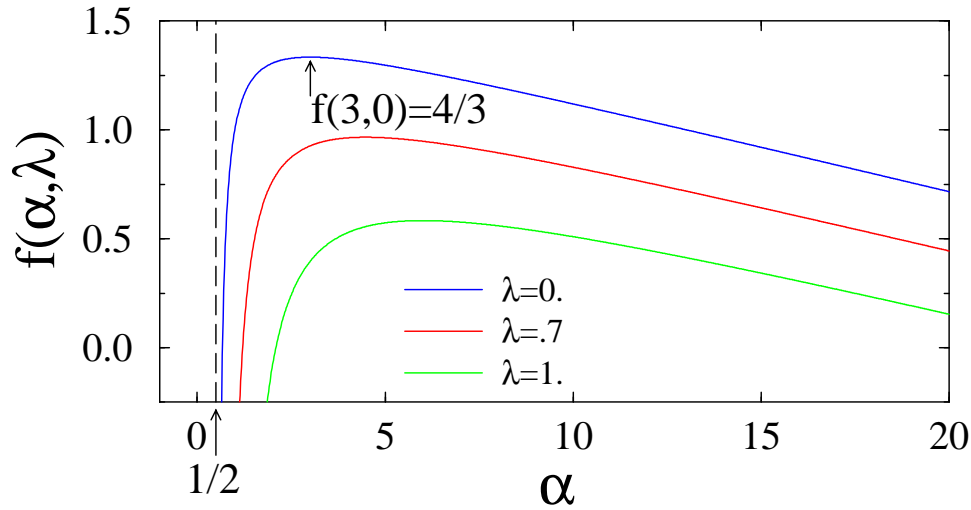


Figure 21. Universal multifractal spectrum  $f(\alpha, \lambda)$  for  $c = 0$  (Brownian frontier, percolation EP and SAW), and for three different values of the spiralling rate  $\lambda$ . The maximum  $f(3;0) = 4/3$  is the Hausdorff dimension of the frontier.

8.3. Conformal Invariance and Quantum Gravity. We now give the main lines of the derivation of exponents  $(n;p)$ , hence  $f(\alpha, \lambda)$  [72]. As usual,  $n$  independent Brownian paths  $B$ , starting at small distance  $r$  away from a point  $w$  on the frontier  $\partial C$ , and diffusing without hitting  $\partial C$ , give a geometric representation of the  $n^{\text{th}}$  moment,  $H^n$ , of the harmonic measure in eq.(8.2) for integer  $n$  (Fig. 20). Convexity yields the analytic continuation to arbitrary  $n$ 's. Let us introduce an abstract (conformal) field operator  $\mathcal{O}_{\partial C^n}$  characterizing the presence of a vertex where  $n$  such Brownian paths and the cluster's frontier diffuse away from each other in the mutually-avoiding configuration  $\partial C^n$  [51, 52]; to this operator is associated a scaling dimension  $x(n)$ . To measure rotations using the moments (8.2) we have to consider expectation values with insertion of the mixed operator

$$(8.9) \quad \mathcal{O}_{\partial C^n} e^{p \arg(\partial C^n)} \sim x(n;p);$$

where  $\arg(\partial C^n)$  is the winding angle common to the frontier and to the Brownian paths (see Fig. (20)), and where  $x(n;p)$  is the scaling dimension of the operator  $\mathcal{O}_{\partial C^n} e^{p \arg(\partial C^n)}$ . It is directly related to  $(n;p)$  by [51]

$$(8.10) \quad x(n;p) = (n;p) + 2;$$

For  $n = 0$ , one recovers the previous scaling dimension

$$\begin{aligned} x(n;p=0) &= x(n); \\ (n;p=0) &= (n) = x(n) - 2; \end{aligned}$$

As in section 6, we use the fundamental KPZ mapping of the CFT in the plane  $C$  to the CFT on a fluctuating abstract random Riemann surface, i.e., in presence of 2D quantum gravity [26], and the universal functions  $U$  and  $V$ , acting on conformal

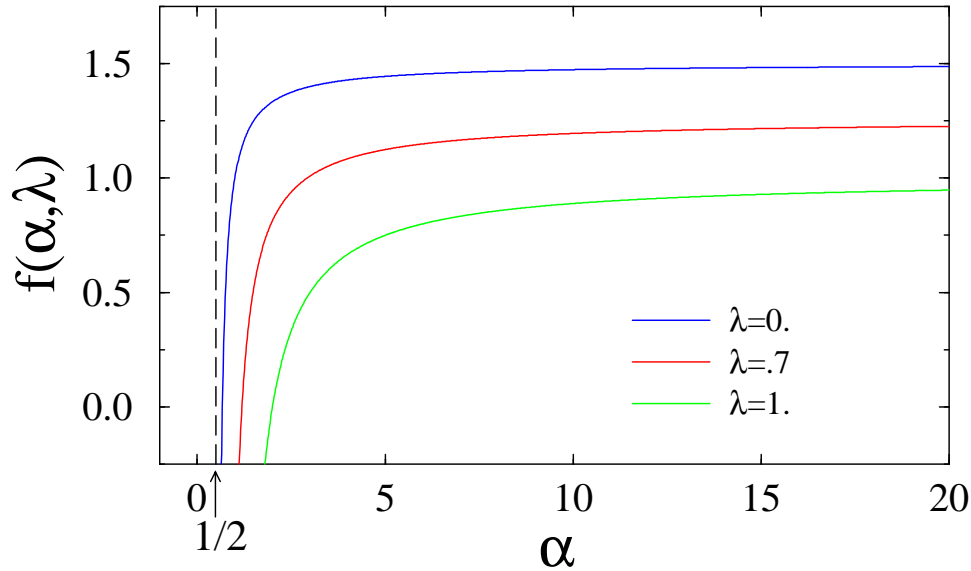


Figure 22. Left-sided multifractal spectra  $f(\alpha, \lambda)$  for the limit case  $c = 1$ , the "ultimate Norway" (frontier of a  $Q = 4$  Potts cluster or  $SLE_{\kappa=4}$ ).

weights, which describe the map:

$$(8.11) \quad U(x) = \frac{x}{1-x}; \quad V(x) = \frac{1-x^2}{4(1-x)^2};$$

with  $V(x) = U(\frac{1}{2}(x+1))$ . As before, the parameter  $\alpha$  is the solution of  $c = 1 - 6^2(1-x)^{-1}$ ;  $\alpha > 0$ :

For the purely harmonic exponents  $x(n)$ , describing the mutually-avoiding set  $\partial C^n$ , we have seen in eqs. (6.27) and (6.22) that

$$(8.12) \quad x(n) = 2V(2U^{-1}(x_1) + U^{-1}(n));$$

where  $U^{-1}(x)$  is the positive inverse of  $U$ ,

$$2U^{-1}(x) = \frac{1}{4(1-x)^2} + \frac{1}{2}x + \frac{1}{4} : \quad ;$$

In (8.12), we recall that the arguments  $x_1$  and  $n$  are respectively the boundary scaling dimensions (b.s.d.) (6.22) of the simple path  $S_1$  representing a semi-infinite random frontier (such that  $\partial C = S_1 \wedge S_1$ ), and of the packet of  $n$  Brownian paths, both diving into the upper half-plane  $H$ . The function  $U^{-1}$  transforms these half-plane b.s.d.'s into the corresponding b.s.d.'s in quantum gravity, the linear combination of which gives, still in QG, the b.s.d. of the mutually-avoiding set  $\partial C^n = (\wedge S_1)^2 \wedge n$ . The function  $V$  naturally maps the latter b.s.d. into the scaling dimension in  $C$ . The path b.s.d.  $x_1$  (6.22) obeys  $U^{-1}(x_1) = (1-x_1)/2$ .

It is now useful to consider  $k$  semi-infinite random paths  $S_1$ , joined at a single

vertex in a mutually-avoiding star configuration  $S_k = S_1 \wedge S_1 \wedge \dots \wedge S_1 = \mathbb{S}^k(S_1)^k$ . (In this notation the frontier near any of its points is a two-star  $\partial C = S_2$ .) The scaling

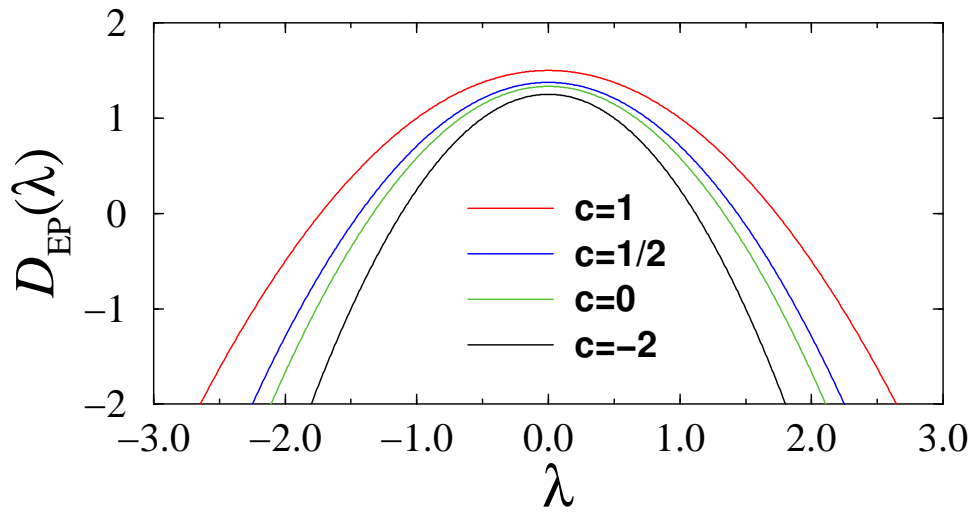


Figure 23. Dimensions  $D_{EP}(\lambda)$  of the external frontiers as a function of rotation rate. The curves are indexed by the central charge  $c$ , and correspond respectively to: loop-erased RW ( $c = 2; SLE_2$ ); Brownian or percolation external frontiers, and self-avoiding walk ( $c = 0; SLE_{8=3}$ ); Ising clusters ( $c = \frac{1}{2}; SLE_3$ );  $Q = 4$  Potts clusters ( $c = 1; SLE_4$ ).

dimension of  $S_k$  can be obtained from the same b.s.d. additivity rule in quantum gravity, as in (6.19) or (8.12) [57]

$$(8.13) \quad x(S_k) = 2V_k U^{-1}(x_1) :$$

The scaling dimensions (8.12) and (8.13) coincide when

$$(8.14) \quad x(n) = x(S_{k(n)})$$

$$(8.15) \quad k(n) = 2 + \frac{U^{-1}(n)}{U^{-1}(x_1)} :$$

Thus we state the scaling star-equivalence

$$(8.16) \quad @C^n(\cdot) S_{k(n)} ;$$

of two mutually-avoiding simple paths  $@C = S_2 = S_1 \wedge S_1$ , further avoiding  $n$  Brownian motions, to  $k(n)$  simple paths in a mutually-avoiding star con guration  $S_{k(n)}$  (Fig. 24). This equivalence plays an essential role in the computation of the complete rotation spectrum (8.10).

8.4. Rotation Scaling Exponents. The Gaussian distribution of the winding angle about the extremity of a scaling path, like  $S_1$ , was derived in [108], using exact Coulomb gas methods. The argument can be generalized to the winding angle of a star  $S_k$  about its center [111], where one finds that the angular variance is reduced by a factor  $1=k^2$  (see also [112]). The scaling dimension associated with the rotation scaling operator  $e^{p \arg(S_k)}$  is found by analytic continuation of the

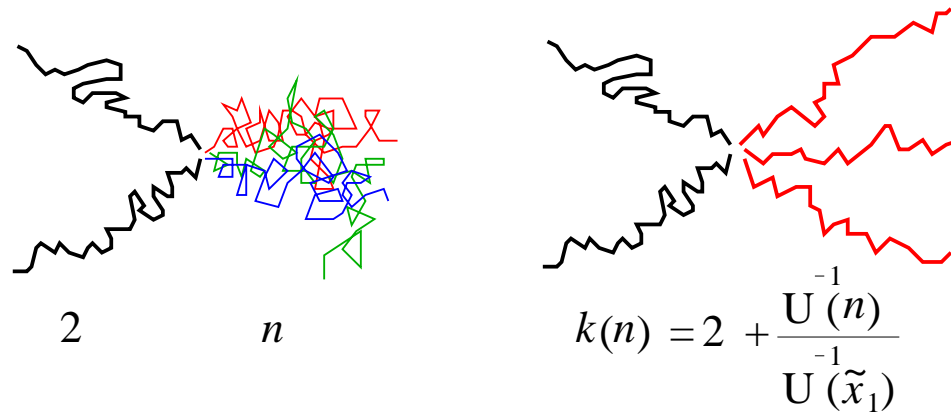


Figure 24. Equivalence (8.15) between two simple paths in a mutually-avoiding configuration  $S_2 = S_1 \wedge S_1$ , further avoided by a packet of  $n$  independent Brownian motions, and  $k(n)$  simple paths in a mutually-avoiding star configuration  $S_{k(n)}$ .

Fourier transforms evaluated there [72]:

$$\chi(S_k; p) = \chi(S_k) \frac{2}{1} \frac{p^2}{k^2};$$

ie., is given by a quadratic shift in the star scaling exponent. To calculate the scaling dimension (8.10), it is sufficient to use the star-equivalence (8.15) above to conclude that

$$\chi(n; p) = \chi(S_{k(n)}; p) = \chi(n) \frac{2}{1} \frac{p^2}{k^2(n)};$$

which is the key to our problem. Using eqs. (8.15), (8.12), and (8.11) gives the useful identity:

$$\frac{1}{8} (1 - \dots)^2 k^2(n) = \chi(n) - 2 + b;$$

with  $b = \frac{1}{2} \frac{(2 - \dots)^2}{1} = \frac{25-c}{12}$ . Recalling (8.10), we arrive at the multifractal result:

$$(8.17) \quad \chi(n; p) = \chi(n) \frac{1}{4} \frac{p^2}{(n) + b};$$

where  $\chi(n) = \chi(n) - 2$  corresponds to the purely harmonic spectrum with no prescribed rotation.

8.5. Legendre Transform. The structure of the full  $\chi$ -function (8.17) leads by a formal Legendre transform (8.3) directly to the identity

$$f(\dots; \dots) = (1 + \dots^2) f(\dots) - b^2;$$

where  $f(\dots) = \chi(n) - 2$ , with  $\dots = d(n) = dn$ , is the purely harmonic MF function. It depends on the natural reduced variable a la Beurling  $(2 \frac{1}{2}; +1)$

$$= \frac{\dots}{1 + \dots^2} = \frac{dx}{dn} (n) = \frac{1}{2} + \frac{1}{2} \frac{b}{2n + b - 2};$$

whose expression emerges explicitly from (8.12). Whence eq.(8.4), Q.E.D.

It is interesting to consider also higher multifractal spectra [60]. For a conformally-invariant scaling curve which is simple, i.e., without double points, like the external frontier @C, here taken alone, define the universal function  $f_2(\delta; \delta^0; \delta^1)$  which gives the Hausdorff dimension of the points where the potential varies jointly with distance  $r$  as  $r^\delta$  on one side of the curve, and as  $r^{\delta^0}$  on the other, given a winding at rate  $\delta^1$ . This function is

$$(8.18) \quad f_2(\delta; \delta^0; \delta^1) = b \frac{1}{2(1-\delta^1)} \frac{1}{1+\delta^2} \frac{1}{2} \frac{1}{2^{-\delta^0}} \frac{1}{2} \\ \frac{b}{2} \frac{2}{2} (\delta + \delta^0);$$

and satisfies the generalization of scaling relation (8.4)

$$(8.19) \quad f_2(\delta; \delta^0; \delta^1) = (1+\delta^2) f_2(\delta; \delta^0; 0) b^{\delta^2}$$

This double multifractality can be generalized to higher ones [60], by considering the distribution of potential between the arms of a rotating star  $S_k$ , with the following poly-multifractal result [113]:

$$(8.20) \quad f_k(f_i; g_i; \delta_i) = b \frac{1}{8(1-\delta_i^k)} k^2 \frac{1}{1+\delta_i^2} \prod_{i=1}^k \frac{1}{2^{-\delta_i}} \frac{1}{2} \\ \frac{b}{2} \frac{2^{X^k}}{2} \delta_i^k :$$

### 9. Duality for $O(N)$ and Potts Models and the Stochastic Lower Evolution

#### 9.1. Geometric Duality in $O(N)$ and Potts Cluster Frontiers.

9.1.1.  $O(N)$  Model. The  $O(N)$  model partition function is that of a gas  $G$  of self- and mutually-avoiding loops on a given lattice, e.g., the hexagonal lattice [15]:

$$(9.1) \quad Z_{O(N)} = \sum_G K^{N_B} N^{N_P};$$

where  $K$  and  $N$  are two fugacities, associated respectively with the total number of occupied bonds  $N_B$ , and with the total number of loops  $N_P$ , i.e., polygons drawn on the lattice. For  $N \geq [2; 2]$ , this model possesses a critical point (CP),  $K_c$ , while the whole "low-temperature" (low- $T$ ) phase, i.e.,  $K_c < K$ , has critical universal properties, where the loops are denser than those at the critical point [15].

9.1.2. Potts Model. The partition function of the  $Q$ -state Potts model on, e.g., the square lattice, with a second order critical point for  $Q \geq [0; 4]$ , has a Fortuin-Kasteleyn representation at the CP:  $Z_{Potts} = \sum_{(C)} Q^{\frac{1}{2} N_P}$ ; where the configurations  $(C)$  are those of unions of clusters on the square lattice, with a total number  $N_P$  of polygons encircling all clusters, and filling the medial square lattice of the original lattice [15, 14]. Thus the critical Potts model becomes a dense loop model, with loop fugacity  $N = Q^{\frac{1}{2}}$ , while one can show that its tricritical point with site

dilution corresponds to the  $O(N)$  CP [44, 97].

9.1.3. Coulomb Gas. The  $O(N)$  and Potts models thus possess the same "Coulomb gas" representations [15, 14, 44, 97]:

$$N = \frac{P}{Q} = 2 \cos g;$$

with  $g \in [1; \frac{3}{2}]$  for the  $O(N)$  CP, and  $g \in [\frac{1}{2}; 1]$  for the low-T  $O(N)$  or critical Potts, xv models; the coupling constant  $g$  of the Coulomb gas also yields the central charge:

$$(9.2) \quad c = 1 - 6(1 - g^2)g;$$

Notice that from the expression (6.15) of  $c$  in terms of  $Q$  one arrives at the simple relation:

$$(9.3) \quad \frac{1}{Q} = 1 - g; \quad g = 1 - \frac{1}{Q}; \quad \frac{1}{Q} = 1 - \frac{1}{g}; \quad g = \frac{1}{1 - \frac{1}{Q}};$$

The above representation for  $N = \frac{P}{Q} \in [0; 2]$  gives a range of values  $2 - c \in [1; 2]$ ; our results also apply for  $c \in (1; 2]$ , corresponding, e.g., to the  $O(N) \in [2; 0]$  branch, with a low-T phase for  $g \in [0; \frac{1}{2}]$ , and CP for  $g \in [\frac{3}{2}; 2]$ :

9.1.4. Hausdorff Dimensions of Hull Subsets. The fractal dimension  $D_{EP}$  of the accessible perimeter, eq. (6.42), is, like  $c(g) = c(g^{-1})$ , a symmetric function of  $g$  and  $g^{-1}$  once rewritten in terms of  $g$ :

$$(9.4) \quad D_{EP} = 1 + \frac{1}{2}g^{-1} \#(1 - g^{-1}) + \frac{1}{2}g \#(1 - g);$$

where  $\#$  is the Heaviside distribution. Thus  $D_{EP}$  is given by two different analytic expressions on either side of the separatrix  $g = 1$ . The dimension of the full hull, i.e., the complete set of outer boundary sites of a cluster, has been determined for  $O(N)$  and Potts clusters [20], and is

$$(9.5) \quad D_H = 1 + \frac{1}{2}g^{-1};$$

for the entire range of the coupling constant  $g \in [\frac{1}{2}; 2]$ . Comparing to eq. (9.4), we therefore see that the accessible perimeter and hull Hausdorff dimensions coincide for  $g = 1$ , i.e., at the  $O(N)$  CP (or for tricritical Potts clusters), whereas they differ, namely  $D_{EP} < D_H$ , for  $g < 1$ , i.e., in the  $O(N)$  low-T phase, or for critical Potts clusters. This is the generalization to any Potts model of the effect originally found in percolation [58]. This can be directly understood in terms of the singly connected sites (or bonds) where fjords close in the scaling limit. Their dimension is given by [20]

$$(9.6) \quad D_{SC} = 1 + \frac{1}{2}g^{-1} - \frac{3}{2}g;$$

For critical  $O(N)$  loops,  $g \in (1; 2]$ , so that  $D_{SC} < 0$ ; hence there exist no closing fjords, thereby explaining the identity:

$$(9.7) \quad D_{EP} = D_H;$$

In contrast, one has  $g \in [\frac{1}{2}; 1)$  and  $D_{SC} > 0$  for critical Potts clusters and for the  $O(N)$  low-T phase. In this case, pinching points of positive dimension appear in the scaling limit, so that  $D_{EP} < D_H$  (Table 1).



Q	0	1	2	3	4
c	-2	0	1/2	4/5	1
D <sub>EP</sub>	5=4	4=3	11=8	17=12	3=2
D <sub>H</sub>	2	7=4	5=3	8=5	3=2
D <sub>SC</sub>	5=4	3=4	13=24	7=20	0

Table 9.1. Dimensions for the critical Q-state Potts model; Q = 0;1;2 correspond to spanning trees, percolation and Ising clusters, respectively.

9.1.5. Duality. We then find from eq. (9.4), with  $g = 1$ :

$$(9.8) \quad (D_{EP} - 1)(D_H - 1) = \frac{1}{4}:$$

The symmetry point  $D_{EP} = D_H = \frac{3}{2}$  corresponds to  $g = 1, N = 2$ , or  $Q = 4$ , where, as expected, the dimension  $D_{SC} = 0$  of the pinching points vanishes.

For percolation, described either by  $Q = 1$ , or by the low-T  $O(N = 1)$  model with  $g = \frac{2}{3}$ , we recover the result  $D_{EP} = \frac{4}{3}$ , recently derived in [53]. For the Ising model, described either by  $Q = 2; g = \frac{3}{4}$ , or by the  $O(N = 1)$  CP with  $g^0 = g^{-1} = \frac{4}{3}$ , we observe that the EP dimension  $D_{EP} = \frac{11}{8}$  coincides, as expected, with that of critical  $O(N = 1)$  loops, which in fact appear as EP's. This is a particular case of a further duality relation between the critical Potts and CP  $O(N)$  models:

$$(9.9) \quad D_{EP}(Q(g)) = D_H[O(N(g^0))]; \text{ for } g^0 = g^{-1}; g = 1:$$

In terms of this duality, the central charge takes the simple expression:

$$(9.10) \quad c = (3 - 2g)(3 - 2g^0):$$

## 9.2. Geometric Duality Property of the SLE

9.2.1. Relation of the SLE trace to Q-Potts frontiers or  $O(N)$  lines. An introduction to the stochastic Loewner evolution process (SLE) can be found in [101], [107]. This process drives a conformally-invariant random path, which essentially describes the boundaries of (Potts) clusters or hulls we have introduced above, or the random lines of the  $O(N)$  model. The random path can be a simple or non simple path with self-contacts. The SLE is parametrized by  $\kappa$ , which describes the rate of an auxiliary Brownian motion, which is the source for the process. When  $\kappa \in [0;4]$ , the random curve is simple, while for  $\kappa \in (4;8)$ , the curve is a self-coiling path. For  $\kappa \geq 8$  the path is space filling. The correspondence to our parameters, the central charge  $c$ , the string susceptibility exponent  $\gamma$ , or the Coulomb gas constant  $g$ , is as follows.

In the original work by Schramm [59], the variance of the Gaussian winding angle  $\theta$  of the single extremity of a SLE of size  $R$  was calculated, and found to be

$$\langle \theta^2 \rangle = \ln R:$$

In [108] we found, for instance for the extremity of a random line in the  $O(N)$  model, the corresponding angular variance

$$\langle \theta^2 \rangle = (4-g) \ln R;$$

from which we immediately infer the identity

$$(9.11) \quad \dots = \frac{4}{g} :$$

The low-temperature branch  $g \in [\frac{1}{2}; 1)$  of the  $O(N)$  model, for  $N \in [0; 2)$ , indeed corresponds to  $\kappa \in (4; 8]$  and describes non simple curves, while  $N \in [2; 0]; g \in [0; \frac{1}{2}]$  corresponds to  $\kappa \in [8; \infty)$ . The critical point branch  $g \in [1; \frac{3}{2}]; N \in [0; 2]$  gives  $\kappa \in [\frac{8}{3}; 4]$ , while  $g \in [\frac{3}{2}; 2]; N \in [2; 0]$  gives  $\kappa \in [2; \frac{8}{3}]$ . The range  $\kappa \in [0; 2)$  probably corresponds to higher multicritical points with  $g > 2$ . Owing to eq. (9.3) for  $\kappa$ , we have

$$(9.12) \quad \dots = 1 - \frac{4}{\kappa}; \quad \dots ;$$

$$(9.13) \quad \dots = 1 - \frac{4}{\kappa}; \quad \dots :$$

9.2.2. Duality. The central charge (6.15) or (9.2) is accordingly:

$$(9.14) \quad c = 1 - 24 \frac{1}{\kappa} - 1 = \dots ;$$

an expression which of course is symmetric under the duality  $\kappa \leftrightarrow 4/\kappa$ , or

$$(9.15) \quad \dots = 16 ;$$

reflecting the symmetry under  $g \leftrightarrow 1/g$  [57]. The self-dual form of the central charge is accordingly:

$$(9.16) \quad c = \frac{1}{4} (6 - \dots) (6 - \dots) :$$

From eqs. (9.5) and (9.4) we respectively find [57]

$$(9.17) \quad D_H = 1 + \frac{1}{8} ;$$

$$(9.18) \quad D_{EP} = 1 + \frac{2}{\kappa} \# (\dots) + \frac{1}{8} \# (4 - \dots) ;$$

in agreement with some results derived later in probability theory [69, 70].

For  $\kappa = 4$ , we have  $D_{EP}(\kappa) = D_H(\kappa)$ . For  $\kappa = 4$ , the self-coiling scaling paths obey the duality equation (9.8) derived above, recast here in the context of the SLE process:

$$(9.19) \quad [D_{EP}(\kappa) - 1] [D_H(\kappa) - 1] = \frac{1}{4} ; \quad \dots ;$$

where now

$$D_{EP}(\kappa) = D_H(\kappa = 16/\kappa) = \dots ;$$

Thus we predict that the external perimeter of a self-coiling SLE $_{\kappa}$  process is, by duality, the simple path of the SLE $_{(16/\kappa) = 4/\kappa}$  process.

The symmetric point  $\kappa = 4$  corresponds to the  $O(N = 2)$  model, or  $Q = 4$  Potts model, with  $c = 1$ . The value  $\kappa = 8/3; c = 0$  corresponds to a self-avoiding walk, which thus appears [52, 53] as the external frontier of a  $\kappa = 6$  process, namely that of a percolation hull [59, 64].

Let us now study more of the SLE's random geometry using the quantum gravity method described here.

Up to now, we have described general conformally-invariant curves in the plane in terms of the universal parameters  $c$  (central charge) or  $\kappa$  (string susceptibility).

The multifractal results described in the sections above thus apply to the SLE after substituting  $\gamma$  to  $\gamma$  or  $c$ . Care should be taken, however, in such a substitution since two dual values of (9.15) correspond to a same value of  $\gamma$ . The reason is that up to now we have considered geometrical properties of the boundaries which actually were self-dual. An example is the harmonic multifractal spectrum of the SLE $_{\kappa}$  frontier, which is identical to that of the smoother (simple) SLE $_{(16/\kappa)} = \gamma = \kappa/4$  path. So we actually saw only the set of simple SLE traces with  $\kappa \leq 4$ . When dealing with higher multifractality, we assumed the random curves to be simple. When dealing with non simple random paths, boundary quantum gravity rules are to be modified as explained now.

### 10. Duality in KPZ

10.1. Dual Dimensions. It will be convenient to introduce the following notations. The standard KPZ map reads:

$$(10.1) \quad x = U(\gamma) = \frac{1}{1 - \gamma^2};$$

where  $x$  is a planar conformal dimension and  $\gamma$  its quantum gravity counterpart, and where we recall that  $\gamma$  is the negative root of

$$(10.2) \quad c = 1 - 6^2(1 - \gamma)^{-1}; \quad \gamma < 0;$$

We introduce the dual quantum dimension of  $\gamma$ ,  $\gamma^0$  such that:

$$(10.3) \quad \gamma^0 = \frac{1}{1 - \gamma};$$

and

$$(10.4) \quad x = U(\gamma) = \frac{1}{1 - \gamma^2};$$

Similarly, let us define the variable  $\gamma^0$ , dual of susceptibility exponent  $\gamma$ , by:

$$(10.5) \quad (1 - \gamma)(1 - \gamma^0) = 1;$$

which is simply the (non-physical!) positive root of eq. (10.2):

$$(10.6) \quad c = 1 - 6^2(1 - \gamma^0)^{-1}; \quad \gamma^0 > 0;$$

The dual equation of (10.3) is then:

$$(10.7) \quad \gamma^0 = \frac{1 - \gamma^0}{1 - \gamma^0};$$

By construction we have the simultaneous equations:

$$(10.8) \quad \gamma = U^{-1}(x); \quad \gamma^0 = \frac{U^{-1}(x)}{1 - U^{-1}(x)};$$

with the positive solution

$$(10.9) \quad U^{-1}(x) = \frac{1}{2} \left[ \sqrt{4(1 - \gamma^0)x + 2} - 1 \right];$$

We define a dual KPZ map  $U_0$  by the same equation as (10.1), with  $\tilde{\cdot}^0$  substituted for  $\tilde{\cdot}$ . It has the following properties:

$$(10.10) \quad x = U_0(\tilde{\cdot}) = U_0(\tilde{\cdot}^0);$$

$$(10.11) \quad \tilde{\cdot}^0 = U_0^{-1}(x) = \frac{U^{-1}(x)}{1};$$

$$(10.12) \quad = U^{-1}(x) = \frac{U_0^{-1}(x)^0}{1^0};$$

10.2. Boundary KPZ for non simple paths. The additivity rules in quantum gravity for the boundary scaling dimensions of mutually-avoiding random paths  $A$  and  $B$  are:

$$(10.13) \quad \tilde{(A \wedge B)} = \tilde{A} + \tilde{B} \quad (\text{simple paths}),$$

$$(10.14) \quad \tilde{\cdot}^0(A \wedge B) = \tilde{\cdot}^0(A) + \tilde{\cdot}^0(B) \quad (\text{non-simple paths}).$$

For simple paths, like random lines in the  $O(N)$  model at its critical point, or the SLE trace for  $\kappa = 4$  the boundary dimensions are additive in quantum gravity, a fundamental fact repeatedly used above. On the other hand, for non-simple paths, the dual dimensions are additive in boundary quantum gravity. This is the case of random lines in the dense phase of the  $O(N)$  model, or, equivalently, of hulls of Fortuin-Kasteleyn clusters in the Potts model, or of the SLE trace. These additivity rules are derived in appendices B and C from the consideration of partition functions on a random surface in the dilute or dense phases. In terms of standard dimensions  $\tilde{\cdot}$  this reads:

$$(10.15) \quad \tilde{(A \wedge B)} = \tilde{A} + \tilde{B} \quad (\text{simple paths}),$$

$$(10.16) \quad \tilde{(A \wedge B)} = \tilde{A} + \tilde{B} \quad (\text{non-simple paths});$$

In the dilute phase the composition rule for boundary dimensions in the upper half-plane  $H$  reads accordingly:

$$(10.17) \quad \varkappa(A \wedge B) = U_0^{-1}(\varkappa(A)) + U_0^{-1}(\varkappa(B));$$

In the dense phase, the new rule (10.14) in terms of dual variables and functions, gives for composite boundary dimensions in  $H$ :

$$(10.18) \quad \varkappa(A \wedge B) = U_0^{-1}(\varkappa(A)) + U_0^{-1}(\varkappa(B));$$

$$(10.19) \quad = U_0^{-1}(\varkappa(A)) + U_0^{-1}(\varkappa(B));$$

So we see that the composition rules (10.18) for non-simple paths are different from the ones for simple paths, when written in terms of the standard string susceptibility exponent  $\varkappa$ , but that they are formally identical in terms of the dual exponent  $\tilde{\cdot}^0$ , as shown by eqs. (10.17) and (10.19).

10.3. Bulk KPZ for non-simple paths. For determining the complete set of scaling dimensions, it remains to relate bulk and boundary dimensions. In the dilute phase, i.e., for simple paths, we have seen the simple relation in a random metric:

$$(10.20) \quad 2 \tilde{\cdot} = \tilde{\cdot}^0;$$

which is established in appendix C (see also appendices A and B). The KPZ map from boundary dimension in quantum gravity to bulk dimension in the plane reads accordingly

$$(10.21) \quad x = 2U(\gamma) = 2U \frac{1}{2}(\tilde{\gamma} + \gamma) = 2V(\tilde{\gamma});$$

where

$$(10.22) \quad V(x) = \frac{1}{4} \frac{x^2}{1-x^2};$$

an expression repeatedly used above. When dealing with non-simple paths, these relations have to be changed to:

$$(10.23) \quad 2 = \tilde{\gamma};$$

as shown in appendices B and C. At this stage, the reader will not be surprised that this relation is just identical to the dual of (10.20)

$$(10.24) \quad 2^0 = \tilde{\gamma}^0;$$

when now written in terms of both dual dimensions and susceptibility exponent. As a consequence, the scaling dimension of a bulk operator in a dense system reads:

$$(10.25) \quad x = 2U(\gamma) = 2U \frac{1}{2} \tilde{\gamma} = \frac{1}{2} \tilde{\gamma} \frac{2}{1-x^2};$$

which by duality can necessarily be written as:

$$(10.26) \quad x = 2V(\tilde{\gamma}^0);$$

$$V(\tilde{\gamma}^0) = \frac{1}{4} \frac{x^2}{1-x^2};$$

as can be checked easily.

As we have seen before, the composition rule for bulk dimensions of simple paths (in the dilute phase) in the plane C follows from (10.21), (10.22), and (10.13):

$$(10.27) \quad x(A \wedge B) = 2U \frac{1}{2} U^{-1}(x(A)) + U^{-1}(x(B)) + \dots;$$

$$(10.28) \quad = 2V U^{-1}(x(A)) + U^{-1}(x(B)) :$$

The composition rule for bulk dimensions of non-simple paths (dense phase) in the plane differs, according to (10.16), (10.23) and (10.25):

$$(10.29) \quad x(A \wedge B) = 2U \frac{1}{2} U^{-1}(x(A)) + U^{-1}(x(B)) \dots;$$

which reads also, according to (10.26) and (10.14):

$$(10.30) \quad x(A \wedge B) = 2V \circ U^{-1}(x(A)) + U^{-1}(x(B)) :$$

This is formally the same as the rule (10.28) in the dilute phase, up to substitution of  $\gamma^0$  for  $\gamma$ , and it applies to the dense phase of the  $O(N)$  model, or to Potts cluster boundaries, and in particular to the SLE<sub>4</sub>.

In summary, the composition rules for planar scaling dimensions, whether on a boundary or in the bulk, take a unique analytic form for both phases (simple or non-simple paths), provided one replaces the string susceptibility exponent in the simple case by its dual variable  $\gamma^0$  in the non-simple case; this can be seen in

(10.28), eqs. (10.17), (10.19) and (10.30).

### 11. SLE and KPZ

11.1. Duality for the SLE. We have seen that the composition rules for dimensions, while they change from the dilute to the dense phase when dealing with the proper KPZ formalism, scaling dimensions and susceptibility exponent, stay invariant when expressed in dual variables. This duality is perfectly adapted to the parameterization of the SLE process. Indeed we have from (9.12) and (9.13)

$$(11.1) \quad \chi = 1 - \frac{4}{\kappa}; \quad \chi^0 = 1 - \frac{4}{\kappa}; \quad \kappa > 4;$$

$$(11.2) \quad \chi = 1 - \frac{4}{\kappa}; \quad \chi^0 = 1 - \frac{4}{\kappa}; \quad \kappa < 4;$$

so that the analytical forms of  $\chi$  and its dual  $\chi^0$  are simply exchanged when passing from simple paths ( $\kappa < 4$ ) to non-simple ones ( $\kappa > 4$ ). Because of the equivalent dual equations (10.10), by choosing either the  $\chi$ -solution or the  $\chi^0$ -solution, depending whether  $\kappa < 4$  or  $\kappa > 4$ , we can write

$$(11.3) \quad \chi = \begin{cases} U_{(\kappa < 4)}(\chi) = U(\chi) & \kappa > 4 \\ U_{\chi^0(\kappa < 4)}(\chi^0) = U(\chi^0) & \kappa < 4 \end{cases}$$

with now a single function, valid for all values of parameter

$$(11.4) \quad U(\chi) = \frac{1}{4} (\chi + 4):$$

Similarly, the inverse KPZ map (10.9) reads, according to (10.11) or (10.12):

$$(11.5) \quad \begin{cases} \chi = U_{(\kappa < 4)}^{-1}(\chi) = U^{-1}(\chi); & \kappa > 4 \\ \chi^0 = U_{\chi^0(\kappa < 4)}^{-1}(\chi^0) = U^{-1}(\chi^0); & \kappa < 4 \end{cases}$$

again with a single expression of the inverse function, valid for any

$$(11.6) \quad U^{-1}(\chi) = \frac{1}{2} \sqrt{16\chi + (\kappa - 4)^2} - \kappa:$$

I emphasize that  $U$  coincides with the KPZ map for  $\kappa > 4$ , while it represents the dual of the latter when  $\kappa < 4$  and then acts on the dual dimension  $\chi^0$ . For instance, we have the important value at the origin

$$(11.7) \quad U^{-1}(0) = \frac{1}{2} [\kappa - 4 + \sqrt{16 - (\kappa - 4)^2}] = 1 - \frac{4}{\kappa} \# (\kappa > 4);$$

which vanishes for simple paths, and is non-trivial for non-simple ones.

It remains to define the analogue of the  $V$  function (10.22) or its dual (10.26):

$$(11.8) \quad \chi = \begin{cases} 2V_{(\kappa < 4)}(\tilde{\chi}) = 2V(\tilde{\chi}) & \kappa > 4 \\ 2V_{\chi^0(\kappa < 4)}(\tilde{\chi}^0) = 2V(\tilde{\chi}^0) & \kappa < 4 \end{cases}$$

with again a single function, valid for all values of parameter

$$(11.9) \quad \begin{aligned} V(\chi) &= U \left( \frac{1}{2} \chi + 1 - \frac{4}{\kappa} \right) \\ &= \frac{1}{16} \left( \chi^2 + 2\chi + \left( \kappa - \frac{4}{\kappa} \right)^2 \right); \end{aligned}$$

but acting on the boundary dimension in quantum gravity or on its dual, depending on whether  $\kappa = 4$  or  $\kappa < 4$ .

11.2. Composition Rules for SLE. Finally we can conclude with general composition rules for the SLE process. Indeed, the boundary rules in  $H$  (10.17) or its dual (10.19), owing to eqs. (11.3) and (11.5), read in a unified way in terms of parameter  $\kappa$ :

$$(11.10) \quad \kappa(A \wedge B) = U U^{-1}(\kappa(A)) + U^{-1}(\kappa(B)) ;$$

valid for the entire range of  $\kappa$ . Similarly, the composition rules for SLE's in the plane  $C$  are found from eqs. (10.28) or (10.30), and recast according to (11.8) and (11.5) into a unified formula, valid for any

$$(11.11) \quad \kappa(A \wedge B) = 2V U^{-1}(\kappa(A)) + U^{-1}(\kappa(B)) :$$

Thus we see that by introducing dual equations, we have been able to unify the composition rules for the SLE in a unique way, which no longer depends explicitly on the range of  $\kappa$ .

### 11.3. Short Distance Expansion (SDE).

11.3.1. Boundary SDE. Consider the power law governing the behavior of two mutually-avoiding random paths  $A$  and  $B$  anchored at the Dirichlet boundary line, and approaching each other at short distance  $r$  along the line. The probability of such an event scales like

$$(11.12) \quad P_{A,B}(r) / r^{\kappa_{A,B}} ; r \rightarrow 0 ;$$

where the short-distance exponent reads [11, 18]:

$$(11.13) \quad \kappa_{A,B} = \kappa(A \wedge B) - \kappa(A) - \kappa(B) :$$

We simply use the fusion rule (11.10) and the quadratic map (11.4) to immediately get

$$(11.14) \quad \kappa_{A,B} = \frac{1}{2} U^{-1}(\kappa_A) U^{-1}(\kappa_B) ;$$

where we use  $\kappa_A = \kappa(A)$  as a short-hand notation. In terms of quantum gravity boundary dimensions, or their dual, this SDE exponent splits into

$$(11.15) \quad \kappa_{A,B} = \frac{1}{2} \begin{matrix} \tilde{\kappa}_A & \tilde{\kappa}_B \\ \tilde{\kappa}_A^0 & \tilde{\kappa}_B^0 \end{matrix} \begin{matrix} 4 \\ 4 \end{matrix} .$$

So we see that the short-distance expansion along the boundary of  $H$  is governed by the product of the quantum boundary dimensions, or of their duals, depending on the phase we are in. In particular, if one chooses the set  $B$  to be the chordal SLE trace itself, its boundary dimension  $\kappa_1 = (6 - \kappa)/2$  is such that  $\tilde{\kappa}_1 = U^{-1}(\kappa_1) = \frac{1}{2}(1 - \kappa)$  in the dilute phase, or  $\tilde{\kappa}_1 = U^{-1}(\kappa_1) = \frac{1}{2} + \kappa$  in the dense phase. That corresponds to the single expression  $U^{-1}(\kappa_1) = 2 = \kappa$ , which is  $\tilde{\kappa}_1$  for  $\kappa = 4$  or  $\tilde{\kappa}_1^0$  for  $\kappa < 4$ . In this case, the expressions (11.14) or (11.15) simplify to

$$(11.16) \quad \begin{aligned} \kappa_{A,1} &= U^{-1}(\kappa_A) = \frac{1}{2} \sqrt{16 \kappa_A + (\kappa_A - 4)^2} + \kappa_A \\ &= \begin{matrix} \tilde{\kappa}_A & 4 \\ \tilde{\kappa}_A^0 & 4 \end{matrix} . \end{aligned}$$

This explains the observation made in [74] that the boundary SDE of any operator with the SLE trace might be seen as exhibiting (boundary) quantum gravity. However, we see that if for  $\kappa \neq 4$  the SDE exponent (11.17) is indeed the KPZ solution  $\tilde{\kappa}$ , for  $\kappa = 4$  it necessarily transforms to the dual dimension  $\tilde{\kappa}^0$  introduced above in (10.3). Moreover, at this stage, this appearance of the quantum gravity dimension might be seen as a coincidence, since the general structure of SDE exponent (11.15) is clearly still quadratic and given by the product of quantum gravity dimensions or their dual.

11.3.2. Bulk SDE. One can also consider the SDE for random paths in the full plane, corresponding to the so-called radial SLE. Consider the power law governing the behavior of two mutually-avoiding random paths A and B approaching each other at short distance  $r$  in the plane, with probability

$$(11.17) \quad P_{A;B}(r) \sim r^{-\kappa_{A;B}}; r \rightarrow 0;$$

where the short-distance exponent now reads:

$$(11.18) \quad \kappa_{A;B} = \kappa(A \wedge B) - \kappa(A) - \kappa(B);$$

We simply use the fusion rule (11.11) and the quadratic maps (11.4) and (11.9) to get

$$(11.19) \quad \kappa_{A;B} = -\frac{U^{-1}(\kappa_A)}{4} - \frac{U^{-1}(\kappa_B)}{4} + \frac{(\kappa_A - \kappa_B)^2}{8};$$

In terms of quantum gravity boundary dimensions, or their dual, this SDE exponent reads

$$(11.20) \quad \kappa_{A;B} = \left( \frac{\tilde{\kappa}_A - \tilde{\kappa}_B}{4} + \frac{(\kappa_A - \kappa_B)^2}{8} \right) \frac{4}{4} \\ = \left( \frac{\tilde{\kappa}_A^0 - \tilde{\kappa}_B^0}{4} + \frac{(\kappa_A - \kappa_B)^2}{8} \right) \frac{4}{4}.$$

So we see that the short-distance expansion in C is again governed by the product of the quantum boundary dimensions, or of their duals, plus a shift term. If one chooses in particular the set B to be the radial SLE trace itself, taken at a typical medialpoint, its boundary scaling dimension  $\kappa_2$  is such that  $\tilde{\kappa}_2 = U^{-1}(\kappa_2) = 1$  in the dilute phase, or  $\tilde{\kappa}_2 = U^{-1}(\kappa_2) = 1 + \frac{c}{12}$  in the dense phase. That corresponds to the single expression  $U^{-1}(\kappa_2) = 2U^{-1}(\kappa_1) = 4 = \tilde{\kappa}_2$  for  $\kappa = 4$  or  $\tilde{\kappa}_2^0$  for  $\kappa \neq 4$ . In this case the expressions (11.19) or (11.20) simplify into

$$(11.21) \quad \kappa_{A;2} = U^{-1}(\kappa_A) + \frac{(\kappa_A - \kappa_2)^2}{8} \\ = \left( \frac{\tilde{\kappa}_A}{4} + \frac{(\kappa_A - \kappa_2)^2}{8} \right) \frac{4}{4} \\ = \left( \frac{\tilde{\kappa}_A^0}{4} + \frac{(\kappa_A - \kappa_2)^2}{8} \right) \frac{4}{4}.$$

So the SDE of the SLE trace with any operator A in the plane again generates the boundary dimension of A in quantum gravity or its dual, modulo a constant shift. Notice that this shift is self-dual with respect to  $\kappa^0 = 16$  and reads also  $\frac{(\kappa - 4)^2}{8} = \frac{1-c}{12}$ .

11.3.3. Kac Spectrum. The Kac spectrum of conformal weights of a conformal field theory of central charge  $c(\kappa)$  can be written with  $\kappa$  as a parameter

$$(11.22) \quad h_{p;q}(\kappa) = \frac{[(1 - \frac{c}{12})p - \frac{c}{24}q]^2}{4(1 - \frac{c}{12})};$$



Notice that if one substitutes the dual parameter  $0$  to  $:$

$$\begin{aligned}
 h_{p;q}^{(0)} &= \frac{[(1-0)p - q]^2 - 0^2}{4(1-0)} \\
 (11.23) \qquad &= h_{q;p}^{(0)}:
 \end{aligned}$$

Hence in metric space the dual dimension is simply that with exchanged indices. By the inverse KPZ relation the dimension  $h_{p;q}^{(0)}$  corresponds to a conformal weight in quantum gravity:

$$(11.24) \qquad \langle \cdot \rangle_{p;q} = U^{-1}(h_{p;q}^{(0)}) = \frac{j(1-0)p - qj + 0}{2}:$$

The dual dimension (10.3) reads:

$$\begin{aligned}
 \langle \cdot \rangle_{p;q}^{(0)} &= \frac{\langle \cdot \rangle_{p;q}}{1} = \frac{j(1-0)q - pj + 0}{2} \\
 (11.25) \qquad &= \langle \cdot \rangle_{q;p}^{(0)} = U_0^{-1}(h_{q;p}^{(0)}):
 \end{aligned}$$

In  $O(N)$  model studies (see, e.g., [15, 28, 114]), it has been observed that the conformal operator  $\langle \cdot \rangle_{p;q}$ , with conformal weights  $h_{p;q}^{(0)}$  (or  $\langle \cdot \rangle_{p;q}$  in QG), and describing a given system of random paths, gets its indices  $p$  and  $q$  interchanged when going from the dilute phase to the dense phase. In the plane, we see from (11.23) that this corresponds to keeping the same indices and formally going to the dual string susceptibility, whereas in quantum gravity, (11.25) shows that this corresponds to keeping the same indices, while performing the double operation of taking the dual dimension together with the dual string susceptibility.

Using (9.12), (9.13), the Kac spectrum (11.22) can be written in terms of parameter  $4$  as:

$$(11.26) \qquad h_{p;q}^{(\langle \cdot \rangle_{p;q}^{(4)})} = \frac{(4p - q)^2 - 4}{16} = \sim_{p;q}; \quad 4;$$

$$(11.27) \qquad h_{p;q}^{(\langle \cdot \rangle_{p;q}^{(4)})} = \frac{(p - 4q)^2 - 4}{16} = \sim_{q;p}; \quad 4;$$

where in this new notation  $\sim_{p;q}$  coincides with  $h_{p;q}^{(0)}$  for  $4$ , and with  $h_{q;p}^{(0)}$  [with interchanged indices] for  $4$ . It also obeys the duality equation:  $\sim_{p;q}^{0=16=} = \sim_{q;p}$ . Notice notably that the convention for placing indices in  $\sim_{p;q}$  is the reverse of that of ref. [74].

The quantum conformal weight (11.24) reads similarly, depending on the  $4$ -range:

$$(11.28) \qquad \langle \cdot \rangle_{p;q}^{(\langle \cdot \rangle_{p;q}^{(4)})} = \frac{j4p - qj + 4}{2}; \quad 4;$$

$$(11.29) \qquad \langle \cdot \rangle_{p;q}^{(\langle \cdot \rangle_{p;q}^{(4)})} = \frac{j p - 4qj + 4}{8}; \quad 4:$$

Let us also introduce a unified notation for the inverse image of  $\sim_{p;q}$  (11.26) by the  $4$ -dependent map  $U^{-1}$  (11.6)

$$\begin{aligned}
 \langle \cdot \rangle_{p;q} &= U^{-1} \sim_{p;q} \\
 (11.30) \qquad &= \frac{j4p - qj + 4}{2}:
 \end{aligned}$$

We therefore get, depending on the range:

$$(11.31) \quad \rho_{p;q} = \begin{pmatrix} \binom{L}{p;q} \\ \binom{L}{q;p} \end{pmatrix} \begin{matrix} 4 \\ 4 \end{matrix}$$

so  $\rho_{p;q}$  is either a conformal weight  $\binom{L}{p;q}$ , or a dual one  $\binom{L}{q;p}$ .

11.4. Scaling Dimensions for Multi-Lines in  $O(N)$ , Potts Models and SLE Process. We shall need in the following the scaling dimensions associated with several (mutually-avoiding) random paths starting from a same small neighborhood, also called star exponents in the above. It is simplest to first give them for the  $O(N)$  model, before transferring them to the SLE. For completeness, these exponents are also derived explicitly from the random lattice approach in appendix B, in particular in the case in presence of a boundary (see also refs. [28, 29, 115]).

11.4.1. Boundary and Bulk Quantum Gravity. Near the boundary of a random surface with Dirichlet conditions, the conformal dimensions read:

$$(11.32) \quad \tilde{\rho}_L = \frac{L}{2} \binom{L}{L+1;1} ;$$

$$(11.33) \quad \tilde{\rho}_L^D = \frac{L}{2} + \binom{L}{1;L+1} ;$$

where the  $\binom{L}{\cdot}$  superscript stands for the dense phase. The quantum bulk dimensions read similarly

$$(11.34) \quad \rho_L = \frac{L}{4} \binom{L}{L=2;0} + \frac{1}{2} ;$$

$$(11.35) \quad \rho_L^D = \frac{L}{4} + \frac{1}{2} \binom{L}{0;L=2} ;$$

In terms of the SLE parameter, the dilute phase corresponds to (9.12) for  $\kappa = 4$ , while the dense one covers (9.13) with  $\kappa = 4$ :

$$(11.36) \quad \tilde{\rho}_L = \frac{2L}{\kappa}; \quad \rho_L = \frac{1}{2} (2L + \frac{\kappa}{2}); \quad \kappa = 4$$

$$(11.37) \quad \tilde{\rho}_L^D = \frac{L}{2} + 1 - \frac{\kappa}{4}; \quad \rho_L^D = \frac{1}{8} (2L + 4 + \frac{\kappa}{2}); \quad \kappa = 4:$$

By using dual dimensions (10.3) for the dense phase, these results are unified into

$$(11.38) \quad \tilde{\rho}_L = \frac{2L}{\kappa} = \binom{L}{L+1;1} ; \quad \kappa = 4$$

$$(11.39) \quad \rho_L = \frac{1}{2} (2L + \frac{\kappa}{2}) = \binom{L}{L=2;0} ; \quad \kappa = 4$$

$$(11.40) \quad \tilde{\rho}_L^D = \frac{2L}{\kappa} = \binom{L}{L+1;1} ; \quad \kappa = 4$$

$$(11.41) \quad \rho_L^D = \frac{1}{2} (2L + \frac{\kappa}{2}) = \binom{L}{L=2;0} ; \quad \kappa = 4:$$

Hence we again observe that in the dense phase the dual dimensions play the role of the original ones in the dilute phase.

11.4.2. Scaling Dimensions in  $H$  and  $C$ . The scaling dimensions  $\kappa_L$  in the standard complex half-plane  $H$ , or  $x_L$  in the complex plane  $C$ , can now be obtained from the quantum gravity ones by the KPZ map (10.1), or, in the SLE formalism, from the  $U$  (11.3) or  $V$  (11.8) adapted KPZ maps. From the last equations (11.38) to (11.41), it is clear that by duality the analytic form of the dimensions stays the same in the two phases (4), and (4). Indeed we get:

$$(11.42) \quad \kappa_L = U(\tilde{\gamma}_L) = \frac{L}{2} (2L + 4) = \gamma_{L+1;1}; \quad (4)$$

$$(11.43) \quad x_L = 2V(\tilde{\gamma}_L) = \frac{1}{8} 4L^2 (4) = \tilde{\gamma}_{L=2;0}; \quad (4)$$

$$(11.44) \quad \kappa_L = U(\tilde{\gamma}_L^D) = \frac{L}{2} (2L + 4) = \gamma_{L+1;1}; \quad (4)$$

$$(11.45) \quad x_L = 2V(\tilde{\gamma}_L^D) = \frac{1}{8} 4L^2 (4) = \tilde{\gamma}_{L=2;0}; \quad (4):$$

We are now in position to determine the multifractal spectrum associated with the harmonic measure near the  $O(N)$  multi-lines, or, equivalently, near the SLE frontier or special points. It also corresponds to the so-called derivative exponents in the SLE formalism [62].

## 12. Multifractal Exponents for the SLE

In sections 6 and 6.3 above we have studied in detail the multifractal spectrum associated with the harmonic measure near a conformally-invariant frontier, generalized to a mixed rotation spectrum in section 8. We also looked at the double-sided distribution of potential near a simple fractal curve. Further generalizations were given to higher multifractal spectra in between the branches of stars made of several simple paths (section 7). One should note at this stage that we used there the quantum gravity formalism in terms of the susceptibility exponent  $\chi$ , which is valid for the "dilute phase" of critical curves, i.e., for simple CI curves. We have seen in previous section 11 how to extend this formalism to the "dense phase", namely to non-simple curves, by using duality. We shall now apply this extended formalism to the multifractal spectrum of the SLE trace. It would be tedious to repeat all previous calculations, so we shall rather concentrate on new extended spectra, and on the basic property of duality (9.8) (9.19) of the SLE trace, which plays an essential role in the construction (6.27) (6.30) of the standard multifractal spectrum  $f(\cdot)$  along any CI random curve.

### 12.1. Boundary Multifractal Exponents.

12.1.1. Definition. Let us start with the exponents associated with geometrical properties of CI curves at the boundary of the half-plane  $H$ . In the SLE language, this corresponds to the chordal case. We look specially at the behavior of powers of the harmonic measure, or in SLE terms, to that of powers of the modulus of the derivative of the Riemann conformal map which maps the SLE trace back to the half-line  $R = \partial H$  [62, 101, 107].

We shall start with the multifractal exponents associated with the  $L$ -leg boundary operator  $\tilde{s}_L$  creating a star made of  $L$  semi-infinite random paths  $S_1^i$ ,  $i$  using in the upper half-plane  $H$  and started at a single vertex on the real line  $\partial H$  in a

mutually-avoiding star configuration

$$S_L = S_1 \wedge S_1 \wedge \dots \wedge S_1 \quad (S_1)^L$$

with  $L$  lines started at the same origin, as seen in sections (8) and (11). Its boundary scaling dimension  $\kappa_L$  is given by eqs. (11.42) or (11.44):

$$(12.1) \quad \kappa(S_L) = \kappa_L = \frac{L}{2} (2L + 4) = \gamma_{L+1;1} ; 8$$

with the inversion formula:

$$(12.2) \quad U^{-1}(\kappa_L) = L U^{-1}(\kappa_1) = \frac{2L}{L+1} = \gamma_{L+1;1} ; 8 :$$

As explained above in section 11, the formalism has now been set up in such a way that the formulae stay valid in both phases  $\kappa < 4$  or  $\kappa > 4$ .

We now dress this  $L$ -star  $S_L$  by a packet of  $n$  independent Brownian paths diffusing away from the apex of the star, located on the boundary, while avoiding the random paths of the star (Fig. 25).

In our standard notation, this reads:

$$S_L \wedge fB_{-B} \quad (B_{g=1})^n \wedge S_{(-B)}^n \quad L \wedge n :$$

We have, with a slight abuse of notation, introduced the short-hand notation:  $L \wedge n = S_L \wedge (-B)^n$ . The corresponding boundary scaling dimension  $\kappa(L \wedge n)$  in  $H$  is given by repeated application of the boundary KPZ construction (11.10):

$$(12.3) \quad \begin{aligned} \kappa(L \wedge n) &= U U^{-1}(\kappa(S_L)) + U^{-1}[\kappa((-B)^n)] \\ &= U L U^{-1}(\kappa_1) + U^{-1}(n) \\ &= U L \frac{2}{L+1} + U^{-1}(n) : \end{aligned}$$

An explicit calculation with (11.4) and (11.6) then gives:

$$(12.4) \quad \kappa(L \wedge n) = n + \frac{L}{L+1} + \frac{1}{2} \frac{16n + (4)^2}{16n + (4)^2} :$$

In particular, for the exponent governing the harmonic measure moments near the origin of a single SLE trace on the boundary @H we find:

$$(12.5) \quad \kappa(1 \wedge n) = n + \frac{1}{2} + \frac{1}{2} \frac{16n + (4)^2}{16n + (4)^2} :$$

12.1.2. Boundary Derivative Exponents. It is interesting to isolate in this exponent the contribution  $\kappa_L$  (12.1) coming from the  $L$  random SLE paths, and which absorbs the non-linearity in  $L$ , and write:

$$(12.6) \quad \kappa(L \wedge n) = \kappa_L + n + \frac{L}{2} \frac{h_p}{16n + (4)^2} + \frac{i}{4}$$

$$(12.7) \quad = \kappa_L + n + L U^{-1}(n) :$$

The structure so obtained is in agreement with the short-distance expansion results (11.14) and (11.15); the mutual-avoidance interaction between the random SLE paths and the random Brownian paths enhances the exponent of independent paths

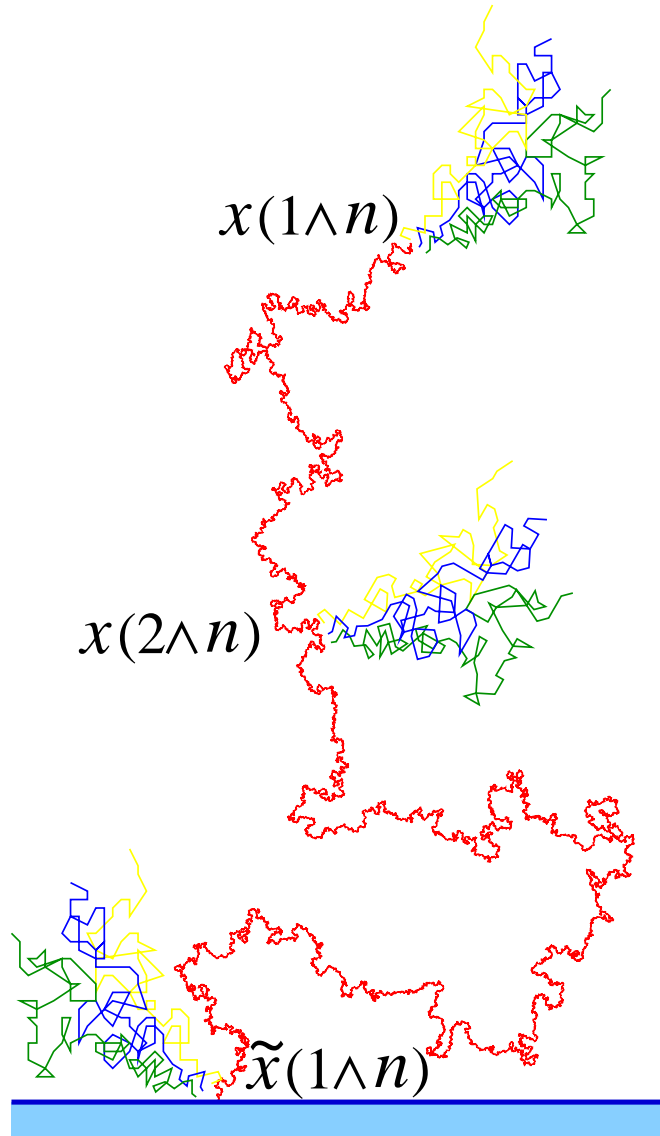


Figure 25. Representation of harmonic moments by packets of independent Brownian paths drifting away from a single SLE trace, hence a  $L = 1$  star  $S_1$ . There are three locations to probe the harmonic measure: at the SLE origin on the boundary, at the SLE tip in the plane, or along the fractal curve itself. The corresponding scaling exponents are respectively  $\kappa(1^n)$  (12.5),  $\kappa(1^n)$  (12.19),  $\kappa(2^n)$  (12.20).

$\kappa_L + n$  by  $L$  times a typical boundary KPZ term. Let us define the subtracted exponent:

$$(12.8) \quad \tilde{\kappa}(L^n) = \kappa(L^n) - \kappa_L :$$

It reads explicitly

$$(12.9) \quad \tilde{\chi}(L^n) = n + L U^{-1}(n) = n + L q(\kappa; n);$$

with, in the notation of ([62, 101, 107]),

$$(12.10) \quad q(\kappa; n) = U^{-1}(n) = \frac{1}{2} \frac{h_p}{16n + (\kappa^2 - 4)} + \frac{i}{4} :$$

12.1.3. Boundary Disconnection Exponents. Notice that for  $n = 0$  the exponent is not necessarily trivial:

$$(12.11) \quad \begin{aligned} \tilde{\chi}(L; n = 0) &= \chi(L^0) - \chi_0 \\ &= L U^{-1}(0); \end{aligned}$$

with

$$(12.12) \quad U^{-1}(0) = \frac{1}{2} \frac{4}{\kappa^2 - 4} :$$

Hence

$$(12.13) \quad \tilde{\chi}(L^0) = \frac{0}{L(1 - 4)} = \frac{4}{4}.$$

So the exponent (12.11) takes non-zero values for  $\kappa > 4$ , i.e. for self-coiling random C I curves. This is typical of a disconnection exponent. Consider a point  $z$  located along the boundary  $\partial H$  at short distance  $r = |z - w|$  from the origin  $w$  where all paths of the SLE star  $S_L$  are started. The probability  $P_{L^0}$  that point  $z$  stays connected to infinity without being encircled by the collection of SLE traces scales like

$$(12.14) \quad P_{L^0}(z) / r^{\tilde{\chi}(L^0)} = r^{L(1 - 4)}; r \neq 0; \quad \kappa > 4:$$

If  $\kappa \leq 4$ , the probability that the random SLE paths return to the boundary is zero, and any point  $w \neq 0$  stays connected to infinity, hence a vanishing disconnection exponent  $\tilde{\chi}_4(L; 0) = 0$ .

### 12.2. Planar Multifractal Exponents.

12.2.1. Construction from Quantum Gravity. In this section we deal with exponents similar to the  $\chi(L^n)$  encountered above, but now for the harmonic measure near the tip of a collection of  $L$  random C I paths in the plane. In the SLE language, these will give derivative exponents, describing the power law decay of the  $n^{\text{th}}$  moment of the modulus of the derivative of the uniformizing Riemann map of the SLE traces to the unit disk  $U$ , this time for chordal SLEs.

We still use the short-hand  $L^n = S_L \wedge (\_B)^n$ . It then suffices to apply the general composition formalism (11.11) in place of (11.10) as in (12.3) above, to get:

$$(12.15) \quad \begin{aligned} \chi(L^n) &= 2V U^{-1}(\chi(S_L)) + U^{-1}[\chi((\_B)^n)] \\ &= 2V L U^{-1}(\chi_1) + U^{-1}(n) \\ &= 2V L \frac{2}{\kappa^2 - 4} + U^{-1}(n) : \end{aligned}$$

Using (11.9) and (11.6), one arrives at the explicit form :

$$(12.16) \quad \chi(L^n) = \frac{n}{2} + B(L) + A(L) \frac{1}{2} \frac{1}{16n + (\kappa^2 - 4)};$$

where the various terms read

$$(12.17) \quad B(L) = \frac{L}{4} (2L + 4) \frac{1}{16} (4)^2$$

$$(12.18) \quad A(L) = \frac{1}{4} L + \frac{1}{4} :$$

Let us specify the first two sets of exponents, corresponding respectively to the tip of the radial SLE ( $L = 1$ ), or to the frontier of the SLE curve ( $L = 2$ ):

$$(12.19) \quad x(1 \wedge n) = \frac{n}{2} + \frac{4 + \frac{P}{16} \frac{1}{n + (4)^2}}{16} + \frac{(6)(2)}{8};$$

$$(12.20) \quad x(2 \wedge n) = \frac{n}{2} + 1 + \frac{1}{4} \frac{h}{4} \frac{P}{16} \frac{i}{n + (4)^2 + 1} \frac{1}{8} :$$

In each equation, the last term corresponds to the scaling dimension  $x_1$  or  $x_2$  of the operator  $s_1$  or  $s_2$ .

12.2.2. Duality for Multifractal Dimensions. It is interesting, at this stage, to return at our original developments in terms of quantum gravity, where the string susceptibility exponent appeared in a natural way. Using (11.1), one finds in the dilute phase ( $\gamma < 4$ ):

$$(12.21) \quad x(L \wedge n) = \frac{n}{2} + B(L) + A(L) \frac{P}{4(1 - \gamma)n + 2}$$

where the various coefficients read

$$(12.22) \quad B(L) = \frac{L}{4} \frac{L}{2} (1 - \gamma) + \frac{1}{4} \frac{1}{1 - \gamma^2}$$

$$(12.23) \quad A(L) = \frac{1}{4} L + \frac{1}{1 - \gamma} :$$

In particular for  $L = 1$  we find:

$$(12.24) \quad x(1 \wedge n) = \frac{n}{2} + \frac{1}{8} (1 - \gamma) \frac{1}{4} \frac{1}{1 - \gamma^2} + \frac{1}{4} \frac{1}{1 - \gamma} \frac{P}{4(1 - \gamma)n + 2} :$$

For  $L = 2$  we get:

$$(12.25) \quad x(2 \wedge n) = \frac{n}{2} + \frac{1}{2} \frac{1}{4} \frac{1}{1 - \gamma^2} + \frac{1}{4} \frac{2}{1 - \gamma} \frac{P}{4(1 - \gamma)n + 2} ;$$

which of course is the same as result (6.28) of section 7 above.

For the dense phase, one either uses (11.2) in (12.16), or formally substitutes everywhere in (12.22) the dual susceptibility exponent  $\gamma^0 = \gamma = (1 - \gamma)$  (10.5) to get

$$(12.26) \quad x^D(L \wedge n) = \frac{n}{2} + B^0(L) + A^0(L) \frac{P}{4(1 - \gamma^0)n + 2}$$

where

$$(12.27) \quad B^0(L) = B^0(L) = \frac{L}{4} \frac{1}{1 - \gamma^0} \frac{L}{2} \frac{1}{1 - \gamma^0{}^2}$$

$$(12.28) \quad A^0(L) = \frac{1}{1 - \gamma^0} A^0(L) = \frac{1}{4} \frac{L}{1 - \gamma^0} :$$

For the first cases  $L = 1$  and  $L = 2$  we respectively find:

$$(12.29) \quad x^D(1^n) = \frac{n}{2} + \frac{1}{4} \frac{1}{1} - \frac{1}{4} \frac{1^2}{1} + \frac{1}{4} \frac{1^p}{4(1^n)n+2};$$

and

$$(12.30) \quad x^D(2^n) = \frac{n}{2} + \frac{1}{2} \frac{1}{4} \frac{1^2}{1} + \frac{1}{4} \frac{2}{1} \frac{1^p}{4(1^n)n+2};$$

We thus observe that the expression for the two-line exponent  $x(2^n)$  is invariant between the two phases. This crucial point explains the fact that when approaching a CI fractal path from outside and converging towards a typical point associated with the two-line operator  $s_2$ , one sees only the external frontier, since all the multifractal exponents (12.25) and (12.30) are identical. This identity expresses the screening of electrostatic interactions by the external perimeter of non-simple paths.

Another way to express this situation is to require the duality identity in the SLE result (12.16)

$$(12.31) \quad x(L^n) = x_{16=}(L^n)$$

which is equivalent to

$$\begin{aligned} B(L) &= B_{0=16=}(L) \\ A(L) &= -A_{0=16=}(L); \end{aligned}$$

One finds from (12.17) a unique solution for  $L = 2$ , which is the geometric duality of frontiers, already seen in sections (9) and (10). It ascribes the simple path SLE  $_{0=16=}$  as the external frontier of SLE  $_4$ , which is a non-simple path.

12.2.3. Planar Derivative Exponents. As a follow up of eqs. (12.19) and (12.20), it is interesting to separate in (12.16) the contribution  $x_L$  of the star  $S_L$  itself

$$(12.32) \quad x(S_L) = x_L = \frac{1}{8} 4L^2 (4^{\frac{3}{2}}) = \sim_{L=2;0};$$

and to write

$$(12.33) \quad x(L^n) = x_L + \frac{n}{2} + \frac{1}{2} L + \frac{1}{4} 1 U^{-1}(n);$$

where

$$(12.34) \quad U^{-1}(n) = \frac{1}{2} h_p \frac{1}{16n + (4^{\frac{3}{2}})} + \frac{i}{4};$$

In analogy to eq. (12.8), one is thus led to define a subtracted exponent

$$(12.35) \quad (L^n) = x(L^n) - x_L;$$

Owing to the results above, this set of exponents reads explicitly:

$$\begin{aligned} (L^n) &= \frac{n}{2} + \frac{1}{2} L + \frac{1}{4} 1 U^{-1}(n) \\ (12.36) \quad &= \frac{n}{2} + \frac{1}{2} L + \frac{1}{4} 1 \frac{1}{2} h_p \frac{1}{16n + (4^{\frac{3}{2}})} + \frac{i}{4}; \end{aligned}$$

These exponents, directly related to the harmonic measure moment exponents (12.15), generalize the so-called derivative exponents introduced in [62]. Indeed, for  $L = 1$ , we find:

$$(12.37) \quad (L = 1; n) = \frac{n}{2} + \frac{1}{16} h_p \frac{1}{16n + (4^{\frac{3}{2}})} + \frac{i}{4};$$



in agreement with ([62, 101, 107]). This particular exponent describes the conformal behavior of the growth process near the tip of the SLE, or, equivalently, that of the harmonic measure seen from that tip. The class (12.36) generalizes it, for  $L = 2$ , to the case of a typical point along the frontier, and to higher branching points for  $L > 2$ .

12.2.4. Planar Disconnection Exponents. Here again, the geometrical situation will strongly depend on the range of values for  $\kappa$ , the fractal sets being directly accessible or not, respectively for  $\kappa \leq 4$  and  $\kappa > 4$ . Indeed, let us consider the values at  $n = 0$ , i.e., the set of disconnection exponents:

$$(12.38) \quad \begin{aligned} (L; n = 0) &= \frac{1}{2} (L + \frac{\kappa}{4} - 1) U^{-1}(0) \\ &= \frac{1}{2} (L + \frac{\kappa}{4} - 1) \frac{4}{\kappa} \#(\kappa > 4): \end{aligned}$$

This explicitly gives

$$(12.39) \quad (L; 0) = \frac{0}{2} (L - 1) (1 - \frac{\kappa}{4}) + \frac{1}{8} (\kappa - 4) \frac{4}{\kappa}$$

For  $L = 1$ , we find the disconnection exponent associated with the tip of the radial SLE, or, equivalently, with the tip of a single line in the  $O(N)$  model:

$$(12.40) \quad (1; 0) = \frac{0}{2} (\kappa - 4) = \frac{4}{\kappa}$$

a result also appearing in [62, 69].

Consider a point  $z \in \mathbb{C}$  located at distance  $r = |z|$  from the origin where all paths of the SLE star  $S_L$  begin. The probability  $P_{L;0}$  that the point  $z$  stays connected to infinity without being encircled by the collection of SLE traces scales like

$$(12.41) \quad P_{L;0}(z) \sim r^{-(L;0)}; r \rightarrow 0:$$

If  $\kappa > 4$ , the random SLE paths are simple curves which cannot encircle any exterior point which thus stays connected to infinity, hence a vanishing disconnection exponent  $\kappa > 4 (L; 0) = 0$ .

### 12.3. Double-Sided Exponents.

12.3.1. Definition. For completeness, let us give the expression for the double-sided exponents corresponding to the double moments of the harmonic measure on both sides of an SLE trace, or, equivalently, to double-sided derivative exponents [62]. For the sake of generality, we shall treat them at level  $L$ , and specify them for  $L = 1; 2$ . We thus have in mind the configuration where two packets of  $n_1$  and  $n_2$  Brownian paths diffuse on both sides of an  $S_L$  multiple SLE trace, hence

$$f_{B_-}^{n_1} \{ \dots \} f_{B_+}^{n_2} \{ \dots \} \quad Bg = \eta(B) (S_1)^L \wedge (B)^{n_2} = n_1 \wedge L \wedge n_2:$$

We have again, with a slight abuse of notation, introduced a short-hand notation:  $n_1 \wedge L \wedge n_2 = (B)^{n_1} \wedge S_L \wedge (B)^{n_2}$ .

12.3.2. Boundary Exponents. Let us start with the halfplane con guration, where all paths start at the same origin w on the halfplane boundary @H . According to the composition rules (11.10), the associated boundary scaling exponent can be constructed immediately as:

$$\begin{aligned} \kappa(n_1 \wedge L \wedge n_2) &= U^{-1}(n_1) + L U^{-1}(\kappa_1) + U^{-1}(n_2) \\ (12.42) \quad &= U^{-1}(n_1) + \frac{2L}{4} + U^{-1}(n_2) : \end{aligned}$$

The calculation gives:

$$\begin{aligned} &\kappa(n_1 \wedge L \wedge n_2) \\ &= \frac{1}{16} \left( 4(L+1) + \frac{p}{16} \frac{h}{n_1 + \frac{4}{p}} + \frac{p}{16} \frac{i_2}{n_2 + \frac{4}{p}} \right) \quad (4) \end{aligned}$$

This is the full boundary scaling dimension of L-SLE paths dressed by  $n_1$  and  $n_2$  Brownian paths. It is interesting to compare it to the dimension  $\kappa_L$  (11.42) or (11.44) of the L-SLEs alone, and define:

$$(12.43) \quad \tilde{\kappa}(n_1 \wedge L \wedge n_2) = \kappa(n_1 \wedge L \wedge n_2) - \kappa_L :$$

We get for this exponent:

$$\begin{aligned} &\tilde{\kappa}(n_1 \wedge L \wedge n_2) \\ &= \frac{1}{16} \left( 4L + 4 + \frac{p}{16} \frac{h}{n_1 + \frac{4}{p}} + \frac{p}{16} \frac{i_2}{n_2 + \frac{4}{p}} \right) \quad (4L + 4) \quad \} \end{aligned}$$

For  $L = 1$ , we find:

$$\begin{aligned} &\tilde{\kappa}(n_1 \wedge 1 \wedge n_2) \\ &= \frac{1}{16} \left( 8 + \frac{p}{16} \frac{h}{n_1 + \frac{4}{p}} + \frac{p}{16} \frac{i_2}{n_2 + \frac{4}{p}} \right) \quad (8) \quad \} ; \end{aligned}$$

also obtained in [62].

12.3.3. Double-Sided Boundary Disconnection Exponents. The values of the generalized disconnection exponents associated with the exponents above are obtained for  $n_1 = n_2 = 0$  as:

$$(12.44) \quad \kappa(0 \wedge L \wedge 0) = U^{-1}(0) + 2U^{-1}(0) :$$

For the exponents (12.43) this gives  $\tilde{\kappa}(0 \wedge L \wedge 0)$  explicitly, with the help of (12.12)  $U^{-1}(0) = \frac{4}{2} \#(4)$ :

$$\begin{aligned} \tilde{\kappa}(0 \wedge L \wedge 0) &= \kappa(0 \wedge L \wedge 0) - \kappa_L \\ &= \frac{1}{2} (4L + 4) - \frac{4}{2} \#(4) : \end{aligned}$$

We therefore find as usual a quite different situation for  $4$  and  $4$ :

$$(12.45) \quad \tilde{\kappa}(0 \wedge L \wedge 0) = \frac{0}{2} (4L + 4) - \frac{4}{2} \#(4) .$$

Notice that the bulk one-sided disconnection exponent (12.38) is related to the double-sided boundary one by the identity

$$(12.46) \quad \kappa(L \wedge 0) = \frac{1}{4} \tilde{\kappa}(0 \wedge L \wedge 0) :$$

12.3.4. Planar Double-Sided Exponents. This time we consider the case where the dressed configuration  $n_1 \wedge n_2$  is located away from the boundary, namely in the plane. The associated dimension is obtained from (11.11) as:

$$\begin{aligned} x(n_1 \wedge L \wedge n_2) &= 2V U^{-1}(n_1) + L U^{-1}(x_1) + U^{-1}(n_2) \\ (12.47) \qquad \qquad &= 2V U^{-1}(n_1) + \frac{2L}{4} + U^{-1}(n_2) : \end{aligned}$$

From (11.9) we find:

$$\begin{aligned} x(n_1 \wedge L \wedge n_2) &= \frac{1}{8} (2L + 4 + \frac{1}{2} \frac{16 n_1 + (4)^2}{16 n_1 + (4)^2} + \frac{1}{2} \frac{16 n_2 + (4)^2}{16 n_2 + (4)^2}) : \end{aligned}$$

The subtracted exponents read accordingly

$$(12.48) \qquad (n_1 \wedge L \wedge n_2) = x(n_1 \wedge L \wedge n_2) - x_1 ;$$

and we get explicitly

$$\begin{aligned} (n_1 \wedge L \wedge n_2) &= \frac{1}{8} (2L + 4 + \frac{1}{2} \frac{16 n_1 + (4)^2}{16 n_1 + (4)^2} + \frac{1}{2} \frac{16 n_2 + (4)^2}{16 n_2 + (4)^2}) - 4L^2 \end{aligned}$$

12.3.5. Double-Sided Bulk Disconnection Exponents. Generalized disconnection exponents associated with the exponents above are obtained for  $n_1 = n_2 = 0$  as:

$$(12.49) \qquad x(0 \wedge L \wedge 0) = 2V \frac{2L}{4} + 2U^{-1}(0) :$$

For the exponent (12.48) this gives explicitly

$$\begin{aligned} (0 \wedge L \wedge 0) &= x(0 \wedge L \wedge 0) - x_1 \\ &= \frac{1}{2} (2L + 4) - 4 \\ (12.50) \qquad \qquad &= \frac{1}{2} (2L + 4) - 4 \end{aligned}$$

12.4. Winding Angle Variance of Multiple SLE Strands. Let us finally return to the winding angle variance at points where  $k$  strands come together in a star configuration  $S_k$ . We have seen in [8] that the variance of  $k$  paths up to distance  $R$  is reduced by a factor  $1/k^2$  with respect to the  $k = 1$  single path case, namely:

$$(12.51) \qquad \ln^2 i_k = \frac{1}{k^2} \ln R :$$

In the case of non-simple paths ( $k > 4$ ), one can further consider the winding at points where  $k$  strands meet together, amongst which adjacent pairs (with  $2j - k$ ) are conditioned not to hit each other [12]. In each pair the two strands, which



Appendix A . Brownian Intersection Exponents from Quantum Gravity

A .1. Non-Intersection Exponents and KPZ . Consider a number  $L$  of independent random walks (or Brownian paths)  $B^{(l)}; l = 1; \dots; L$  in  $(\mathbb{R}^d)$ ; started at fixed neighboring points, and the probability

$$P_L(t) = P \left[ \bigcap_{l=1}^L (B^{(l)}[0;t] \cap B^{(l')}[0;t]) = \emptyset \right];$$

that their paths do not intersect up to time  $t$ . At large times and for  $d < 4$ ; one expects this probability to decay as  $P_L(t) \sim t^{-\gamma_L}$ , where  $\gamma_L(d)$  is a universal exponent depending only on  $L$  and  $d$ .

For  $L$  walks with Dirichlet boundary conditions in  $H$ , and started at neighboring points near the boundary, the non-intersection probability  $P_L^{\sim}(t)$  scales as  $P_L(t) t^{-\tilde{\gamma}_L}$ , with a boundary exponent  $\tilde{\gamma}_L$ . In two dimensions, the exponent values are

$$(A.1) \quad \gamma_L = h_{0;L}^{(c=0)} = \frac{1}{24} (4L^2 - 1);$$

and for the halfplane

$$(A.2) \quad 2\tilde{\gamma}_L = h_{1;2L+2}^{(c=0)} = \frac{1}{3} L (1 + 2L);$$

where  $h_{p;q}^{(c)}$  denotes the Kac conformal weight

$$(A.3) \quad h_{p;q}^{(c)} = \frac{[(m+1)p - m q]^2 - 1}{4m(m+1)};$$

of a minimal conformal field theory of central charge  $c = 1 - 6/m(m+1)$ ;  $m \in \mathbb{N}$  [12]. For Brownian motions  $c = 0$ ; and  $m = 2$ :

This appendix provides the main lines of a derivation of these exponents. One considers the random walks on a random lattice with planar geometry, or, in other words, in presence of two-dimensional quantum gravity [26]. There, the conformal dimensions of non-intersecting walks are obtained from an exact solution. We then use the non-linear KPZ map which exists between conformal weights on a random surface and  $\gamma^{(0)}$  in the plane (2.9),

$$(A.4) \quad \gamma^{(0)} = U(\gamma) = \frac{(\gamma)}{(1-\gamma)};$$

where  $\gamma$ , the string susceptibility exponent, is related to the central charge:

$$(A.5) \quad c = 1 - 6\gamma^2 = (1-\gamma);$$

for a minimal model of the series (A.3),  $\gamma = 1-m$ , and with  $\gamma^{(0)} = h_{p;q}^{(c)}$ : For Brownian motions  $\gamma = 1=2$ , and the KPZ relation becomes

$$(A.6) \quad \gamma^{(0)} = U_{(\gamma=1=2)}(\gamma) = \frac{1}{3} (1 + 2\gamma);$$

which indeed bears a striking resemblance to (A.2). Eqs. (A.1) and (A.2) then correspond to

$$(A.7) \quad \begin{aligned} \gamma_L &= \frac{1}{2} L - \frac{1}{2}; & \gamma_L &= U_{(\gamma=1=2)}(\gamma_L) \\ \tilde{\gamma}_L &= L; & 2\tilde{\gamma}_L &= U_{(\gamma=1=2)}(\tilde{\gamma}_L); \end{aligned}$$

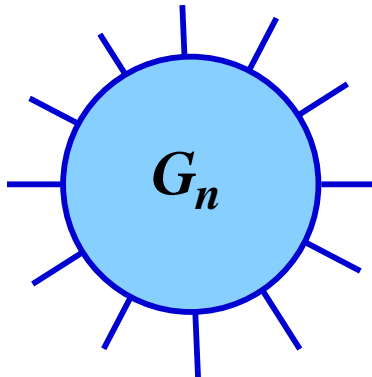


Figure 26. A planar random disk with  $n$  external legs.

A.2. Planar Random Graphs. Consider the set of planar random graphs  $G$ , built up with, e.g., trivalent vertices and with a fixed topology, here that of a sphere ( $S$ ) or a disk ( $D$ ). The partition function is defined as

$$(A.8) \quad Z(\lambda; \mu) = \sum_G \frac{1}{S(G)} e^{-\sum_j \mu_j};$$

where  $\chi$  denotes the Euler characteristic  $\chi = 2(S); 1(D)$ ;  $\sum_j \mu_j$  is the number of vertices of  $G$ ,  $S(G)$  its symmetry factor. The partition sum converges for all values of the parameter  $\mu$  larger than some critical  $\mu_c$ . At  $\mu = \mu_c^+$ ; a singularity appears due to the presence of infinite graphs in (A.8)

$$(A.9) \quad Z(\lambda; \mu) \sim (\mu - \mu_c)^{2 - \text{str}(\mu)};$$

where  $\text{str}(\mu)$  is the string susceptibility exponent. For pure gravity as described in (A.8), with central charge  $c = 0$ ; one has  $\text{str}(\mu) = 2 - \frac{5}{4}$  [84].

The two-puncture partition function will play an important role. It is defined as

$$(A.10) \quad Z[\text{two punctures}] = \frac{\partial^2}{\partial \mu^2} Z(\lambda; \mu) = \sum_{G(\mu)} \frac{1}{S(G)} \sum_j \mu_j^2 e^{-\sum_j \mu_j};$$

It scales as:

$$(A.11) \quad \frac{\partial^2}{\partial \mu^2} Z(\lambda; \mu) \sim (\mu - \mu_c)^{2 - \text{str}(\mu)};$$

The restricted partition function of a planar random graph with the topology of a disk and a fixed number  $n$  of external vertices (26),

$$(A.12) \quad G_n(\lambda) = \sum_{n \text{ leg planar } G} e^{-\sum_j \mu_j};$$

can be calculated through the large  $N$  limit of a random  $N \times N$  matrix integral [109]. It has an integral representation

$$(A.13) \quad G_n(\lambda) = \int_a^b d\mu (\mu)^n;$$

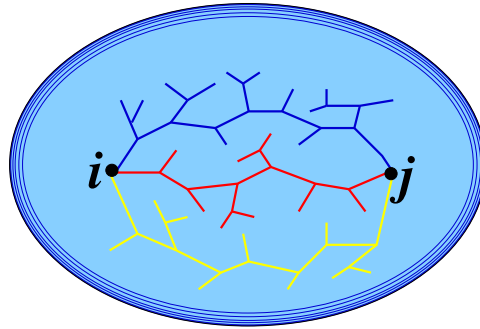


Figure 27.  $L = 3$  mutually-avoiding random trees on a random sphere.

where  $\rho(\lambda)$  is the spectral eigenvalue density of the random matrix, for which the explicit expression is known as a function of  $\lambda$ ; [109]. The support  $[a;b]$  of the spectral density depends on  $\lambda$ .

A.3. Random Walks on Random Graphs.

A.3.1. Representation by Trees. Imagine putting a set of  $L$  random walks  $B^{(l)}; l = 1; \dots; L$  on the random graph  $G$  with the special constraint that they start at the same vertex  $i \in G$ ; end at the same vertex  $j \in G$ , and have no intersections in between. Consider the set  $B^{(l)}[i;j]$  of the points visited on the random graph by a given walk  $B^{(l)}$  between  $i$  and  $j$ , and for each site  $k \in B^{(l)}[i;j]$  the first entry, i.e., the edge of  $G$  along which the walk  $(l)$  reached  $k$  for the first time. The union of these edges form a tree  $T_{i,j}^{(l)}$  spanning all the sites of  $B^{(l)}[i;j]$ , called the forward tree. An important property is that the measure on all the trees spanning a given set of points visited by a RW is uniform [110]. This means that we can also represent the path of a RW by its spanning tree taken with uniform probability. Furthermore, the non-intersection property of the walks is by definition equivalent to that of their spanning trees.

A.3.2. Bulk tree partition function. One introduces the  $L$  tree partition function on the random lattice (Fig. 27)

$$(A.14) \quad Z_L(\lambda; z) = \sum_{\text{planar } G} \frac{1}{S(G)} e^{-\lambda \sum_{i,j \in G} X_{ij}} \prod_{l=1}^L \sum_{T_{i,j}^{(l)}} z^{\sum_{i,j} X_{ij}}$$

where  $\sum_{i,j} X_{ij}$  is a set of  $L$  trees, all constrained to have sites  $i$  and  $j$  as end-points, and without mutual intersections; a fugacity  $z$  is in addition associated with the total number  $\sum_{i,j} X_{ij} = \sum_{l=1}^L \sum_{i,j} X_{ij}^{(l)}$  of vertices of the trees. In principle, the trees spanning the RW paths can have divalent or trivalent vertices on  $G$ , but this is immaterial to the critical behavior, as is the choice of purely trivalent graphs  $G$ , so we restrict ourselves here to trivalent trees.

A.3.3. Boundary Partition Functions. We generalize this to the boundary case where  $G$  now has the topology of a disk and where the trees connect two sites  $i$  and

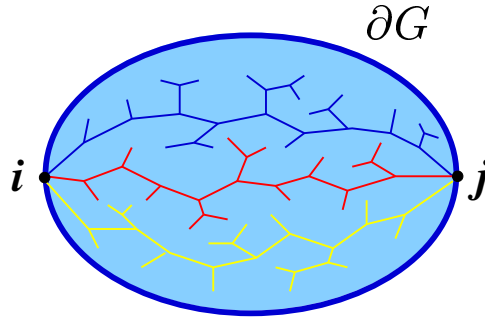


Figure 28.  $L = 3$  mutually-avoiding random trees traversing a random disk.

$j$  on the boundary  $\partial G$  (Fig. 28)

$$(A.15) \quad Z_L(\cdot; z; \mathbf{z}) = \int_{\text{disk } G} e^{-\int_{i,j \in \partial G} \mathbf{z} \cdot \mathbf{g} \cdot j} \prod_{i,j \in \partial G} \prod_{l=1}^L T_{i,j}^{(l)} z^{T_j};$$

where  $\mathbf{z}$  is the fugacity associated with the boundary's length.

The partition function of the disk with two boundary punctures is defined as

$$(A.16) \quad Z(\bullet \circlearrowleft \bullet) = \int_{\text{disk } G} e^{-\int_{i,j \in \partial G} \mathbf{z} \cdot \mathbf{g} \cdot j} \int_{\partial G} \mathbf{z}^2 = Z_{L=0}(\cdot; \mathbf{z});$$

and formally corresponds to the  $L = 0$  case of the  $L$ -tree boundary partition functions (A.15).

A.3.4. Integral representation. The partition function (A.14) has been calculated exactly in previous work [28], while (A.15) was first considered in [50]. The twofold grand canonical partition function is calculated first by summing over the abstract tree configurations, and then gluing patches of random planar lattices in between these trees. A tree generating function is defined as  $T(\mathbf{x}) = \sum_{n \geq 1} x^n T_n$ ; where  $T_1 = 1$  and  $T_n$  is the number of rooted planar trees with  $n$  external vertices (excluding the root). It reads [28]

$$(A.17) \quad T(\mathbf{x}) = \frac{1}{2} (1 + \sqrt{1 - 4\mathbf{x}});$$

The result for (A.14) is then given by a multiple integral:

$$(A.18) \quad Z_L(\cdot; z) = \int_{\mathbf{y}^1} \prod_{l=1}^L d_{\mathbf{y}^l}(\mathbf{y}^l) T(\mathbf{z}_{l-1}; \mathbf{z}_{l+1});$$

with the cyclic condition  $\mathbf{y}_{L+1} = \mathbf{y}_1$ . The geometrical interpretation is quite clear (Fig. 1). Each patch  $l = 1; \dots; L$  of random surface between trees  $T^l, T^{(l)}$  contributes as a factor a spectral density  $d_{\mathbf{y}^l}(\mathbf{y}^l)$  as in eq. (A.13), while the backbone of the each tree  $T^{(l)}$  contributes an inverse "propagator"  $T(\mathbf{z}_{l-1}; \mathbf{z}_{l+1})$ ; which couples the eigenvalues  $\mathbf{y}_{l-1}; \mathbf{y}_{l+1}$  associated with the two patches adjacent to  $T^{(l)}$ :

$$(A.19) \quad T(\mathbf{x}; \mathbf{y}) = [1 - T(\mathbf{x}) - T(\mathbf{y})]^{-1};$$



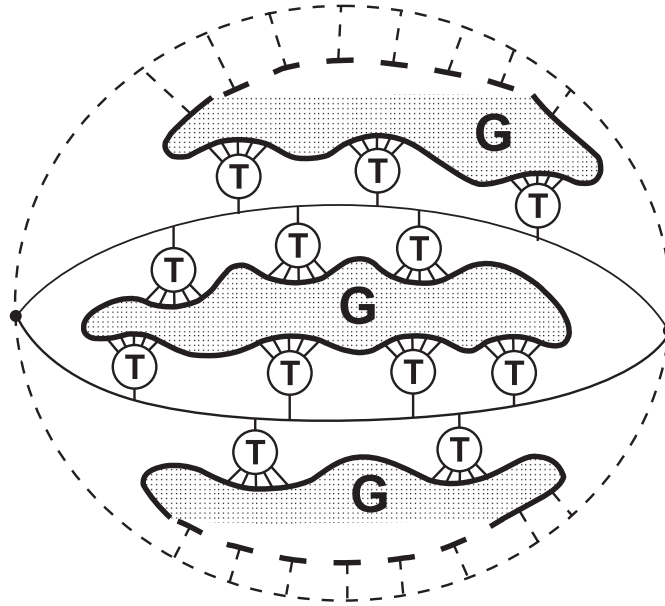


Figure 29. Random trees on a random surface. The shaded areas represent portions of random lattices  $G$  with a disk topology (generating function (A.12, A.13));  $L = 2$  trees connect the end-points, each branch giving a generating function  $T$  (A.17). Two possible topologies are represented: for the disk, the dashed lines represent the boundary, whereas for the sphere the top and bottom dashed lines should be identified with one another, as should the upper and lower grey patches.

The integral representation of the boundary partition function (A.15) is

$$Z_L(\gamma; z; \mathbf{z}) = \int_a^{z_b} \prod_{l=1}^L d_{l-1}(\gamma_l) T(z_l; z_{l+1}) (1 - z_1)^{-1} (1 - z_{L+1})^{-1}; \tag{A.20}$$

with two extra propagators  $L$  describing the two boundary segments:

$$L(z) = (1 - z)^{-1}; \tag{A.21}$$

This gives for the two-puncture disk partition function (A.16)

$$Z(\bullet \circlearrowleft \bullet) = \int_a^{z_b} d(\gamma) (1 - z)^2; \tag{A.22}$$

A.4. Critical Behavior.

A.4.1. Singularity Analysis. The critical behavior of the double grand canonical partition function  $Z_L(\gamma; z)$  (A.18) is obtained by taking the double scaling limit  $z \rightarrow z_c$  (in finite random surface) and  $n \rightarrow \infty$  (in finite trees or RW's). The latter critical fugacity is obtained as the smallest  $z$  where  $T(z_l; z_{l+1})$  (A.19) diverges. This occurs near the upper edge of the support of  $\gamma$ , i.e., when  $z \rightarrow z_b$ , thus for  $4z_c b(\gamma) = 1$  (see (A.17)).

Hereafter we denote  $c = : \dots$ , and  $z = : z$ . In the grand-canonical formalism, their inverses scale like the mean or typical sizes  $\mathbb{E} j$  of the lattice and  $\mathbb{T} j$  of the trees:

$$(A.23) \quad \mathbb{E} j \sim (\dots)^{-1}; \mathbb{T} j \sim (z)^{-1}.$$

Thus we are typically interested in the limits  $\dots \rightarrow 0$  and  $z \rightarrow 0$ .

For  $\dots \neq b$  and for  $\dots \neq 0$ , one knows that  $\dots$  has the singular behavior (up to constant coefficients) [109, 28]

$$(A.24) \quad (\dots; \dots) \sim (\dots)^{\frac{1}{2}} (b - \dots)^{\frac{1}{2}} + (b - \dots)^{\frac{3}{2}}.$$

Because of the coupling via propagators  $T$  of the  $\dots$ 's to  $z$ , hence to  $z \rightarrow 0$ , and by homogeneity, each integration of a density in (A.18) contributes a singular power behavior

$$(A.25) \quad Z \sim \int d \dots \sim (\dots)^{\frac{1}{2}} (z)^{\frac{3}{2}} + (z)^{\frac{5}{2}};$$

while each propagator  $T$  (A.19), because of (A.17), contributes a square root singularity

$$(A.26) \quad T \sim (z)^{\frac{1}{2}}.$$

We therefore arrive at a formal power behavior

$$(A.27) \quad Z_L \sim (\dots)^{\frac{1}{2}} (z) + (z)^{\frac{5}{2}} i_L.$$

The analysis of this singular behavior is best performed by using finite-size scaling (FSS) between the various random sets [28]. One balances the two terms of  $Z_L$  (A.27) against each other so that

$$(A.28) \quad z \sim (\dots)^{\frac{1}{2}}.$$

This corresponds to a dilute phase where

$$(A.29) \quad \mathbb{T} j \sim \mathbb{E} j^{\frac{1}{2}};$$

so that the number of sites visited by the random walks grows like the square root of the lattice size. The partition function (A.27) then scales as

$$(A.30) \quad Z_L(\dots; z) \sim (\dots - c)^L.$$

**A.4.2. Bulk Quantum Gravity Conformal Weights.** The partition function  $Z_L$  (A.18) represents a random surface with two punctures where two conformal operators of conformal weights  $i_L$  are located, here at the two vertices of  $L$  non-intersecting RW's. It scales as

$$(A.31) \quad Z_L \left[ Z \left( \begin{array}{c} \bullet \\ \bullet \end{array} \right) \right] \mathbb{E} j^{2 i_L} = \frac{c^2}{c-2} Z_{=2}(\dots) \mathbb{E} j^{2 i_L};$$

where the two-puncture partition function (A.10) scales as in (A.11). Eq. (A.30) immediately gives

$$(A.32) \quad 2 i_L - \text{str}(\dots = 2) = L;$$

where  $\text{str}(\gamma = 2) = \gamma - 1 = 2$ , or

$$(A.33) \quad \gamma_L = \frac{1}{2} \gamma_L + \frac{1}{2} \gamma ;$$

which is the first of eqs. (A.7), QED.

A.4.3. Boundary Exponents. For the boundary partition function  $Z_L$  (A.20) a similar analysis can be performed near the triple critical point  $(c; z_c; z_c = 1/b(c))$ ; where the boundary length also diverges through the singular behavior of its generating function  $L$  (A.21). A triple finite-size scaling then occurs, with the further equivalence for  $z = z_c$

$$(A.34) \quad z = z_c \left( \frac{1}{z} \right)$$

obtained by homogeneity since in (A.20)  $z$  and  $z$  are coupled to the same spectral parameters in propagators  $T$  and  $L$ , hence  $z = z$ . This amounts to the geometrical triple scaling:

$$(A.35) \quad |G| \sim |G|^{1/2} |T|;$$

with a natural scaling of the boundary length with respect to the area. The latter is characteristic of dilute systems, and is more complex for dense ones (like SLE<sub>4</sub>). See appendices B and C, where a general study of boundary quantum gravity can be found, with applications to the  $O(N)$  model, and to the SLE.

The scaling behavior of  $Z_L$  (A.20) is obtained using the symbolic notation

$$(A.36) \quad Z_L = d^{L+1} ? T^L ? L^2;$$

where the  $?$  operation represents the factorisation of scaling components in terms of (A.25), (A.26) and where the formal powers also represent repeated  $?$  operations. One has

$$(A.37) \quad L \sim (z)^{-1};$$

By analogy to eq. (A.27) one therefore arrives at a formal power behavior

$$(A.38) \quad Z_L = d ? T ? d ? L^2;$$

This can be simply recast as

$$(A.39) \quad Z_L = Z_L ? d ? L^2;$$

Notice that the last two factors precisely correspond to the scaling of the two-puncture boundary partition function (A.22)

$$(A.40) \quad Z(\bullet \circlearrowleft \bullet) = Z_0 d ? L^2;$$

A.4.4. Boundary Conformal Weights. Partition function  $Z_L$  (A.15) corresponds to the insertion of two boundary operators of dimensions  $\tilde{\gamma}_L$ ; integrated over the boundary  $\partial G$ ; on a random surface with the topology of a disk, or in graphical terms:

$$(A.41) \quad Z_L = Z(\bullet \circlearrowleft \bullet) |G|^{2\tilde{\gamma}_L} ;$$

We can use the punctured disk partition function scaling (A.40) to divide (A.39) and get

$$(A.42) \quad Z_L = Z(\text{punctured disk}) Z_L;$$

where the equivalences hold true in terms of scaling behavior. Comparing eqs. (A.31) to (A.41)–(A.42), and using FSS equation (A.35) gives the general identity between boundary and bulk exponents:

$$(A.43) \quad \tilde{\gamma}_L = 2 \gamma_L - \text{str}(\gamma = 2):$$

From the bulk conformal weight (A.32), one finds

$$(A.44) \quad \tilde{\gamma}_L = L;$$

which is the second of eqs. (A.7), QED.

Applying KPZ relation (A.6) to  $\gamma_L$  and  $\tilde{\gamma}_L$  yields exponents  $\gamma_L$  (A.1), and  $2\tilde{\gamma}_L$  (A.2), QED.

Notice the peculiar relation (A.43) between boundary and bulk exponents, which is also linear in terms of the numbers of Dirichlet-like mutually-avoiding components. This is a part of the general results established in appendices B and C.

### A.5. Generalized Non-Intersection Exponents.

A.5.1. Definitions. Eqs. (A.18) and (A.20) give the key to many generalizations. Indeed the product of identical propagators  $T^L$  there can be replaced by a product of different propagators  $T_{n_1}$ , corresponding to different geometrical objects, as obvious from the cyclic construction (see figure 29).

Consider in particular configurations made of  $L$  mutually-avoiding bunches  $l = 1; \dots; L$ , each of them made of walks transparent to each other, i.e.,  $n_l$  independent RW's [48]. The probability of non-intersection of the  $L$  packets scales as

$$(A.45) \quad P_{n_1; \dots; n_L}(t) \sim t^{-(n_1; \dots; n_L)}$$

and near a Dirichlet boundary

$$(A.46) \quad P'_{n_1; \dots; n_L}(t) \sim t^{-\tilde{(n_1; \dots; n_L)}}$$

The original case of  $L$  mutually-avoiding RW's now corresponds to  $n_1 = \dots = n_L = 1$ . The generalizations of exponents  $(n_1; \dots; n_L)$  and  $\tilde{(n_1; \dots; n_L)}$  as well as  $2\tilde{(n_1; \dots; n_L)}$  describing these  $L$  packets can be calculated from quantum gravity.

A.5.2. Random Lattice Partition Functions. On a random lattice, each bunch will contribute a certain inverse propagator  $T_{n_1}$  and yield instead of (A.18)

$$(A.47) \quad Z_{fn_1; \dots; n_L}(g; \mathfrak{n}) = \sum_{a=1}^Z \prod_{l=1}^L \mathfrak{Y}_l^{n_l} d_{l-1}^{(1)} T_{n_1};$$

or for (A.20)

$$(A.48) \quad Z'_{fn_1; \dots; n_L}(g; \mathfrak{n}) = \sum_{a=1}^Z \prod_{l=1}^L \mathfrak{Y}_l^{n_l+1} d_{l-1}^{(1)} T_{n_1 L_1 L_{L+1}};$$

Recall that the two-puncture boundary partition function reads

$$(A.49) \quad Z(\bullet \circlearrowleft \bullet) = d^{-2} \int L^2$$

In terms of scaling behavior, we can thus rewrite the above integral representations as in (A.36) and (A.40)

$$(A.50) \quad Z_{fn_1; Lg;n} = \frac{Z_{fn_1; Lg;n}}{Z(\bullet \circlearrowleft \bullet)}$$

$$(A.51) \quad \int d^2x \int_{T_{n_1}} \prod_{l=1}^n \dots$$

A.5.3. Bulk and Boundary Quantum Gravity Conformal Weights. From the definition of bulk quantum gravity conformal weights, the bulk partition function has to be identified, as in (A.31), to

$$(A.52) \quad Z_{fn_1; Lg;n} = Z(\bullet \circlearrowleft \bullet) \int G^{2fn_1g} \int G^{str(=2) 2fn_1g}$$

while the normalized boundary partition function scales, as in (A.41), as

$$(A.53) \quad \frac{Z_{fn_1; Lg;n}}{Z(\bullet \circlearrowleft \bullet)} \int G^{2fn_1g}$$

The relative scaling of the boundary length with respect to the area,  $\int G \int G^{1=2}$ , together with (A.50), (A.52), and (A.53), immediately gives the relation between bulk and boundary conformal weights:

$$(A.54) \quad \tilde{fn}_1; Lg;n = 2fn_1; Lg;n_{str(=2)} = 2fn_1; Lg;n \frac{1}{2}$$

where we have used the value  $str(=2) = 1=2$  for pure quantum gravity ( $c=0$ ).

A.5.4. Single Packet Partition Functions. Introduce now the partition functions corresponding to the existence of only one packet of  $n_1$  independent random walks on the random lattice, namely  $Z(n_1) = Z_{fn_1=0; 1; n_L \neq 0g}$  and  $Z'(n_1) = Z'_{fn_1=0; 1; n_L \neq 0g}$ . Using the same notation as in (A.47) and (A.48), we rewrite them as

$$(A.55) \quad Z(n_1) = \int d^2x \int_{T_{n_1}} \dots$$

$$(A.56) \quad Z'(n_1) = \int d^2x \int_{T_{n_1}} \prod_{l=1}^n \dots$$

As before, these equations imply in terms of scaling behavior

$$(A.57) \quad Z(n_1) = \frac{Z'(n_1)}{Z(\bullet \circlearrowleft \bullet)} \int d^2x \int T$$

A.5.5. Conformal Weights. As usual, the definition of the conformal weights is expressed as:

$$(A.58) \quad Z(n_1) = Z(\bullet \bullet) \mathfrak{G} j^{2(n_1)} \mathfrak{G} j^{\text{str}(=2) 2(n_1)};$$

$$(A.59) \quad \frac{Z(n_1)}{Z(\bullet \bullet)} = \mathfrak{G} j^{2\tilde{n}(n_1)};$$

where now  $\tilde{n}(n)$  and  $\tilde{\sim}(n)$  are the bulk and boundary quantum conformal weights of a single bunch of  $n$  transparent walks on the random surface. From (A.57) we conclude as in (A.54) that:

$$(A.60) \quad \begin{aligned} \tilde{\sim}(n_1) &= 2(n_1) - \text{str}(=2) \\ &= 2(n_1) + \frac{1}{2}; \end{aligned}$$

A.5.6. Factorization Properties. The factorization property (A.51), together with (A.57), immediately gives in terms of scaling behavior as represented by the  $\mathfrak{?}$  operation:

$$(A.61) \quad Z(fn_1; \mathbb{L}g; n) \stackrel{Y^L}{=} \mathfrak{?} fZ(n_1)g$$

$$(A.62) \quad \stackrel{Y^L}{=} \mathfrak{?} \frac{Z(n_1)}{Z(\bullet \bullet)} \frac{Z(fn_1; \mathbb{L}g; n)}{Z(\bullet \bullet)}$$

Running these scaling relations backwards, with the help of definitions (A.52), (A.53), (A.58) and (A.59), immediately gives the basic additivity of boundary conformal dimensions, or shifted bulk ones, in presence of gravity:

$$(A.63) \quad \begin{aligned} \tilde{\sim}(fn_1; \mathbb{L}g; n) &= \sum_{l=1}^{X^L} \tilde{\sim}(n_1) \\ &= \sum_{l=1}^{X^L} 2(n_1) + \frac{1}{2} = 2(fn_1; \mathbb{L}g; n) + \frac{1}{2}; \end{aligned}$$

A.5.7. Exponents  $\tilde{\sim}(n)$ . It does not seem to be easy to calculate the random lattice partition functions (A.55) or (A.56) corresponding to a packet of  $n$  transparent walks for  $n \notin 1$ , since the walks, as the forward trees spanning the visited sites, will overlap strongly and enclose arbitrarily many patches of random lattice. In other words, the explicit form of propagator  $T_n$  is not easily accessible for  $n \geq 2$ . For  $n = 1$  it is given by the expression (A.19) in terms of the tree generating function (A.17).

We know, however, the exact value of the Dirichlet boundary exponent  $\tilde{\sim}(n)$  in presence of quantum gravity corresponding to such a bunch of  $n$  transparent random walks. Indeed, in the standard half-plane  $H$ , it must correspond to a boundary conformal weight

$$(A.64) \quad \tilde{\sim}^{(0)}(n) = U(\tilde{\sim}(n));$$

which is its image by the KPZ map (A.6):

$$(A.65) \quad U(\tilde{\sim}(n)) = U_{(\text{str}(=2))}(\tilde{\sim}(n)) = \frac{1}{3}(1 + 2\tilde{\sim}(n));$$

In the half-plane with Dirichlet boundary conditions, for  $n$  independent Brownian paths, one has by simple additivity

$$(A.66) \quad \tilde{\gamma}^{(0)}(n) = n \tilde{\gamma}^{(0)}(1) = n;$$

since for a single Brownian path one has by elementary means:  $\tilde{\gamma}^{(0)}(1) = 1$ . The inverse of KPZ map (A.6) then gives the result

$$(A.67) \quad \tilde{\gamma}(n) = U^{-1}(n) = \frac{1}{4} \left( \sqrt{24n+1} - 1 \right);$$

This quantum gravity boundary conformal weight is highly non-trivial since the random walks (in the scaling limit, the Brownian paths), while independent in a fixed metric, are strongly coupled by the fluctuations of the metric in quantum gravity.

A.5.8. Back to the Complex (Half-) Plane. Using once again the KPZ relation (A.65) for  $\tilde{\gamma}_{1g}$  and  $\tilde{\gamma}_{1g}$  gives the general results in the standard complex half-plane  $H$  or plane  $C$

$$\begin{aligned} 2\tilde{\gamma}(n_1; L); n &= \tilde{\gamma}^{(0)}(n_1); L g; n U \tilde{\gamma}_{1g} \\ \tilde{\gamma}(n_1; L); n &= \tilde{\gamma}^{(0)}(n_1); L g; n U (\tilde{\gamma}_{1g}) : \end{aligned}$$

Using eqs. (A.63) and (A.67) finally gives

$$(A.68) \quad \begin{aligned} & 2\tilde{\gamma}(n_1; L); n U \tilde{\gamma}_{1g}; L g; n \\ & \tilde{\gamma}(n_1; L); n V \tilde{\gamma}_{1g}; L g; n \\ & \tilde{\gamma}_{1g}; L g; n \prod_{l=1}^P U^{-1}(n_l) = \prod_{l=1}^P \frac{1}{4} \left( \sqrt{24n_l+1} - 1 \right) \end{aligned}$$

with

$$(A.69) \quad \begin{aligned} & U(\cdot) = U_{(\cdot=1=2)}(\cdot) = \frac{1}{3} (1+2) \\ & V(\cdot) = U \frac{1}{2} \frac{1}{2} = \frac{1}{24} (4^2 - 1); \end{aligned}$$

which is the quantum gravity geometric structure announced in section 2, QED.

### Appendix B. $O(N)$ Model Multi-Line Exponents from Quantum Gravity

Let us derive here the  $O(N)$  multi-line exponents (11.32), (11.33), (11.34), and (11.35) from their study on a random lattice. We shall in particular focus on the relationship between boundary and bulk exponents. The approach will be similar to the one followed in appendix A for multiple tree exponents. (See also refs. [28, 29, 115].)

#### B.1. Random Lattice Partition & Two-Point Functions.

B.1.1. Partition Function. Consider again the set of planar random graphs  $G$ , built up with, e.g., trivalent vertices and with a fixed topology. The partition function of the  $O(N)$ -loop model is defined as

$$(B.1) \quad Z_{O(N)}(\gamma; K; \nu) = \sum_{G(\gamma)} \frac{1}{S(G)} e^{\sum_j \nu_j} W_{O(N)}(G)$$

$$(B.2) \quad W_{O(N)}(G) = \sum_{L \subseteq G} K^{\sum_j \ell_j} N^{\text{Card}L};$$

where  $\chi$  denotes the fixed Euler characteristic of the lattice  $G = G(\gamma)$ ;  $\sum_j \nu_j$  is the number of vertices of  $G$ ,  $S(G)$  its symmetry factor. In the  $O(N)$  weight  $W_{O(N)}(G)$ , the sum runs also over all self-avoiding loop configurations  $L$  on  $\sum_j \nu_j$  with a fugacity  $K$  for the total occupied length  $\sum_j \ell_j$  and a fugacity  $N$  for the total number of loops  $\text{Card}L$ . Notice that the effective fugacity associated with bonds occupied by  $O(N)$  loops is

$$z = e^{-K};$$

The Euler characteristic is

$$(B.3) \quad \chi = 2 - 2H - B;$$

where  $H$  and  $B$  respectively are the numbers of handles and boundaries of  $G$ . In the following we shall consider explicitly the cases of the spherical topology ( $\chi = 2$ ), and of the disk ( $\chi = 1$ ).

The partition function of the random lattice with two punctures will play an important role later. It is defined by twice differentiating the one above with respect to the "chemical potential", or "cosmological constant",

$$(B.4) \quad \frac{\partial^2}{\partial \nu^2} Z_{O(N)}(\gamma; K; \nu) = \sum_{G(\gamma)} \frac{1}{S(G)} \sum_j \nu_j^2 e^{\sum_j \nu_j} W_{O(N)}(G)$$

$$(B.5) \quad = : Z_{O(N)}[\text{disk with two punctures}]$$

with an intuitively obvious graphical representation for this two-puncture partition function.

For a given  $\gamma$ , the partition sum  $Z_{O(N)}$  converges for all values of the parameter  $K$  smaller than some critical  $K_c(\gamma)$ . For  $K > K_c(\gamma)$  the loops fill the lattice and force it to become infinite: this is the dense phase. There is also a critical line  $K = K_c(K)$ , such that at  $K = K_c(K)$  a singularity appears, solely due to the presence of infinite graphs in (B.1), and where the loops stay non-critical. This corresponds to pure gravity. The two critical regimes meet for  $\gamma = \gamma_c$  such that  $K_c = K_c(K_c)$ . Then the loops, for  $K > K_c(\gamma)$ , and the non-occupied part of the random lattice, for  $K < K_c(\gamma)$ ; become infinite simultaneously: this is the dilute phase [28].

B.1.2. Disk Green's Function. The disk partition function, or rather here, Green's function, associated with a planar random graph with the topology of a disk, and bearing a sea of  $O(N)$  loops, with a fixed number  $n$  of external vertices (Fig. 30), is defined as

$$(B.6) \quad G_{O(N),n}(\gamma; K) = \sum_{n \text{ leg planar } G} e^{\sum_j \nu_j} \sum_{L \subseteq G} K^{\sum_j \ell_j} N^{\text{Card}L};$$



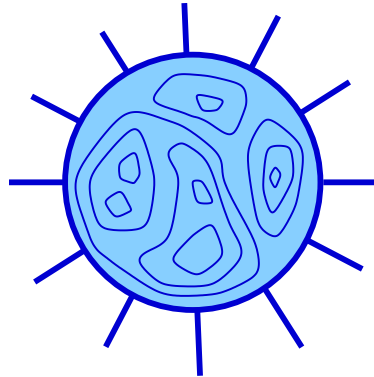


Figure 30. Planar random disk with a sea of  $O(N)$  loops, and a fixed number  $n$  of external vertices.

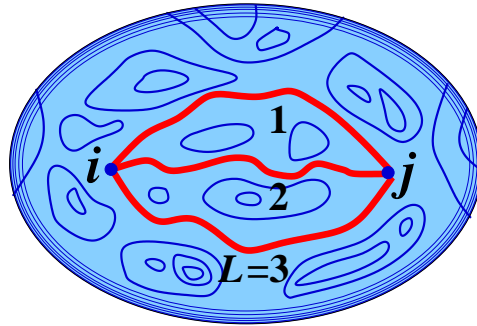


Figure 31. The watermelon configuration of  $L = 3$  random lines among  $O(N)$  loops on the random sphere, building up partition function (B.7).

B.1.3. Bulk Two-Point Partition Function. Now, let us consider a set of  $L$  self- and mutually-avoiding walks  $\gamma_{ij} = f_{ij}^{(l)}; l = 1; \dots; L$  on the random graph  $G$  with the constraints that they start at the same vertex  $i \in G$  (or near it, if  $L = 4$ ), end at (or near) the same vertex  $j \in G$ , and have no mutual intersections in between (Fig. 31). The  $L$ -walk partition function on the random lattice with a spherical topology reads [28]

$$(B.7) \quad Z_{O(N);L}(i; j; z) = \sum_{\text{planar } G} \frac{1}{S(G)} e^{-\beta G} W_{O(N)}(G) \sum_{i, j \in G} \sum_{\substack{\gamma_{ij}^{(l)} \\ l=1; \dots; L}} z^{j_{ij}^{(l)}};$$

a fugacity  $z$  is associated with the total number  $j_{ij} = \sum_{l=1}^L j_{ij}^{(l)}$  of bonds occupied by the  $L$  walks. At a later stage, it will be convenient to keep  $z$  distinct from the effective fugacity  $z = e^{-K}$  associated with the bonds occupied by the  $O(N)$  loops.

B.1.4. Boundary Two-Point Partition Function. We generalize this to the boundary case where  $G$  now has the topology of a disk and where the  $L$  lines connect two

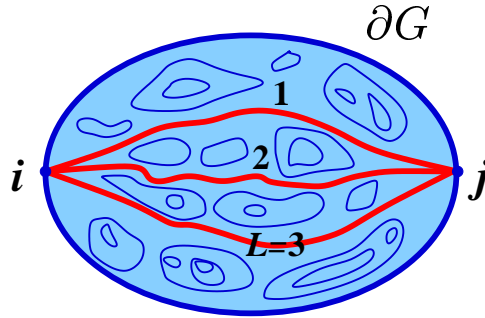


Figure 32. The boundary watermelon configuration of  $L = 3$  random lines among  $O(N)$  loops on the random disk, building up partition function (B.8).

sites  $i$  and  $j$  on the boundary  $\partial G$  (Fig. 32):

$$(B.8) \quad Z_{O(N);L}(\cdot; z; \mathbf{z}) := \int_{\text{disk } G} e^{-\beta \int \mathbb{W}_{O(N)}(G)} \mathbf{z}^{\beta G} \prod_{i,j \in \partial G} \prod_{l=1;\dots;L} z^{j_{ij}^{(l)}}$$

where  $\mathbf{z}$  is the new fugacity associated with the boundary's length. The partition function of the disk with two boundary punctures will play an important role in the sequel. It corresponds to eq. (B.8) in the absence of the  $L$  lines, and is defined as

$$(B.9) \quad Z_{O(N)}(\bullet\text{---}\bullet) := Z_{O(N);L=0}(\cdot; z; \mathbf{z}) = \int_{\text{disk } G} e^{-\beta \int \mathbb{W}_{O(N)}(G)} \mathbf{z}^{\beta G} \int_{\partial G} \mathbf{z}^2 :$$

B.2. Random Matrix and Spectral Representation.

B.2.1. Disk Green's Function. First, the disk partition function (B.6) can be calculated through the large  $N$  limit of a random  $N \times N$  matrix integral [29]. It has an integral representation

$$(B.10) \quad G_{O(N);m}(\cdot; K) = \int_a^b d \rho_{O(N)}(\cdot; K)^n ;$$

where  $\rho_{O(N)}(\cdot; K)$  is the spectral eigenvalue density of the random matrix model as a function of  $\cdot$ ,  $K$  and  $N$ . The support  $[a;b]$  of the spectral density depends on  $\cdot$ ,  $K$ , and  $N$ . An explicit expression for  $\rho_{O(N)}(\cdot)$  is known along the critical line  $K = K_c(\cdot)$  [29].

B.2.2. Spherical Two-Point Partition Function. The partition function (B.7) was calculated exactly in previous work [28]. The two-fold grand canonical partition function is calculated first by summing over the  $L$ -line configurations, and then by gluing patches of random lattices in between these lines. In fact, it can also be obtained directly from the tree case of appendix A, by remarking that from each site belonging to one of the  $L$  traversing lines, only a single edge of the random lattice now grows, instead of a rooted tree. That amounts exactly to replacing the series giving the tree propagator  $T(x)$  (A.17) of appendix A by its first term,  $x$ .

The result for (B.7) is then given by a multiple integral similar to (A.18):

$$(B.11) \quad Z_{O(N);L}(\lambda; z) = \int_{a=1}^b \prod_{l=1}^L d\lambda_{l, O(N)}(\lambda) \prod_{l=1}^L L(z_l; z_{l+1});$$

with the cyclic condition  $\lambda_{L+1} = \lambda_1$ . Each patch  $l=1; \dots; L$  of random surface between lines  $l; l+1$  contributes as a factor an  $O(N)$  spectral density  $d\lambda_{l, O(N)}(\lambda)$  as in eq. (B.10), while each line  $l$  contributes an inverse "propagator"  $L(z_l; z_{l+1})$ ; similar to (A.19) which couples the adjacent eigenvalues  $\lambda_l; \lambda_{l+1}$ :

$$(B.12) \quad L(x; y) = (1 - x - y)^{-1};$$

B.2.3. Boundary Two-Point Partition Function. The integral representation of the boundary two-point partition function (B.8) is similarly

$$(B.13) \quad Z_{O(N);L}(\lambda; z; z) = \int_{a=1}^b \prod_{l=1}^L d\lambda_{l, O(N)}(\lambda) \prod_{l=1}^L L(z_l; z_{l+1}) (1 - z_1)^{-1} (1 - z_{L+1})^{-1}$$

with two extra propagators  $L(z_{1 \text{ or } L+1})$  describing the two boundary lines between  $i$  and  $j$ . Hence one sees here that the exterior boundary lines and the  $L$  interior random paths play very similar roles. This is the case for Dirichlet boundary conditions.

B.2.4. Disk Partition Function. The partition function of the disk with two boundary punctures (B.9) is given by the non-trivial case  $L = 0$  of (B.13)

$$(B.14) \quad Z_{O(N)}(\text{disk with two punctures}) = Z_{O(N);L=0}(\lambda; z; z) = \int_a^b d\lambda (\lambda) (1 - z)^{-2};$$

where we again used the graphical representation of the boundary two-puncture partition function.

### B.3. Scaling Behavior.

B.3.1. Eigenvalue Density. The critical behavior of the  $O(N)$  model corresponds, for the eigenvalue density  $\rho(\lambda)$ , as usual to the vicinity of the end-point  $b$  of the spectrum [28, 29]. The critical line  $K_c(\lambda)$  mentioned above is given by the critical effective loop fugacity  $z = z_c(\lambda)$  with

$$z_c(\lambda) = e^{-K_c(\lambda)} = (2b)^{-1}$$

This can be seen also in the critical behavior of the double-grand canonical partition function  $Z_{O(N);L}(\lambda; z)$  (B.11) associated with  $L$  non-intersecting lines on the  $O(N)$  random lattice. The critical point of the L watermelon lines is indeed obtained in the integral representation for the smallest  $z$  where  $L(z_1; z_{l+1})$  (B.12) diverges. This occurs near the upper edge  $b$  of the support of  $d\lambda_{O(N)}(\lambda)$ , i.e., when

$\lambda = b$ , thus again for  $z = z_c(\lambda)$ , with  $2z_c b = 1$  (see (B.12)). At this critical value of the fugacity, both the internal  $O(N)$  loops and the  $L$  random lines become infinite. As explained above, for reaching the dilute phase a further double scaling is necessary. One can let  $\lambda \rightarrow b$  simultaneously, in a finite-size scaling scheme, or right away set  $\lambda = b$ , and afterwards let  $z \rightarrow z_c(\lambda)$ .

The eigenvalue density is known exactly along the critical line  $K = K_c(\lambda)$  or, equivalently,  $z = z_c(\lambda)$  [29]. We shall only need its behavior for small and

near the upper end of the spectrum, i.e., for  $b \rightarrow 1$ . There  $\rho_{(N)}$  has the double singular behavior (up to constant coefficients) [29, 28]

$$(B.15) \quad \rho_{(N)}(\beta; K_c(\beta)) \sim (\beta - 1)^{-1} + (\beta - 1)^{-1+};$$

where  $\beta$  parametrizes the fugacity  $N$  in the  $O(N)$  model:

$$(B.16) \quad N = 2 \cos(\beta); \quad 0 < \beta < \pi$$

This behavior (B.15) will be sufficient to determine the critical behavior of the various partition functions.

**B.3.2. Spherical Two-Point Partition Function.** We just have seen the scaling behavior of the eigenvalue density along the critical line  $z = z_c(\beta)$ , and in the vicinity the double scaling critical point  $\beta = \pi$ , up to the double critical point  $z = 1$ . In order for the two-point partition function (B.11) to stay finite, it is now crucial to keep the fugacity  $z$  of the watermelon lines in the propagators  $L$  such that  $z < (2b)^{-1}$ , hence away from the critical value  $z = z_c(\beta)$  of the internal loops. Let us thus introduce the shifted quantities

$$(B.17) \quad z = z_c(\beta) + \tilde{z}$$

$$(B.18) \quad \beta = \pi - \tilde{\beta};$$

in terms of which all the scaling analysis, to which we now turn, will be performed.

In multiple integral (B.11), each integration of density  $\rho_{(N)}$  (B.15) yields by homogeneity (power counting) a singular power behavior

$$(B.19) \quad d \rho_{(N)}(\beta) \sim (\tilde{z})^{-2} + (\tilde{z})^{-2+};$$

Each propagator  $L$  (B.12), when integrated over its variables, brings in a singularity

$$(B.20) \quad L \sim (\tilde{z})^{-1};$$

We therefore arrive at a formal power behavior

$$(B.21) \quad Z_{O(N);L} \sim (\tilde{z})^{-L} = (\tilde{z})^{-1 \cdot L};$$

where (B.19) gives the explicit scaling:

$$(B.22) \quad Z_{O(N);L} \sim (\tilde{z})^{-L} + (\tilde{z})^{-L+};$$

**B.3.3. Boundary Two-Point Partition Function.** For the boundary partition function  $Z_{O(N);L}$  (B.13) a similar analysis is performed near the critical point  $z_c = 1/b$ ; where the boundary length also diverges. For Dirichlet boundary conditions, the scaling limit requires the further equivalence of boundary and bulk loops, i.e., for the shifted boundary fugacity  $\tilde{z} = z$  the equivalence:

$$(B.23) \quad z = \tilde{z};$$

The formal scaling of the boundary two-point partition function is therefore:

$$(B.24) \quad Z_{O(N);L} \sim (\tilde{z})^{-L} (\tilde{z})^{-2}$$

Using equivalence (B.23) and (B.19) yields the explicit scaling behavior

$$(B.25) \quad \tilde{Z}_{O(N);L} \sim (z)^{L+1} (z)^{-1}$$

$$(B.26) \quad \tilde{Z}_{O(N);L} \sim (z)^{L+1} + (z)^{L+1} (z)^{-1} :$$

B.4. Partition Function Scaling Identities. In order to simplify the scaling analysis, it is worth noticing several fundamental scaling relations between partition functions, which are structural and do not require the precise knowledge of the eigenvalue density.

B.4.1. Bulk-Boundary Relation. One first notices that one can also rewrite (B.24) as the scaling identity

$$(B.27) \quad \tilde{Z}_{O(N);L} \sim (z)^{L+1} (z)^{-2}$$

where, owing to (B.21) and (B.24), one respectively recognizes the sphere and the boundary two-point partition functions, which are thus linked by a fundamental relation, first observed in [50]:

$$(B.28) \quad \tilde{Z}_{O(N);L} \sim \frac{\tilde{Z}_{O(N);L}}{\tilde{Z}_{O(N)}(\bullet \circ \bullet)} :$$

B.4.2. Recursion Relation. We can also write (B.24), together with (B.23), as a ratio

$$(B.29) \quad \tilde{Z}_{O(N);L} \sim \frac{(z)^{L+2} (z)^{-(L+1)} (z)^{-2}}{(z)^{-2}} (z)^{-1} :$$

Comparing to (B.25) for  $L + 1$  gives a recursion relation between the two-point boundary partition functions at levels  $L$  and  $L + 1$ :

$$(B.30) \quad \tilde{Z}_{O(N);L} \sim \frac{\tilde{Z}_{O(N);L+1}}{\tilde{Z}_{O(N)}(\bullet \circ \bullet)} (z)^{-1} ;$$

a recursion relation which will prove very useful for an easy calculation of scaling exponents.

B.5. Quantum Gravity Conformal Weights.

B.5.1. Finite Size Scaling (FSS). In the grand-canonical ensemble, and in the critical regime  $z \neq 0$  for (B.18) the average size  $\langle |G| \rangle$  of the lattice  $G$  scales as

$$(B.31) \quad \langle |G| \rangle \sim (z)^{-1} ;$$

Let us denote by  $\mathcal{E}_L$  the set of lattice edges occupied by the  $L$  watermelon lines. Its average size  $\langle |\mathcal{E}_L| \rangle$  in the grand-canonical ensemble scales in the critical regime  $z \neq 0$  for (B.17) as

$$(B.32) \quad \langle |\mathcal{E}_L| \rangle \sim (z)^{-1} :$$

Finally, the average size of the boundary line  $\partial G$  scales as

$$(B.33) \quad \langle |\partial G| \rangle \sim (z)^{-1} :$$

Hereafter we shall keep the simplified notations  $\langle \cdot \rangle$ ,  $\langle \cdot \rangle_G$  and  $\langle \cdot \rangle_j$  for those averages. The fugacities  $\mu$  and  $z$  associated with the two random sets  $G$  and  $\mathcal{J}$  are expected to have the relative scaling [28]

$$(B.34) \quad \langle \mu \rangle \sim \langle z \rangle^{\frac{2}{\gamma}} ;$$

where  $\gamma$  (denoted  $\gamma_D=2$  in [28]) is a critical exponent to be determined. It depends on the nature of the critical phase. Thus the sizes of the two random sets  $G$  and  $\mathcal{J}$  are expected to have the relative scaling [28]

$$(B.35) \quad \langle |G| \rangle \sim \langle |\mathcal{J}| \rangle^{\frac{2}{\gamma}}$$

For Dirichlet boundary conditions, we have seen that the boundary line and the watermelon lines are similar, and eqs. (B.23), (B.32), and (B.33) give

$$(B.36) \quad \langle |G| \rangle \sim \langle z \rangle^{-1} \sim \langle \mu \rangle^{-1} \langle |\mathcal{J}| \rangle$$

so that we deal with the finite-size scaling regime

$$(B.37) \quad \langle \mu \rangle \sim \langle z \rangle^{\frac{2}{\gamma}} \sim \langle z \rangle^2$$

or, equivalently

$$(B.38) \quad \langle |G| \rangle \sim \langle |\mathcal{J}| \rangle^{\frac{2}{\gamma}} \sim \langle |\mathcal{J}| \rangle$$

**B.5.2. String Susceptibility Exponent.** Let us first consider the partition function (B.1) in the scaling regime. The string susceptibility exponent  $\gamma_{str}(\gamma)$  is defined by the scaling behavior of the partition function:

$$(B.39) \quad Z_{O(N)}(\mu; K_c; \gamma) \sim \langle \mu \rangle^{-\gamma_{str}(\gamma)} ;$$

where the exponent depends on the topology. Because of the scaling (B.31), one also has

$$(B.40) \quad Z_{O(N)}(\mu; K_c; \gamma) \sim \langle |G| \rangle^{\gamma_{str}(\gamma) - 2} ;$$

The two-puncture partition function (B.4) scales accordingly as:

$$(B.41) \quad \frac{\mathcal{G}^2}{\mathcal{G}} Z_{O(N)}(\mu; K_c; \gamma) \sim \langle \mu \rangle^{-\gamma_{str}(\gamma)} \langle |G| \rangle^{\gamma_{str}(\gamma)} ;$$

The value of  $\gamma_{str}$  can be derived from the exact solution of the  $O(N)$  model [84, 28] (actually here also for the simple topologies of the sphere or of the disk from the scaling equations above). The general formula for  $\gamma_{str}$  is also known from the Liouville theory [27]. It reads in terms of the central charge  $c$ :

$$(B.42) \quad \gamma_{str}(\gamma) = 2 - \frac{25 - c}{24} + \frac{P}{(1 - c)(25 - c)} ;$$

A particularly important one is the string susceptibility exponent of the spherical topology  $\gamma_{str}(\gamma=2)$ , in terms of which the KPZ formula is written. For other topologies we have:

$$(B.43) \quad \gamma_{str}(\gamma=2) - 2 = \frac{1}{2} [\gamma_{str}(\gamma=2) - 2] = \frac{1}{2} (\gamma - 2) ;$$

In particular, for the disk topology,  $\gamma=1$ , we find:

$$(B.44) \quad \gamma_{str}(\gamma=1) = 1 + \frac{1}{2} ;$$

B.5.3. Bulk Conformal Dimensions. We first consider the planar topology ( $\chi = 2$ ). The two-puncture partition function (B.5) and (B.41) then scales as

$$(B.45) \quad Z_{O(N)}[\text{two punctures}] \sim \mathfrak{G} j^{\text{str}(\chi=2)} :$$

In quantum gravity, the bulk conformal weight  $\tilde{h}_L$  is then defined by the scaling of the two-point function  $Z_{O(N);L}$ , properly normalized, with respect to the average size of the lattice:

$$(B.46) \quad Z_{O(N);L} = Z_{O(N)}[\text{two punctures}] \mathfrak{G} j^{2-L} :$$

This definition takes into account the fact that the order  $L$  two-point partition function  $Z_{O(N);L}$  contains, in addition to the insertion of two operators creating  $L$  lines, the two-puncture partition function on the sphere. Thus we have by definition:

$$(B.47) \quad Z_{O(N);L} \sim \mathfrak{G} j^{\text{str}(\chi=2) - 2L} :$$

B.5.4. Boundary Conformal Dimensions. For measuring length scales along a fluctuating boundary, there are two natural possibilities: use the boundary length  $\mathfrak{G} j$  or the square root  $\sqrt{\mathfrak{G} j}$  of the fluctuating area. They differ a priori since we have seen that  $\mathfrak{G} j \sim \mathfrak{G} j^2$ , with  $\chi = 1$ . In boundary quantum gravity, the proper conformal weights are defined in terms of the effective length  $\sqrt{\mathfrak{G} j} \sim \mathfrak{G} j$ .

Let us first consider the disk partition function with two punctures (B.14). We write its scaling as:

$$(B.48) \quad Z_{O(N);L=0} = Z_{O(N)}[\text{two punctures}] \mathfrak{G} j^{\text{str}(\chi=1) - 2} \mathfrak{P} \frac{1}{\mathfrak{G} j}^{2 - 2\tilde{h}_0} :$$

The first power law accounts for the scaling of the disk partition function (B.40) for an Euler characteristic  $\chi = 1$ , with a susceptibility exponent  $\text{str}(\chi = 1)$ , while the second term takes into account the integration and the conformal weight  $\tilde{h}_0$  of the two punctures along the boundary.

For the order  $L$  boundary partition function  $Z_{O(N);L}$ , we similarly define boundary conformal weights  $\tilde{h}_L$ , such that:

$$(B.49) \quad Z_{O(N);L} \sim \mathfrak{G} j^{\text{str}(\chi=1) - 2} \mathfrak{P} \frac{1}{\mathfrak{G} j}^{2 - 2\tilde{h}_L} :$$

We thus have the simple scaling relation

$$(B.50) \quad \frac{Z_{O(N);L}}{Z_{O(N)}[\text{two punctures}]} = \frac{Z_{O(N);L}}{Z_{O(N);L=0}} \mathfrak{P} \frac{1}{\mathfrak{G} j}^{2\tilde{h}_0 - 2\tilde{h}_L} :$$

Measuring scaling behavior in terms of the boundary length  $\mathfrak{G} j$  leads to the definition of another set of boundary quantum gravity dimensions  $\tilde{h}_L^0$ , such that

$$(B.51) \quad Z_{O(N);L} \sim \mathfrak{G} j^{\text{str}(\chi=1) - 2} \mathfrak{G} j^{2 - 2\tilde{h}_L^0} ;$$

or, equivalently

$$(B.52) \quad \frac{Z_{O(N);L}}{Z_{O(N)}[\text{two punctures}]} = \frac{Z_{O(N);L}}{Z_{O(N);L=0}} \mathfrak{G} j^{2\tilde{h}_0 - 2\tilde{h}_L^0} :$$

Because of the FSS relation (B.38) we immediately have:

$$(B.53) \quad \tilde{h}_L^0 - 1 = (\tilde{h}_L - 1) :$$

B.5.5. The Exponent  $\gamma$ . The scaling exponent  $\gamma$  can be related to the bulk conformal weight  $\gamma_2$  and to the boundary conformal weight  $\tilde{\gamma}_0$  as follows. The derivative operator  $\partial_z$  inserts a factor  $j \cdot j \cdot \mathfrak{g}^{1/2}$  equal to the total length of the random lines in partition functions. But by definition it also geometrically represents the insertion of a puncture on the watermelon lines, with a local Gibbs weight  $\mathfrak{g}^{1/2}$ , since  $L = 2$  random strands originate from this puncture. We therefore conclude that:

$$(B.54) \quad \frac{1}{2} = 1 - \gamma_2:$$

Similarly, differentiating a boundary partition function with respect to the boundary fugacity  $z$  with the operator  $\partial_z$  gives a factor  $j \cdot G \cdot j \cdot \mathfrak{g}^{1/2}$  in that partition function. But it also represents the insertion of a puncture operator along the boundary line, with by definition a local Gibbs weight  $\mathfrak{g}^{1/2}$ . We therefore arrive at the second identity

$$(B.55) \quad \frac{1}{2} = 1 - \tilde{\gamma}_0:$$

A first general identity follows:

$$(B.56) \quad 2 - \gamma_2 = 1 + \tilde{\gamma}_0;$$

which we see as characteristic of Dirichlet boundary conditions in quantum gravity. It means that the fractal dimension of random lines in the bulk is the same as that of boundary lines.

B.5.6. Bulk-Boundary Relation between Conformal Weights. In the above we observed the scaling relation (B.28) between the two-point function on the sphere and those on the disk. Relations (B.47) and (B.50) immediately imply the general identity between boundary and bulk exponents:

$$(B.57) \quad \tilde{\gamma}_L - \tilde{\gamma}_0 = 2 - L - \text{str}(\gamma = 2):$$

B.5.7. Recursion for Conformal Weights. We also observed the scaling recursion relation (B.30) between boundary partition functions, which, owing to (B.36) and (B.38) can be rewritten as

$$(B.58) \quad \frac{Z_{O(N);L+1}}{Z_{O(N)}(\bullet \circ \bullet)} = Z_{O(N);L} \cdot \mathfrak{g}^{1/2}:$$

It is now sufficient to apply definitions (B.49) and (B.50) to get the recursion relation

$$(B.59) \quad \tilde{\gamma}_0 - \tilde{\gamma}_{L+1} = 1 - \tilde{\gamma}_L + [\text{str}(\gamma = 1) - 2] \cdot \frac{1}{2}:$$

We finally use (B.43) for  $\text{str}(\gamma = 1) - 2 = \frac{1}{2} [\text{str}(\gamma = 2) - 2]$ , and the expression (B.55) of  $\tilde{\gamma}_0$  to arrive at the recursion:

$$(B.60) \quad \tilde{\gamma}_{L+1} = \tilde{\gamma}_L + \frac{1}{2} \tilde{\gamma}_0 + 1 - \text{str}(\gamma = 2);$$

which finally gives

$$(B.61) \quad \tilde{\gamma}_L = \tilde{\gamma}_0 + \frac{L}{2} \tilde{\gamma}_0 + 1 - \text{str}(\gamma = 2):$$



The bulk conformal weights immediately follow from (B.57):

$$(B.62) \quad \Delta_L = \frac{L}{4} h_{\text{str}(L=2)} + \frac{1}{2} h_{\text{str}(L=2)} + 1$$

Notice that for  $L = 2$ , one has identically  $\Delta_2 = \frac{1}{2}(\Delta_0 + 1)$ , in agreement with (B.56).

**B.5.8. Dilute and Dense Phases.** At this stage, it is remarkable that the multi-line exponents of the  $O(N)$  model (B.61) and (B.62) have been entirely determined from the existence and structure of the spectral representation of the two-point functions (B.11), and (B.13) implying necessary scaling relations, and without using the precise scaling behavior (B.15) of the eigenvalue density, nor the equivalent forms (B.22) and (B.26).

The exponents so found (B.61) and (B.62) depend on only one unknown, the boundary conformal weight  $\tilde{\Delta}_0$  associated with a boundary puncture on a random surface. In the Euclidean half-plane  $H$ , its scaling dimension is given by the KPZ equation:

$$(B.63) \quad \kappa_0 = U(\tilde{\Delta}_0) = \tilde{\Delta}_0 \frac{\tilde{\Delta}_0}{1};$$

where  $\kappa = \text{str}(L=2)$ . It corresponds to a point insertion along  $\partial H$ , and therefore is expected to vanish, so that  $\tilde{\Delta}_0$  is solution of  $\kappa_0 = U(\tilde{\Delta}_0) = 0$ . One solution is trivially  $\tilde{\Delta}_0 = 0$ , while the other is negative:  $\tilde{\Delta}_0 = -1$ . We thus find from (B.55) the two possibilities:

$$(B.64) \quad \begin{aligned} & \text{I} \quad \tilde{\Delta}_0 = 0; \quad \Delta_0 = 1 \\ & \text{II} \quad \tilde{\Delta}_0 = -1; \quad \Delta_0 = \frac{1}{2} \end{aligned}$$

This is where the nature of the critical phase enters. In case I above,  $\Delta_0 = 1$  gives  $\langle G_j | \bar{G}_j \rangle$ , i.e., the boundary is smooth, with a fractal dimension half that of the random surface. This is what is expected for the dilute phase. Another way to describe the dilute phase is to balance the two scaling terms in (B.11) or (B.13), requiring the same scaling for both [28]. This gives  $\Delta_0 = \frac{1}{2}$  (independently of  $L$ ), thus from (B.37)  $\Delta_0 = 1$ , as announced. Thus one is led to conclude that case II above must correspond to the dense phase.

**B.5.9. Quantum Gravity Conformal Weights.** It is interesting to note that the relation (B.57) between bulk and boundary conformal weights then takes two different forms, depending on the nature of the critical phase:

$$(B.65) \quad \begin{aligned} & \text{Dilute} \quad \Delta_L = \tilde{\Delta}_L; \quad \tilde{\Delta}_0 = 0; \quad \Delta_0 = \frac{1}{2}; \quad \Delta_1 = 1 \\ & \text{Dense} \quad \Delta_L = \tilde{\Delta}_L; \quad \tilde{\Delta}_0 = -1; \quad \Delta_0 = \frac{1}{2}; \quad \Delta_1 = \frac{1}{2} \end{aligned}$$

The naive expressions of the boundary conformal weights follow from (B.61):

$$(B.66) \quad \tilde{\Delta}_L = \begin{cases} \frac{L}{2} (1 - \Delta_0) = \binom{L}{L+1,1}; & \tilde{\Delta}_0 = 0; \quad \Delta_0 = 1 \text{ (dilute)} \\ \frac{L}{2} + \frac{1}{2} = \binom{L}{1;L+1}; & \tilde{\Delta}_0 = -1; \quad \Delta_0 = \frac{1}{2} \text{ (dense)}, \end{cases}$$

while the bulk conformal weights immediately follow from (B.62):

$$(B.67) \quad \begin{aligned} & \begin{cases} \delta \\ \gamma \end{cases} \\ & \begin{aligned} & \frac{1}{2} + \frac{L}{4} (1 - \delta) = \binom{\delta}{L=2;0}; \quad \delta_0 = \frac{\delta}{2}; \quad \delta = 1 \text{ (dilute)} \\ & \frac{1}{2} + \frac{L}{4} = \binom{\delta}{0;L=2}; \quad \delta_0 = \frac{\delta}{2}; \quad \delta = \frac{1}{1-L} \text{ (dense)}. \end{aligned} \end{aligned}$$

Hence we have established all the  $O(N)$  watermelon conformal weights in boundary and bulk quantum gravity, namely equations (11.32–11.35), QED.

B.5.10. Dual Conformal Weights. In section 12.2.1, we introduced the dual  $\delta_0$  of a conformal weight by eq. (10.3)

$$(B.68) \quad \delta_0 = \frac{1}{1 - \delta};$$

such that  $U(\delta) = \delta_0$ . These dual dimensions are natural in the description of the dense phase. Indeed, while we stated in (10.13) or (10.14) that in the dilute phase (or for simple SLE paths) the boundary scaling dimensions are additive, their duals retain the additivity property in the dense phase (or for non-simple SLE paths), a fact which will be established in all generality in the next appendix.

The nature of these dual dimensions remained slightly mysterious, however. It is interesting to observe their appearance in eq. (B.51). Indeed, when measuring lengths there in terms of the boundary length  $|\partial G_j|$ , instead of the square root  $\sqrt{|\partial G_j| |\partial G_j|}$  of the area, a new exponent  $\tilde{\delta}_L^0$  appeared, such that

$$(B.69) \quad \tilde{\delta}_L^0 = 1 + (\tilde{\delta}_L - 1) = \frac{\tilde{\delta}_L}{1 - \tilde{\delta}_0}:$$

In the dilute phase, the two boundary lengths scale in the same way,  $\delta = 1$ ,  $\tilde{\delta}_0 = 0$ , and the boundary conformal weights are unchanged:  $\tilde{\delta}_L^0 = \tilde{\delta}_L$ :

In the dense phase, we have found  $\tilde{\delta}_0 = \frac{1}{1-L}$ ;  $\delta = \frac{1}{1-L}$ , and the new dimension  $\tilde{\delta}_L^0$  (B.69) is just the dual one (B.68)

$$(B.70) \quad \tilde{\delta}_L^0 = \frac{\tilde{\delta}_L}{1 - \tilde{\delta}_0} = \frac{\tilde{\delta}_L}{1}:$$

Furthermore, since the dual boundary puncture dimension  $\tilde{\delta}_0^0 = 0$  in the dense phase, the cyclicity of eq. (B.52) clearly shows the dual exponents  $\tilde{\delta}_L^0$  to be linear in  $L$ , in agreement with (10.14), QED. Indeed eq. (B.66) gives for the dense phase:

$$(B.71) \quad \tilde{\delta}_L^0 = \frac{1}{1} \frac{L}{2} = (1 - \delta_0) \frac{L}{2};$$

in agreement with duality eqs. (10.5), (11.25), (11.32), and (11.33) of section 12, QED.

B.5.11. Coulomb Gas Formulae. For pedagogical purposes, we have given above a derivation of the exponents based on general principles only, in terms of the susceptibility exponent  $\chi$ . We could also have derived these results from expressions (B.22) and (B.26) in terms of parameter  $\beta$  (B.16). This analysis again leads to distinguish the two cases of dilute and dense phases, and one respectively finds for bulk and boundary exponents:

$$(B.72) \quad \begin{aligned} & \begin{cases} \delta \\ \gamma \end{cases} \\ & \begin{aligned} & \frac{1}{4} (1 + \delta) - \frac{1}{2} = \binom{\delta}{L}; \quad \delta = 1 \text{ (dilute)} \\ & \frac{1}{4} L - \frac{1}{2(1-L)} = \binom{\delta}{L}; \quad \delta = 1 \text{ (dense)}. \end{aligned} \end{aligned}$$

$$(B.73) \quad \begin{aligned} & \langle \tilde{\gamma}_L = 2 \gamma_L = \frac{1}{2}L(1 + \gamma); \quad \gamma = \gamma; \quad \gamma = 1 \text{ (dilute)} \\ & \gamma = \frac{1}{2}L(1 - \gamma); \quad \gamma = \frac{1}{1 - \gamma}; \quad \gamma = 1 \text{ (dense)}. \end{aligned}$$

In terms of the Coulomb gas coupling constant,  $g$ , parametrizing the  $O(N)$  model, one has

$$(B.74) \quad \begin{aligned} N &= 2 \cos \gamma; \quad \gamma = 0 \quad 1 \\ &\langle \gamma = 2 [L; 2] \text{ (dilute)} \\ (B.75) \quad & \gamma = 2 \cos g; \quad \gamma = 2 [0; 1] \text{ (dense)}. \end{aligned}$$

We thus have:

$$(B.76) \quad \begin{aligned} & \langle \gamma = 1 + 2 [L; 2]; \quad \gamma = 1 \quad g \text{ (dilute)} \\ & \gamma = 1 - 2 [0; 1]; \quad \gamma = 1 \quad g^{-1} \text{ (dense)}. \end{aligned}$$

Finally, the dilute and dense exponents can be recast in terms of the Coulomb gas coupling constant. The bulk ones read as

$$(B.77) \quad \begin{aligned} & \langle \gamma_L = \frac{1}{4}gL + \frac{1}{2}(1 - g) \quad \gamma = 1 \quad g; \quad \gamma = 1 \text{ (dilute)} \\ & \gamma_L = \frac{1}{4}L + \frac{1}{2}(1 - g^{-1}) \quad \gamma = 1 \quad g^{-1}; \quad \gamma = g \text{ (dense)}, \end{aligned}$$

and the boundary ones

$$(B.78) \quad \begin{aligned} & \langle \tilde{\gamma}_L = 2 \gamma_L = \frac{1}{2}gL; \quad \gamma = 1 \quad g; \quad \gamma = 1 \text{ (dilute)} \\ & \gamma_L = 2 \gamma_L = \frac{1}{2}L + 1 - g^{-1}; \quad \gamma = 1 \quad g^{-1}; \quad \gamma = g \text{ (dense)}. \end{aligned}$$

B.5.12. Conformal Weights for the Stochastic Loewner Evolution. The quantum gravity conformal weights for the SLE are obtained either directly from the Coulomb gas ones above, by the simple substitution  $\gamma = 4 - g$ , or by using in eqs. (10.5), (11.25), (11.32), and (11.33) the parametrization  $\gamma = 1 - 4 = -3$  for the dilute phase, i.e., for simple paths SLE<sub>4</sub>, and  $\gamma = 1 - 4 = -3$  for the dense phase, i.e., for non-simple paths SLE<sub>4</sub>. We find:

$$(B.79) \quad \begin{aligned} & \langle \tilde{\gamma}_L = \frac{2L}{L+1}; \quad \gamma = 1 \quad (4) \\ & \gamma_L = \frac{L}{2} + 1 - \frac{1}{4} = \frac{0-16}{1;L+1}; \quad \gamma = \frac{4}{4} \quad (4); \end{aligned}$$

while the bulk conformal weights are:

$$(B.80) \quad \begin{aligned} & \langle \tilde{\gamma}_L = \frac{1}{2}(1 - \frac{4}{4}) + \frac{L}{4} = \frac{0-16}{L=2;0}; \quad \gamma = 1 \quad (4) \\ & \gamma_L = \frac{1}{2}(1 - \frac{4}{4}) + \frac{L}{4} = \frac{0-16}{0;L=2}; \quad \gamma = \frac{4}{4} \quad (4); \end{aligned}$$

where we recall the definition (11.30),

$$p_{j|q} = \frac{\Delta p - qj + \frac{4}{2}}{2}$$

These are eqs. (11.36) and (11.37) or, equivalently, (11.38) to (11.41), QED.

Appendix C . Boundary-Bulk Exponents & Boundary Fusion Rules in Quantum Gravity

C .1. Structural Conformal Weight Relations. The aim of this last appendix is to establish two different basic scaling relations in quantum gravity, which we often encountered in calculating critical exponents.

C .1.1. From the Boundary to the Bulk. The first one concerns the relation between quantum gravity bulk conformal weights  $\chi$ , and their Dirichlet boundary counterparts  $\tilde{\chi}$ :

$$(C.1) \quad \chi_{\text{str}(\Sigma=2)} = \tilde{\chi} + \tilde{\chi}_0;$$

where  $\chi_{\text{str}(\Sigma=2)}$  is the string susceptibility exponent of the random surface with the sphere topology, bearing a certain conformal field theory of central charge  $c(\Sigma)$ , and where  $\tilde{\chi}_0$  is the conformal weight of the boundary puncture operator.

C .1.2. Dirichlet Random Sets and Conformal Weight Additivity. The second one is the additivity property of boundary conformal weights,  $\tilde{\chi}_A$  and  $\tilde{\chi}_B$ , corresponding to two random sets A and B living on the random disk, and mutually-avoiding each other, namely experiencing mutual Dirichlet conditions, in addition to those felt at the disk boundaries. This restriction has been noted  $A \wedge B$  throughout the paper. This additivity property reads, in its general setting:

$$(C.2) \quad \tilde{\chi}_{A \wedge B} + \tilde{\chi}_0 = \tilde{\chi}_A + \tilde{\chi}_0 + \tilde{\chi}_B + \tilde{\chi}_0;$$

C .1.3. KPZ Original and Modified Maps. We recall the form of the function involved in the KPZ equation:

$$(C.3) \quad h = U(\cdot) = \frac{1}{1 - \kappa(\cdot)^2};$$

which maps the quantum conformal weights onto (classical) Kac-like conformal weights  $h$  in the plane or half-plane. For the SLE process, we introduced a modified KPZ map:

$$(C.4) \quad U(\cdot) = \frac{1}{4} (\kappa^2 + 4);$$

with inverse:

$$(C.5) \quad U^{-1}(x) = \frac{1}{2} \sqrt{16x + (\kappa^2 + 4)} - \kappa^2;$$

C .1.4. Conformal Weight of the Boundary Puncture. We have seen in appendix B that  $\tilde{\chi}_0$  satisfies

$$(C.6) \quad U(\tilde{\chi}_0) = 0;$$

and takes one of the two values  $(0; \infty)$ , depending whether one is at a dilute critical point, or in a dense phase.

C .1.5. Additivity Rule for the SLE Process. As shown in section 11, when using the  $U^{-1}$  inverse function, instead of the original one  $U^{-1}$ , the additivity rule (C.2) can be recast in a unique formula, independently of the value of  $\tilde{\chi}_0$ , and of the range of  $\kappa$ :

$$(C.7) \quad U^{-1}(\kappa_{A \wedge B}) = U^{-1}(\kappa_A) + U^{-1}(\kappa_B);$$

where the conformal weights  $\kappa$  are those on the boundary of the half-plane  $H$

$$(C.8) \quad \kappa = U(\tilde{\chi});$$

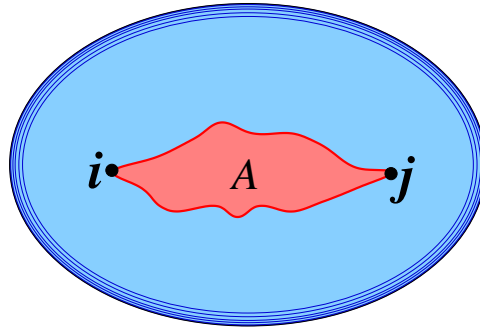


Figure 33. Two-point correlator of a random set  $A$  on a random sphere, corresponding to the partition function (C.11).

C.2. Partition Functions.

C.2.1. Two-Puncture Partition Functions. We consider a random lattice  $G$  bearing a given statistical system, whose critical properties correspond to a conformal field theory with central charge  $c$ , and string susceptibility exponent  $\gamma$ . The two-puncture partition function in the spherical topology reads

$$(C.9) \quad Z(\text{two punctures}) = \frac{\partial^2}{\partial z^2} Z(\text{disk}) = \sum_{\text{planar } G} \frac{1}{S(G)} \int \int e^{\int W(G)};$$

where  $W(G)$  is the weight due to the background statistical system borne by the random lattice, depending on some unspecified fugacities, and where  $Z$  is the partition function of the random lattice and statistical system in the absence of punctures. The two-puncture boundary partition function is, in a similar way:

$$(C.10) \quad Z(\text{two punctures on boundary}) = \frac{\partial}{\partial z} \frac{\partial^2}{\partial z^2} Z(\text{disk}; z) = \sum_{\text{disk } G} e^{\int W(G)} \int \int z^{\gamma G};$$

where  $Z$  is the disk partition function without punctures.

C.2.2. General Two-Point Partition Functions. Imagine a random set  $A$  on a random lattice  $G$ . We have in mind random sets  $A$  like the random trees of appendix A, the random lines of the  $O(N)$  model in appendix B, or random paths similar to the SLE process, i.e., frontier hulls of Potts or  $O(N)$  models. One can then define two-point partition functions, which connect two arbitrary points  $i$  and  $j$  in  $G$  (Fig. 33), as the watermelon ones  $Z_{O(N);L}$  (B.7) or  $Z'_{O(N);L}$  (B.8) in appendix B.

The existence of the random set  $A$  at a given point  $i \in G$  is associated with a conformal field operator  $\phi_A(i)$  creating the process at  $i$ , and belonging to the conformal field theory borne by  $G$ . We write the two-point partition function in a symbolic way

$$(C.11) \quad Z_A = \langle \phi_A(i) \phi_A(j) \rangle = \sum_{\text{planar } G} \frac{1}{S(G)} e^{\int W(G)} \sum_{i,j \in G} \sum_{A_{i,j} \subset G} Z^{A_{i,j}};$$

where the average  $\langle \dots \rangle$  is calculated with grand-canonical Gibbs weights;  $W(G)$  again is the weight of the random lattice bearing the background statistical system,

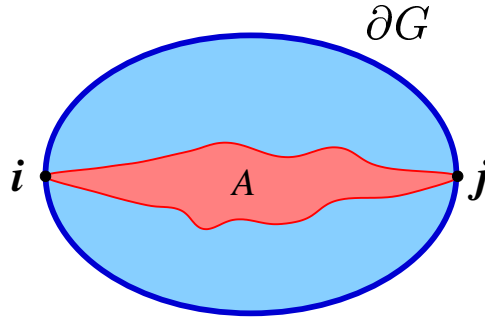


Figure 34. Two-point boundary correlator of a random set  $A$  on a random disk, corresponding to the partition function (C.12).

depending on some associated fugacities, and  $z$  is a fugacity associated with the number of sites occupied by random set  $A_{ij}$  between  $i$  and  $j$ .

Similarly, the two-point boundary partition function reads as in (B.8) (Fig. 34):

$$\begin{aligned}
 Z_A &= \mathbb{h} \prod_{i,j \in \partial G} \tilde{z}_A(i) \tilde{z}_A(j) \\
 \text{(C.12)} \quad &= \int_{\text{disk } G} e^{-\beta \mathcal{W}(G)} z^{\#\partial G} \prod_{i,j \in \partial G} z^{\#A_{ij}};
 \end{aligned}$$

where  $z$  is the new fugacity associated with the boundary's length.

Consider now two sets  $A$  and  $B$  starting and ending at the same vertices  $i$  and  $j$  on  $G$ , and in a mutually-avoiding configuration  $A \wedge B$  (Fig. 35). Their two-point partition function is defined as:

$$\begin{aligned}
 Z_{A \wedge B} &= \mathbb{h} \prod_{i,j \in \partial G} \tilde{z}_{A \wedge B}(i) \tilde{z}_{A \wedge B}(j) \\
 \text{(C.13)} \quad &= \int_{\text{planar } G} \frac{1}{S(G)} e^{-\beta \mathcal{W}(G)} \prod_{i,j \in \partial G} z^{\#A_{ij}} z^{\#B_{ij}};
 \end{aligned}$$

where a common fugacity is attributed to the total number of sites of  $A \wedge B$  between  $i$  and  $j$ ,  $\tilde{z}_{A \wedge B}(i,j) = \tilde{z}_{A_{ij}} + \tilde{z}_{B_{ij}}$ .

The boundary partition function is similarly (Fig. 36):

$$\begin{aligned}
 Z_{A \wedge B} &= \mathbb{h} \prod_{i,j \in \partial G} \tilde{z}_{A \wedge B}(i) \tilde{z}_{A \wedge B}(j) \\
 \text{(C.14)} \quad &= \int_{\text{disk } G} e^{-\beta \mathcal{W}(G)} z^{\#\partial G} \prod_{i,j \in \partial G} z^{\#A_{ij}} z^{\#B_{ij}};
 \end{aligned}$$

### C.3. Spectral representation.

C.3.1. Partition Function in Spherical Topology: In the random lattice representations by eigenvalue densities of random matrices like those used in appendices A and B, the two-point partition function in spherical topology in general can be written as in (A.18) or (B.11)

$$\text{(C.15)} \quad Z_A = \int d(\cdot) \mathcal{T}_A(z; \cdot);$$

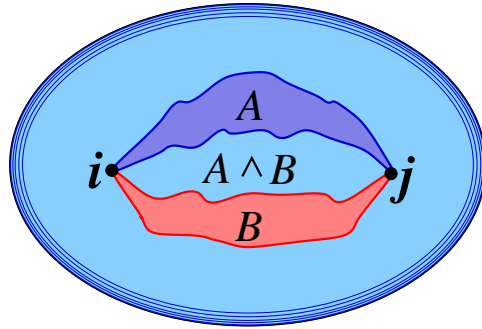


Figure 35. Two-point correlation of mutually-avoiding random sets  $A \wedge B$  on a random sphere, as they appear in the partition function (C.13).

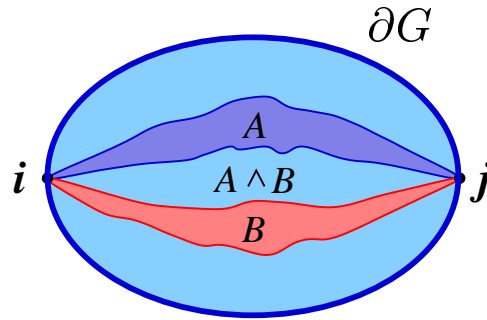


Figure 36. Two-point boundary correlation of mutually-avoiding random sets  $A \wedge B$  on a random disk, as they appear in the partition function (C.14).

where the patch of random surface outside set  $A$  contributes an spectral density  $\rho(\gamma)$ , while  $A$  contributes an inverse "propagator"  $T_A(z; \gamma_1; \gamma_2)$ ; similar to (A.19) or (B.12), the form of which depends on the nature of set  $A$ . The variables are the fugacity  $z$  of set  $A$  and the spectral parameter  $\gamma$ , repeated here since it characterizes both sides of the random surface patch adjacent to  $A$ .

C.3.2. Boundary Two-Point Partition Function (C.12): Its integral representation is similarly

$$(C.16) \quad Z_A = \int \prod_{l=1}^Z \gamma_l^2 d\gamma_l(\gamma_l) T_A(z; \gamma_1; \gamma_2) \frac{L(z_1)^{-1} L(z_2)^{-1}}{(1 - z_1)^{-1} (1 - z_2)^{-1}}$$

with two extra propagators  $L(z_{1[or2]})$  describing the two boundary lines between  $i$  and  $j$ :

$$(C.17) \quad Z_A = \int \prod_{l=1}^Z \gamma_l^2 d\gamma_l(\gamma_l) T_A(z; \gamma_1; \gamma_2) L(z_1) L(z_2);$$

using the simplified notation (see (B.12))

$$(C.18) \quad L(x) = L(x;0) = (1-x)^{-1};$$

C.3.3. Two-Puncture Boundary Partition Function: (C.10) can be written as the limit case where  $A$  is a boundary puncture, noted  $\bullet$ :

$$(C.19) \quad \begin{aligned} Z = Z(\bullet \circ \bullet) &= \int_{\mathbb{Z}} d(\cdot) (1-z)^2 \\ &= \int_{\mathbb{Z}} d(\cdot) L^2(z); \end{aligned}$$

C.3.4. Dirichlet Mutually-Avoiding Sets  $A \wedge B$ : The mutual-avoidance  $A \wedge B$  requires the random sets  $A$  and  $B$  to be separated by a connected piece of random lattice  $G$ . Thus the spectral representation associated with partition functions (C.13) and (C.14) requires to integrate over an extra eigenvalue density  $\rho$  in between the two propagators  $T_A$  and  $T_B$  associated with traversing random sets  $A$  and  $B$ . Thus partition functions (C.13) and (C.14) can be written as

$$(C.20) \quad Z_{A \wedge B} = \int_{\mathbb{Z}} \int_{\mathbb{Y}^2} d_1(\rho) T_A(z; \rho; 2) T_B(z; 2; \rho);$$

$$(C.21) \quad \begin{aligned} Z_{A \wedge B} &= \int_{\mathbb{Z}} \int_{\mathbb{Y}^3} d_1(\rho) T_A(z; \rho; 2) T_B(z; 2; \rho) \\ &\quad (1-z_1)^{-1} (1-z_3)^{-1} \\ &= \int_{\mathbb{Z}} \int_{\mathbb{Y}^3} d_1(\rho) T_A(z; \rho; 2) T_B(z; 2; \rho) L(z_1) L(z_3); \end{aligned}$$

C.4. Quantum Gravity Conformal Weights.

C.4.1. Bulk Conformal Dimensions. We first consider the planar topology ( $\chi = 2$ ). The two-puncture partition function (C.9) scales as

$$(C.22) \quad Z[\bullet \circ \bullet] \sim \mathfrak{J}^{j^{\text{str}}(\chi=2)};$$

In quantum gravity, the bulk conformal weight  $\Delta_A$  of operator  $\mathcal{O}_A$  is then defined by the scaling of the two-point function  $Z_A$ , properly normalized, with respect to the average size of the lattice:

$$(C.23) \quad Z_A = Z[\bullet \circ \bullet] \sim \mathfrak{J}^{2\Delta_A};$$

This definition takes into account the fact that the two-point partition function  $Z_A$  contains, in addition to the insertion of two  $\mathcal{O}_A$  operators, the two-puncture partition function on the sphere. Thus we have by definition:

$$(C.24) \quad Z_A \sim \mathfrak{J}^{j^{\text{str}}(\chi=2) + 2\Delta_A};$$

C.4.2. Boundary Conformal Dimensions. Let us first consider the disk partition function with two punctures (C.10). We write its scaling as:

$$(C.25) \quad Z = Z(\bullet \circ \bullet) \sim \mathfrak{J}^{j^{\text{str}}(\chi=1) + 2\Delta_A} \frac{P}{\mathfrak{J}^j} \sim \mathfrak{J}^{2\tilde{\Delta}_0};$$

As in eq. (B.48) of appendix B, the first power law accounts for the scaling of the disk partition function for an Euler characteristic  $\chi = 1$ , with a susceptibility



exponent  $\text{str}(\gamma) = 1$ , while the second term takes into account the integration and the conformal weight  $\tilde{\gamma}_0$  of the two punctures along the boundary.

For the boundary partition function  $Z_A$ , we similarly define boundary conformal weights  $\tilde{\gamma}_A$ , such that:

$$(C 26) \quad Z_A = \int \mathcal{G}^{j^{\text{str}(\gamma)=1}} \int \mathcal{P} \frac{1}{\mathcal{G}^j} \int \mathcal{L}^{2\tilde{\gamma}_A} ;$$

By using (C 25) we thus have the simple scaling relation

$$(C 27) \quad \frac{Z_A}{Z(\bullet \circlearrowleft \bullet)} = \frac{\tilde{Z}_A}{Z} \int \mathcal{G}^{j^{\text{str}(\gamma)=1}} \int \mathcal{P} \frac{1}{\mathcal{G}^j} \int \mathcal{L}^{2\tilde{\gamma}_0 + 2\tilde{\gamma}_A} ;$$

One can also measure the scaling behavior in terms of the boundary length  $\int \mathcal{G}^j = \int \mathcal{G}^{j=2}$ , where, as shown in appendix B,  $\text{str}(\gamma) = 1 \Rightarrow \tilde{\gamma}_0$ . This leads to the definition of another set of boundary quantum gravity dimensions,  $\tilde{\gamma}_A^0$ , such that

$$(C 28) \quad Z_A = \int \mathcal{G}^{j^{\text{str}(\gamma)=1}} \int \mathcal{G}^j \int \mathcal{L}^{2\tilde{\gamma}_A^0} ;$$

or, equivalently,

$$(C 29) \quad \frac{Z_A}{Z} = \int \mathcal{G}^j \int \mathcal{L}^{2\tilde{\gamma}_0 + 2\tilde{\gamma}_A^0} ;$$

This gives as in (B 53) of appendix B, the dimension:

$$(C 30) \quad \tilde{\gamma}_A^0 - 1 = (\tilde{\gamma}_A - 1) ;$$

Hence

$$(C 31) \quad \tilde{\gamma}_A^0 = \frac{\tilde{\gamma}_A}{1} \frac{\tilde{\gamma}_0}{\tilde{\gamma}_0} ;$$

which is the dual dimension (10.3) when  $\tilde{\gamma}_0 = 1$ , i.e., in the dense phase.

### C 5. Derivation of Quantum Gravity Scaling Relations.

C 5.1. Relation between Bulk and Boundary Exponents. We now have to characterize the scaling behavior of partition functions, as represented by spectral multiple integrals such as (C 15), (C 17), or (C 19). Similarly to the study done in appendix B [see, e.g., eqs. (B 19), (B 20), and (B 21)], it is useful to introduce a notation characterizing the various scaling factors in the multiple integrals. We thus write these partition functions (C 15), (C 17), and (C 19) as

$$(C 32) \quad Z_A = \int \mathcal{G}^j \int \mathcal{L}^{2\tilde{\gamma}_A} ;$$

$$(C 33) \quad Z_A = \int \mathcal{G}^j \int \mathcal{L}^{2\tilde{\gamma}_A} \int \mathcal{L}^{2\tilde{\gamma}_0} ;$$

$$(C 34) \quad Z(\bullet \circlearrowleft \bullet) = Z = \int \mathcal{G}^j \int \mathcal{L}^{2\tilde{\gamma}_0} ;$$

where the  $\int$  notation naturally resembles that representing convolutions. Each factor  $X$  of a  $\int$ -product brings in its own contribution to the scaling behavior of the partition function. Ultimately, this scaling behavior is measured in terms of area  $\int \mathcal{G}^j$  and is formally written as

$$(C 35) \quad X = \int \mathcal{G}^j \int \mathcal{L}^{2\tilde{\gamma}_X} ;$$



Considering its ratio to the two-puncture boundary partition function gives:

$$(C.48) \quad \frac{\mathbb{Z}_{A \wedge B}}{\mathbb{Z}} = \mathbb{Z}_{A \wedge B}^{\#} \mathbb{Z}^{\#} = 2 + [\Gamma_A] + [\Gamma_B];$$

where use was made of the scaling dimension (C.39). Comparing to (C.41) finally gives

$$(C.49) \quad \frac{\tilde{\mathbb{Z}}_{A \wedge B}}{\tilde{\mathbb{Z}}} = \frac{\tilde{\mathbb{Z}}_A}{\tilde{\mathbb{Z}}} + \frac{\tilde{\mathbb{Z}}_B}{\tilde{\mathbb{Z}}};$$

From eq. (C.44) we conclude:

$$(C.50) \quad \tilde{\mathbb{Z}}_{A \wedge B} \tilde{\mathbb{Z}}_0 = \tilde{\mathbb{Z}}_A \tilde{\mathbb{Z}}_0 + \tilde{\mathbb{Z}}_B \tilde{\mathbb{Z}}_0;$$

which is eq. (C.2), QED.

## References

- [1] Paul Levy, *Processus stochastiques et mouvement brownien* (Gauthier-Villars, Paris, 1965).
- [2] B.Mandelbrot, *The Fractal Geometry of Nature* (Freeman, New-York, 1982).
- [3] K.Symonzyk, in *Local Quantum Theory*, edited by R.Jost (Academic, London, New-York, 1969).
- [4] P.-G.de Gennes, *Phys. Lett. A* 38, 339 (1972).
- [5] J.des Cloizeaux and G.Jannink, *Polymers in Solution, their Modeling and Structure* (Clarendon, Oxford, 1989).
- [6] M.Aizenman, *Phys. Rev. Lett.* 47, 1 (1981); *Commun. Math. Phys.* 86, 1 (1982); D.C.Brydges, J.Frohlich, and T.Spencer, *Commun. Math. Phys.* 83, 123 (1982).
- [7] G.F.Lawler, *Commun. Math. Phys.* 86, 539 (1982); *Intersection of Random Walks* (Birkhauser, Boston, 1991).
- [8] M.E.Fisher, *J. Stat. Phys.* 34, 667 (1984).
- [9] M.Aizenman, *Commun. Math. Phys.* 97, 91 (1985); G.Felder and J.Frohlich, *ibid.*, 111; G.F.Lawler, *ibid.*, 583.
- [10] B.Duplantier, *Commun. Math. Phys.* 117, 279 (1987).
- [11] A.A.Belavin, A.M.Polyakov and A.B.Zamolodchikov, *Nucl. Phys. B* 241, 333 (1984).
- [12] D.Friedan, J.Qiu, and S.Shenker, *Phys. Rev. Lett.* 52, 1575 (1984).
- [13] see, e.g., J.L.Cardy, in *Phase Transitions and Critical Phenomena*, edited by C.Domb and J.L.Lebowitz, (Academic, London, 1987), Vol. 11.
- [14] M.den Nijs, *J. Phys. A* 12, 1857 (1979); *Phys. Rev. B* 27 1674 (1983).
- [15] B.Nienhuis, *Phys. Rev. Lett.* 49, 1062 (1982); in *Phase Transitions and Critical Phenomena*, edited by C.Domb and J.L.Lebowitz, (Academic, London, 1987), Vol. 11.
- [16] J.L.Cardy, *Nucl. Phys. B* 240 [FS12], 514 (1984).
- [17] H.Saleur, *J. Phys. A* 19 L807 (1986).
- [18] B.Duplantier, *Phys. Rev. Lett.* 57, 941 (1986); *J. Stat. Phys.* 54, 581 (1989).
- [19] B.Duplantier and H.Saleur, *Phys. Rev. Lett.* 57, 3179 (1986).
- [20] H.Saleur and B.Duplantier, *Phys. Rev. Lett.* 58, 2325 (1987).
- [21] J.L.Cardy, *J. Phys. A* 25, L201 (1992).
- [22] R.Langlands, P.Pouliot, and Y.Saint-Aubin, *Bull. AMS* 30, 1 (1994).
- [23] M.Aizenman, in *Mathematics of Multiscale Materials; the IMA Volumes in Mathematics and its Applications*, K.M.Golden et al. eds, Springer-Verlag (1998).
- [24] I.Benjamini, and O.Schramm, *Commun. Math. Phys.* 197, 75 (1998).
- [25] V.A.Kazakov, *Phys. Lett. A* 119, 140 (1986).
- [26] A.M.Polyakov, *Mod. Phys. Lett. A* 2, 893 (1987); V.G.Knizhnik, A.M.Polyakov and A.B.Zamolodchikov, *Mod. Phys. Lett. A* 3, 819 (1988).
- [27] F.David, *Mod. Phys. Lett. A* 3, 1651 (1988); J.Distler and H.Kawai, *Nucl. Phys. B* 321, 509 (1988).
- [28] B.Duplantier and I.K.Kostov, *Phys. Rev. Lett.* 61, 1436 (1988); *Nucl. Phys. B* 340, 491 (1990).

- [29] I. K. Kostov, *Mod. Phys. Lett. A* 4, 217 (1989); M. Gaudin and I. K. Kostov, *Phys. Lett. B* 220, 200 (1989).
- [30] B. B. Mandelbrot, *J. Fluid Mech.* 62, 331 (1974).
- [31] H. G. E. Hentschel and I. Procaccia, *Physica (Amsterdam)* 8D, 835 (1983).
- [32] U. Frisch and G. Parisi, in *Proceedings of the International School of Physics "Enrico Fermi"*, course LXXXV III, edited by M. G. Hil (North-Holland, New York, 1985) p. 84.
- [33] T. C. Halseth, M. H. Jensen, L. P. Kadano, I. Procaccia, and B. I. Shraiman, *Phys. Rev. A* 33, 1141 (1986).
- [34] M. Cates and J. M. Deutsch, *Phys. Rev. A* 35, 4907 (1987); B. Duplantier and A. Ludwig, *Phys. Rev. Lett.* 66, 247 (1991); C. von Ferber, *Nucl. Phys. B* 490, 511 (1997).
- [35] T. C. Halseth, P. Meakin, and I. Procaccia, *Phys. Rev. Lett.* 56, 854 (1986).
- [36] T. C. Halseth, *Multifractality, Scaling, and Diffusive Growth in Fractals: Physical Origin and Properties*, L. Pietronero, ed. (Plenum Publishing Co., New York, 1989).
- [37] P. Meakin, *Fractals, Scaling and Growth Far from Equilibrium*, Cambridge Nonlinear Science Series 5 (1999); B. B. Mandelbrot and C. J. G. Evertsz, *Nature* 348, 143 (1990).
- [38] M. E. Cates and T. A. Witten, *Phys. Rev. Lett.* 56, 2497 (1986); *Phys. Rev. A* 35, 1809 (1987).
- [39] G. F. Lawler, *The frontier of a Brownian path is multifractal*, preprint (1998).
- [40] B. Duplantier and K.-H. Kwon, *Phys. Rev. Lett.* 61, 2514 (1988).
- [41] B. Li, and A. D. Sokal, *J. Stat. Phys.* 61, 723 (1990); E. E. Puckette, and W. Wemer, *Elect. Comm. in Probab.* 1, 5 (1996).
- [42] K. Burdzy and G. F. Lawler, *Probab. Th. Rel. Fields* 84, 393 (1990); *Ann. Probab.* 18, 981 (1990).
- [43] G. F. Lawler, *Duke Math. J.* 47, 655 (1980), 53, 249 (1986).
- [44] B. Duplantier, *J. Stat. Phys.* 49, 411 (1987); B. Duplantier and F. David, *J. Stat. Phys.* 51, 327 (1988).
- [45] S. Majumdar, *Phys. Rev. Lett.* 68, 2325 (1992); B. Duplantier, *Physica A* 191, 516 (1992).
- [46] R. W. Kenyon, *Acta Math.* 185, 239 (2000).
- [47] R. W. Kenyon, *J. Math. Phys.* 41, 1338 (2000).
- [48] W. Wemer, *Probab. Th. Rel. Fields* 108, 131 (1997).
- [49] G. F. Lawler and W. Wemer, *Ann. Probab.* 27, 1601 (1999).
- [50] B. Duplantier, *Phys. Rev. Lett.* 81, 5489 (1998).
- [51] B. Duplantier, *Phys. Rev. Lett.* 82, 880 (1999).
- [52] B. Duplantier, *Phys. Rev. Lett.* 82, 3940 (1999).
- [53] M. Aizenman, B. Duplantier and A. Aharony, *Phys. Rev. Lett.* 83, 1359 (1999).
- [54] B. Duplantier, in *Fractals: Theory and Applications in Engineering*, M. Dekking et al. eds., pp. 185-206 (Springer-Verlag, 1999).
- [55] G. F. Lawler and W. Wemer, *J. European Math. Soc.* 2, 291 (2000).
- [56] J. L. Cardy, *J. Phys. A* 32, L177 (1999).
- [57] B. Duplantier, *Phys. Rev. Lett.* 84, 1363 (2000).
- [58] T. Gossmann and A. Aharony, *J. Phys. A* 20, L1193 (1987).
- [59] O. Schramm, *Israel Jour. Math.*, 118, 221 (2000).
- [60] B. Duplantier, *J. Stat. Phys.* 110, 691 (2003); [arXiv:cond-mat/0207743](https://arxiv.org/abs/cond-mat/0207743).
- [61] The duality prediction follows immediately from the  $g \leftrightarrow 1/g$  duality results of [57], and the  $g \leftrightarrow 4/g$  correspondence between the SLE parameter and the Coulomb gas constant  $g$ . It was in particular stated at the Strasbourg RCP 25 meeting of March 2000.
- [62] G. F. Lawler, O. Schramm, and W. Wemer, *Acta Math.* 187, (I) 237, (II) 275 (2001), [arXiv:math.PR/9911084](https://arxiv.org/abs/math.PR/9911084), [arXiv:math.PR/0003156](https://arxiv.org/abs/math.PR/0003156); *Ann. Inst. Henri Poincaré PR* 38, 109 (2002), [arXiv:math.PR/0005294](https://arxiv.org/abs/math.PR/0005294).
- [63] G. F. Lawler, O. Schramm, and W. Wemer, *Acta Math.* 188 (2002) (to appear), [arXiv:math.PR/0005295](https://arxiv.org/abs/math.PR/0005295), *Math. Res. Lett.* 8, 401 (2001).
- [64] S. Smirnov, *C. R. Acad. Sci. Paris Ser. I Math.*, 333, 239 (2001)
- [65] G. F. Lawler, O. Schramm, and W. Wemer, *Electronic J. of Probability* 7, 2002, paper no. 2, [arXiv:math.PR/0108211](https://arxiv.org/abs/math.PR/0108211).
- [66] S. Smirnov, and W. Wemer, *Math. Res. Lett.* 8, 729 (2001), [arXiv:math.PR/0109120](https://arxiv.org/abs/math.PR/0109120).
- [67] G. F. Lawler, O. Schramm, and W. Wemer, [arXiv:math.PR/0112234](https://arxiv.org/abs/math.PR/0112234).
- [68] G. F. Lawler, O. Schramm, and W. Wemer, [arXiv:math.PR/0204277](https://arxiv.org/abs/math.PR/0204277).
- [69] S. Rohde and O. Schramm, [arXiv:math.PR/0106036](https://arxiv.org/abs/math.PR/0106036).
- [70] V. Beara, [arXiv:math.PR/0211322](https://arxiv.org/abs/math.PR/0211322), [arXiv:math.PR/0204208](https://arxiv.org/abs/math.PR/0204208).

- [71] I. A. B i n d e r, Harmonic Measure and Rotation of Simply Connected Planar Domains, PhD Thesis, Caltech (1998).
- [72] B. D u p l a n t i e r and I. A. B i n d e r, Phys. Rev. Lett. 89, 264101 (2002); arXiv:cond-mat/0208045.
- [73] G. F. L a w l e r, O. S c h r a m m, and W. W e m e r, arXiv:math.PR/0209343.
- [74] M. B a u e r, and D. B e r n a r d, Phys. Lett. B 543, 135 (2002) [arXiv:math-ph/0206028]; arXiv:hep-th/0210015; arXiv:hep-th/0301064.
- [75] R. F r i e d r i c h and W. W e m e r, arXiv:math.PR/0209382; arXiv:math-ph/0301018.
- [76] V. F a t e e v, A. Z a m o l d c h i k o v, A. L. Z a m o l d c h i k o v, arXiv:hep-th/0001012.
- [77] B. P o n s o t and J. T e c h n e r, Nucl. Phys. B 622, 309 (2002); arXiv:hep-th/0110244.
- [78] I. K. K o s t o v, arXiv:hep-th/0212194.
- [79] J. L. C a r d y, arXiv:math-ph/0301039.
- [80] W. W e m e r, arXiv:math.PR/0302115.
- [81] J. D u b e d a t, arXiv:math.PR/0303128.
- [82] See, e.g., A. M. P o l y a k o v, Gauge Fields and Strings (Harwood-Academic, Chur, 1987).
- [83] D. V. B o u l a t o v, et al., Nucl. Phys. B 275, 641 (1986); F. D a v i d, Nucl. Phys. B 257, 45, 543 (1985); J. A m b j o m, B. D u r h u u s, and J. F r o h l i c h, *ibid.*, 433.
- [84] I. K. K o s t o v and M. L. M e h t a, Phys. Lett. B 189, 118 (1987).
- [85] G. F. L a w l e r, Israel Jour. Math., 65, 113 (1989).
- [86] G. F. L a w l e r, *Elect. Comm. in Probab.* 1 (29) (1996).
- [87] C. v o n F e r b e r and Y. H o l o v a t c h, Europhys. Lett. 39, 31 (1997); Phys. Rev. E 56, 6370 (1997).
- [88] B. B. M a n d e l b r o t, and C. J. G. E v e r t s z, Nature 348, 143 (1990).
- [89] S. K a k u t a n i, Proc. Imp. Acad. Sci. (Tokyo) 20, 706 (1942).
- [90] N. G. M a k a r o v, Proc. London Math. Soc. 51, 369 (1985).
- [91] M. A i z e n m a n and A. B u r c h a r d, Duke Math. J. 99, 419 (1999).
- [92] A. B e u r l i n g, The collected works of Arne Beurling. Vol. 1, Contemporary Mathematicians, Birkhauser Boston Inc., Boston, MA, 1989, Complex analysis, Edited by L. Carleson, P. Malliavin, J. Neuberger and J. W e m e r.
- [93] R. C. B a l l and R. B l u m e n f e l d, Phys. Rev. A 44, R828 (1991).
- [94] R. C. B a l l, B. D u p l a n t i e r, and T. C. H a l s e y, unpublished (1999).
- [95] J. L. J a c o b s e n and P. Z i n n - J u s t i n, arXiv:cond-mat/0207063.
- [96] J. L. C a r d y, *ibid.*, and Lectures on Conformal Invariance and Percolation, Chuo University, Tokyo (2001).
- [97] B. D u p l a n t i e r, Phys. Rep. 184, 229 (1989).
- [98] P. M e a k i n et al., Phys. Rev. A 34, 3325 (1986); see also: P. M e a k i n, *ibid.* 33, 1365 (1986); in Phase Transitions and Critical Phenomena, vol. 12, edited by C. Domb and J.L. Lebowitz (Academic, London, 1988).
- [99] P. M e a k i n and B. S a p o v a l, Phys. Rev. A 46, 1022 (1992).
- [100] T. C. H a l s e y and M. L e i b i g, Ann. Phys. (N.Y.) 219, 109 (1992).
- [101] G. F. L a w l e r, ESI preprint 2001, An introduction to the stochastic Loewner evolution, <http://www.math.duke.edu/~jose/esi.html>.
- [102] M. B. H a s t i n g s, Phys. Rev. Lett. 88, 055506 (2002).
- [103] R. B a l i a n and B. D u p l a n t i e r, Ann. Physics 112, 165 (1978), p.183.
- [104] B. D u p l a n t i e r and J. L. C a r d y, private discussion (A s p e n, 1999).
- [105] J. L. C a r d y, Nucl. Phys. B 300, 377 (1988).
- [106] A. A h a r o n y and J. A s i k i a i n e n, arXiv:cond-mat/0206367.
- [107] W. W e m e r, Saint-Flour lectures notes (2002), [www.math.u-psud.fr/~wemer/](http://www.math.u-psud.fr/~wemer/).
- [108] B. D u p l a n t i e r and H. S a l e u r, Phys. Rev. Lett. 60, 2343 (1988).
- [109] E. B r e z i n, C. I t z y k s o n, G. P a r i s i, J.-B. Z u b e r, Commun. Math. Phys. 59, 35 (1978).
- [110] D. A l d o u s, SIAM J. Disc. Math. 3, 450 (1990); A. B r o d e r, in 30th Annual Sym. Foundations Computer Sci. 442, (IEEE, New York, 1989).
- [111] B. D u p l a n t i e r, unpublished.
- [112] B. W i e l a n d and D. B. W i l s o n, Phys. Rev. E, to be published.
- [113] B. D u p l a n t i e r and I. A. B i n d e r, to be published.
- [114] B. D u p l a n t i e r and H. S a l e u r, Nucl. Phys. B 290 [FS20] 291 (1987).
- [115] V. K a z a k o v and I. K. K o s t o v, Nucl. Phys. B 386, 520 (1992).